

DISS. ETH Nr. 19923

**Development of a siRNA Screening Strategy for
Host Cell Factors Involved in Virus Infection**

ABHANDLUNG
zur Erlangung des Titels
DOKTOR DER WISSENSCHAFTEN
der
ETH ZÜRICH

vorgelegt von
Thomas Heger
Diplom-Biochemiker, Universität Tübingen

geboren am 28. 03. 1978

Deutscher Staatsbürger

Angenommen auf Antrag von

Prof. Dr. Ari Helenius, Referent
Prof. Dr. Daniel Gerlich, Korreferent

2011

ZUSAMMENFASSUNG

RNA Interferenz mit siRNA hat sich zu einer bedeutenden Technologie entwickelt, um gezielt die Aktivität einzelner zellulärer Gene herunterzuregulieren und dabei die Auswirkungen auf zelluläre Funktionen untersuchen zu können. Viren sind eine der bedeutendsten Gruppen von Pathogenen für Mensch und Tier. Sie sind intrazelluläre Parasiten und benötigen deshalb zelluläre Proteine und Funktionen, um sich vermehren zu können. Bei vielen Viren sind die Funktionen ihrer viralen Proteine bereits gut untersucht. Die Interaktion mit der Wirtszelle dagegen ist oft nur unzulänglich untersucht. Ein vielversprechender Ansatz, um essenzielle Wirtsfunktionen zu entdecken ist der systematische „Knock-Down“ von Wirtsproteinen und das Bestimmen von Veränderungen in der Virusinfektion in Zellkultur.

In dieser Arbeit haben wir eine siRNA Screening Plattform entwickelt und getestet, um neue Wirtsproteine zu finden, die essenziell für Virusinfektion sind. Wir verwendeten eine siRNA-Bibliothek, die 108 Gene umfasst, welche wichtige Rollen in solchen zellulären Funktionen spielen, die potenziell von Viren genutzt werden. Diese umfassen Endozytosewege, Rezeptorsignaltransduktion, Endosomen, ER- und Golgi-vermittelte Sekretion und andere. Wir haben eine vielseitige und benutzerfreundliche Bildanalyse-Software entwickelt und intensiv getestet, welche integraler Bestandteil der Screening-Strategie ist. Insgesamt screeneten wir sechs unterschiedliche Viren aus diversen Familien und Genera, Semliki Forest Virus (SFV), Simian Virus 40 (SV40), Uukuniemi Virus, Vaccinia Virus, Influenza A Virus und Vesikuläre Stomatitis Virus. Wir stellten die Qualität des Screening-Prozesses sicher, in dem wir drei siRNA verwendeten, die gegen dasselbe Gen gerichtet sind; ausserdem waren alle siRNA als Duplikate per Replikat vorhanden, und wir screeneten alle Viren und Zelllinien in Triplikaten. Ein stringentes Prüfen auf korrekte Phänotypen der Kontrollen und Zelltoxizität basierend der Anzahl der Zellen war eine weitere Massnahme. Bei einigen Viren konnten wir zwei Zelllinien screenen. Vorläufige Hits wurden daraus unter Anwendung zweier unterschiedlicher Analyse-Methoden bestimmt. Strikte Kriterien wurden bei der Hitbestimmung aus siRNA Phänotypen angewandt. Wir entdeckten viele erwartete und neue Hits für die meisten hier gescreenten Viren. Aus diesen konnten wir viele Hits für SFV and SV40 validieren.

Das Screening von SFV identifizierte Proteine, welche wichtig sind für Clathrin-vermittelte Endozytose und die Funktionen von frühen Endosomen. Ausserdem sind Proteine, die assoziiert sind mit Rezyklierungsendosomen, Ubiquitinierung und Protein Kinase C, vorhanden. Wir konnten dazu Syntaxin-5 identifizieren und validieren, welches als SNARE Protein eine wichtige Rolle im ER-Golgi-Transport spielt – es ist auch wichtig für erfolgreiche Infektion mit SFV. Umfassende Validierung mit Hilfe von Inhibitoren von diversen Signalwegen bestätigte die Resultate des

Screenings für SFV. Insbesondere wurden die wichtigen Funktionen, die Ansäuerung, Clathrin-vermittelte Endozytose sowie frühe Endosomen für die Infektion von SFV haben, bestätigt. Interessanterweise zeigt unsere genaue Untersuchung der Funktion von Proteinkinase C, dass diese Enzymfamilie eine duale Rolle während der SFV-Infektion spielt. Eine liegt dabei in einem Schritt vor der Fusion der viralen Hülle mit der Endosomenmembran, während der andere Schritt nach der Fusion anzusiedeln ist.

Beim SV40-Screening konnten wir überraschend klar zeigen, dass der Virus von endosomalen Proteinen abhängt. Weder Clathrin- noch Caveolin-assoziierte Hits wurden dabei gefunden. Validierung erfolgte mit zeitaufgelöster Mikroskopie, unter Zuhilfenahme von Inhibitoren und dominant-negativen Konstrukten. Wir konnten zeigen, dass SV40-Aufnahme und Infektion von endosomalem Sortieren und Ansäuern abhängt. Der Virus colokalisiert mit Markern von frühen und, bei fortgeschrittenen Zeiten, auch späten Endosomen sowie Lysosomen. Dieses Resultat widerspricht einer älteren Hypothese, nach der SV40 in sogenannte „Caveosomen“ während seines Weges von der Plasmamembran zum ER sortiert wird. Diese Organellen seien pH-neutral. Wichtig ist, dass unsere Ergebnisse eine kürzliche Publikation bestätigt, wonach diese „Caveosomen“ keine unabhängigen Organellen sind, sondern lediglich modifizierte Endosomen in Cav1-EGFP-überexprimierenden Zellen. Interessanterweise fanden wir auch bei SV40, wie zuvor bei SFV, einen frühen Schritt während der Internalisierung, der Proteinkinase C-abhängig ist. Dies deutet auf PKC als einen wichtigen Faktor während des frühendosomalen Sortierens hin, wie auch bei SFV.

Zusammenfassend konnten wir einige zelluläre Funktionen verifizieren, auf die das Screening hinwies, und auch zum Teil die Schritte des viralen Vermehrungszyklus, bei denen sie eine Rolle spielen, identifizieren. Wir konnten viele der Screening-Hits validieren und zeigen, dass unsere Screeningstrategie im Labormassstab reproduzierbare Daten liefert und sehr nützlich zur Beantwortung virologischer Fragestellungen ist.

SUMMARY

RNA interference with small interfering RNA has evolved to a powerful technology to silence single cellular genes and investigate the effects of the knock-down on cellular functions. Viruses belong to the most fatal pathogens of humans and livestock. They are intracellular parasites and require cellular proteins and pathways to propagate. For many viruses much is known about the function of viral proteins. However, the interaction of the virus with the host organism is broadly elusive. A promising approach to shed light on basic cellular functions that are essential for virus amplification is to systematically knock-down host proteins and measure changes of virus infection in cell culture.

In this study, we develop and test a siRNA screening platform to find novel host proteins essential for virus infection. We screen a siRNA library, which targets 108 selected genes that play important roles in cellular pathways that are potentially used by viruses. These comprise endocytosis pathways, receptor signaling, endosomal compartments, ER and Golgi-mediated secretion, vesicle trafficking, and many more. We developed and intensively tested a versatile and user-friendly image analysis software, called *InfectionCounter*, that is integral part of the screening strategy. In total we screened six different viruses from diverse families and genera, Semliki Forest Virus (SFV), Simian Virus 40 (SV40), Uukuniemi virus, vaccinia virus, influenza A virus, and vesicular stomatitis virus. We insured quality of screening by using three siRNA targeting the same gene, all siRNA in duplicates per replicate, three independent replicates, and stringent assessment of control effects and cell toxicity. For some viruses two cell lines were screened and preliminary hits with two different analysis methods were determined. Stringent criteria were applied to determine hits from siRNA effects. We found many expected and novel hits for most of the viruses. The final hits were validated for SFV and SV40.

The screen for SFV identified proteins involved in clathrin-mediated endocytosis and early endosomal functions. Moreover, the importance of recycling endosomal proteins and factors involved in ubiquitination as well as protein kinase C members were obvious. We identified and validated syntaxin-5 as a strong hit; it is a SNARE protein important for ER-Golgi transport, as important for SFV receptor secretion. Extensive validation with small compound inhibitors against diverse pathways verified the screen and confirmed the important roles of acidification, clathrin-dependent endocytosis and early endosomes in infection of SFV. Interestingly, protein kinase C shows a dual role during infection, one in a pre-fusion step, another in post-fusion processes.

The SV40 screen revealed surprisingly clearly that the virus strongly depends on endosomal proteins. Neither clathrin- nor caveolin-associated hits were found in the list. We validated the data from the screen in detail using time lapse microscopy, small molecule inhibitors, dominant negative constructs.

We could clearly confirm that SV40 entry and infection depends on endosomal sorting and acidification. The virus colocalizes with early endosomal and, later in entry, late endosomal and lysosomal markers. This is in stark contrast to a previous hypothesis that the virus uses pH-neutral “caveosomes” as sorting stations on its journey from the plasma membrane to the ER. Importantly, our study confirms recent findings that “caveosomes” are not independent organelles but modified lysosomes in caveolin-1-EGFP overexpressed cells. Interestingly, we found a PKC-dependent step early in SV40 entry, similar to SFV, which might indicate an early endosomal step that requires PKC.

In summary, we could verify several cellular pathways and partly localize their function within the virus life cycle for SFV and SV40. This validates many of the screening hits for these viruses and underlines our lab-scale siRNA screening approach as reproducible and very useful to challenge virological issues.

TABLE OF CONTENTS

1	INTRODUCTION	1
1.1	Endocytosis Pathways	1
1.1.1	Clathrin-Mediated Endocytosis	1
1.1.2	Caveolae-dependent Endocytosis	4
1.1.3	Caveolae-independent Endocytosis by Lipid Rafts	5
1.1.4	Macropinocytosis	7
1.2	Endosomes	10
1.2.1	Early Endosomes	10
1.2.2	Endosomal Recycling Pathways	12
1.2.3	Degradative Pathway	13
1.3	Viruses	14
1.3.1	Semliki Forest Virus	14
1.3.2	Simian Virus 40	16
1.3.3	Vesicular Stomatitis Virus	17
1.3.4	Influenza A Virus	18
1.3.5	Uukuniemi Virus	19
1.3.6	Vaccinia Virus	20
1.4	RNA Interference	20
1.5	Image Analysis Software	21
1.5.1	Canny Edge Detection	22
1.6	Objective of the PhD Thesis	23
2	RESULTS	24
2.1	Development of an Image Analysis Software	24
2.1.1	Rationale	24
2.1.2	Working Principle of <i>InfectionCounter</i>	24
2.1.3	Special Features of the Program	26
2.1.4	Test of the Program	27
2.2	RNAi Screening for Host Cell Factors Important for Virus Infection	32

2.2.1	Introduction	32
2.2.2	General Screening Procedure	32
2.3	Usual Suspects Miniscreens of Six Different Viruses.....	34
2.3.1	Screening of Semliki Forest Virus (SFV).....	35
2.3.2	Screening of Simian Virus 40, Vesicular Stomatitis Virus, Vaccinia Virus, Uukuniemi Virus, and Influenza A Virus	40
2.3.3	Comparison of hit lists from different viruses.....	43
2.4	Analysis and Validation of Screening Hits.....	45
2.4.1	Western Blot Analysis to Quantify Knock-down efficiency.....	45
2.4.2	Screening of Semliki Forest Virus (SFV).....	46
2.4.3	Screening of Simian Virus 40 (SV40).....	54
3	DISCUSSION.....	59
4	MATERIALS AND METHODS.....	69
4.1	Software Development.....	69
4.2	Cell Culture	69
4.3	Drugs and Plasmids	69
4.4	Viruses and Virus Preparation.....	70
4.4.1	SFV.....	70
4.4.2	VSV	70
4.4.3	SV40.....	71
4.4.4	Influenza A Virus	71
4.4.5	Vaccinia virus.....	71
4.4.6	Uukuniemi Virus	71
4.5	FACS Analysis of SFV Infection.....	72
4.6	Protocols for RNAi screening	72
4.6.1	Plate Layout.....	72
4.6.2	General Transfection Protocol.....	73
4.6.3	Virus Infection Assays for Screening.....	73
4.6.4	Imaging.....	75
4.6.5	Normalization and Standardization	75

4.6.6	Hit Definition	76
4.6.7	Bioinformatic tools.....	76
5	SUPPLEMENTARY INFORMATION.....	77
6	ABBREVIATIONS.....	78
7	REFERENCES	79
8	ACKNOWLEDGEMENTS	93
9	CURRICULUM VITAE	94

1 INTRODUCTION

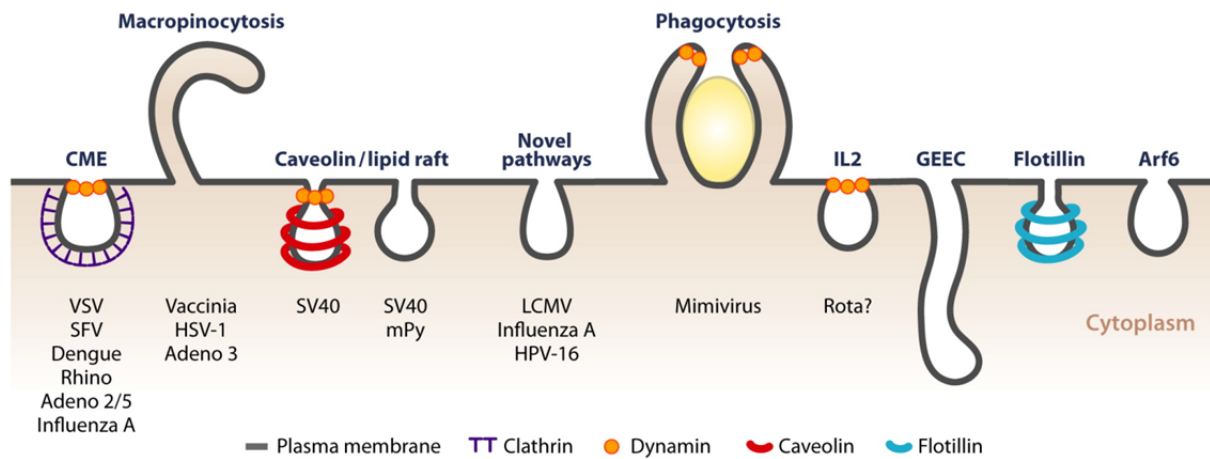
1.1 Endocytosis Pathways

The plasma membrane separates the cell interior from its environment. The uptake of macromolecules, nutrients, particles and even whole organisms across the plasma membrane in membrane-enclosed vesicles is called endocytosis. Endocytosis is crucial for cellular basic functions such as immune response, intracellular communication, development, and signaling into the cell. Endocytosis encompasses two broad categories, the uptake of larger particles, which is called phagocytosis, and pinocytosis, the internalization of fluids and solutes. While only specialized cells such as macrophages are capable of phagocytosis, pinocytosis can be found in most cells. Until now several pathways of pinocytic uptake could be identified: clathrin-mediated endocytosis, macropinocytosis, caveolae / raft-mediated endocytosis, and several other less characterized non-clathrin pathways (Doherty and McMahon 2009).

Many viruses exploit the different endocytosis pathways to get into the cell (Fig. 1). They bind to receptors at the plasma membrane, are internalized into endocytic vesicles and subsequently transported to the sites of viral replication (Gruenberg and van der Goot 2006; Mercer, Schelhaas et al. 2010). It becomes increasingly clear that the interaction of viruses and their host cells is a complex process. Any information about viral and cellular factors during the viral life cycle is potentially important to understand this process and helps to develop strategies against pathogenic viruses (Mercer, Schelhaas et al. 2010).

1.1.1 Clathrin-Mediated Endocytosis

Clathrin-mediated endocytosis (CME) is the best understood endocytic pathway. Receptors and cargo are engulfed at the plasma membrane forming clathrin-coated pits (CCP) that finally undergo fission to clathrin-coated vesicles (CCV). The coat protein clathrin is a trimer consisting of one heavy chain protein (CLTC) and one of two expressed light chain molecules (CLTA, CLTB) forming a triskelion. Many triskelions build a homooligomeric basket structure around the forming membrane vesicle. By its heavy chain each triskelion is bound to adaptor proteins such as AP2 linking the coat to membrane-associated and transmembrane proteins such as receptors. Together with the clathrin and adaptor complexes a huge protein machinery consisting of several hundreds of accessory proteins are involved to form a vesicle (Schmid and McMahon 2007).



AR Mercer J, et al. 2010.
Annu. Rev. Biochem. 79:803–33

Figure 1

Cellular endocytosis pathways. The cell employs multiple endocytic mechanisms for pinocytic uptake (CME – clathrin-mediated endocytosis, macropinocytosis, Caveolin/lipid raft-dependent pathways, and other poorly characterized routes). Phagocytosis is the uptake of large particles and a feature of specialized cells such as macrophages. Several routes are dependent on the small GTPase dynamin (orange circles) that is implicated in fission of endocytic vesicles. Several pathways are mostly defined by physiological cargo and have not yet been assigned to viruses (IL2 – Interleukin 2 beta, GEEC pathway, Arf6-dependent pathway, and flotillin-mediated pathway). From (Mercer, Schelhaas et al. 2010)

In the first step of CCP formation receptors, patches of the phospholipid phosphatidylinositol-4,5-bisphosphate (PI4,5P2) that are synthesized by phosphoinositole-5-kinases, and adaptors nucleate at the plasma membrane. This initiates and promotes clathrin polymerization. Since clathrin alone cannot induce membrane curvature (Nossal 2001) accessory proteins are involved in this step. Among them are multi-domain proteins from the epsin-family that insert amphipathic helix domains into the bilayer (Ford, Mills et al. 2002) or BAR domain-containing proteins such as Amphiphysin (Peter, Kent et al. 2004) and sortin nexin 9 (SNX9) (Lundmark and Carlsson 2003) that sense and stabilize membrane curvature. They also bind clathrin and AP-2, and recruit dynamin to the closing vesicle (Lundmark and Carlsson 2004). Another important protein that was first described by its role in EGF receptor endocytosis, Eps15, works as a scaffolding factor that binds AP-2 through its beta subunit (Schmid, Ford et al. 2006).

Depending on cargo different adaptor proteins are recruited to the forming CCP. G-protein coupled receptors (GPCRs) bind to beta-arrestins, which in turn interact with clathrin, PIP2, and AP-2 (Laporte, Oakley et al. 2000; Wolfe and Trejo 2007). ARH and disabled-2 (dab2) are adaptors for the receptor of low density lipoprotein (LDL) (Maurer and Cooper 2006), while numb has an analogue role for internalization of the notch receptor (Santolini, Puri et al. 2000).

Fission of deeply invaginated CCP into a CCV is mediated by the small GTPase dynamin-2 (DNM2) (Hinshaw 2000; Sever 2002). DNM2 is the ubiquitously expressed prototypic member of a dynamin and dynamin-related protein family involved in membrane fusion and fission. It further comprises

dynamamin-1 (DNM1) and dynamamin-3 (DNM3), specifically expressed in brain and testis, respectively. Additionally, there is a mitochondrial dynamamin-related protein (DRP1) that is implicated in mitochondrial fission (De Vos, Allan et al. 2005) and structural linkage to the actin cytoskeleton (Bereiter-Hahn, Voth et al. 2008). Dynamamin is a multi-domain protein consisting of five functionally different domains. At the N-terminus a highly homologous GTPase domain is situated in all members of the family, followed by a helical middle domain, a Pleckstrin homology (PH) domain, a GTPase effector domain (GED), and a proline-arginine domain (PRD) that allows interactions with SH3 domain containing binding partners. In solution dynamamin forms tetramers, with the helical middle and GTPase effector domain intertwining to a stalk (Schmid and Frolov 2011). On the one end of the stalk reside the PH domains connecting the complexes with PI4,5P2 lipid patches of membranes, on the other end the GTPase and PRD domains (Muhlberg, Warnock et al. 1997).

By several techniques such as TIRF and EM it was shown that dynamamin self-assembles late during the fission process in spirals around the constricting neck of the vesicle (Takei, McPherson et al. 1995; Merrifield, Feldman et al. 2002; Schmid and Frolov 2011) (Fig. 1). The mechanism of mediating fission is still under debate. It has first proposed that dynamamin acts as a mechanochemical enzyme that twists around the neck and thereby closes it under GTP cleavage supported by the GED domain. However, more recent data showed that self-assembly and GTPase activity negatively regulated dynamamin function indicating rather a regulating role in the fission process (Hinshaw and Schmid 1995; van der Blik 1999; Danino, Moon et al. 2004; Roux, Uyhazi et al. 2006; Mettlen, Pucadyil et al. 2009).

After fission the coat is released from the nascent vesicle. Two factors are crucial for uncoating, hsc70 and auxilin/GAK. Hsc70, heat shock cognate 70, is a member of the 70kDa family of heat shock proteins that work as molecular chaperones (Chappell, Welch et al. 1986; Eisenberg and Greene 2007). The neuron-specific protein Auxilin and its ubiquitous homolog cyclin-G-associated kinase GAK bind through their HPD motif to hsc70 and to specific phosphoinositide head groups in the CCV by their PTEN-like domain. Studies show that auxilin/GAK first binds to CCV, recruits hsc70 (Ahle and Ungewickell 1990; Ungewickell, Ungewickell et al. 1995; Kanaoka, Kimura et al. 1997), and transfers clathrin triskelia from the basket to the chaperone hsc70 (Gruschus, Greene et al. 2004). Due to their binding capability to dynamamin it is thought that both proteins are already recruited to the closing neck and support CCV budding (Newmyer, Christensen et al. 2003). Another protein that is recruited to the nascent vesicle, synaptojanin, hydrolyzes PI4,5P2 by its phosphatase activity (Wenk and De Camilli 2004). This activity finally dissociates adaptors such as AP-2 (Eisenberg and Greene 2007). The vesicle is trafficked within a short time to early endosomes and fuses with their limiting membrane to release its cargo.

CME is used for the cellular uptake of many physiological cargos such as transferrin, growth hormones, LDL. Also viruses take advantage of this route into the cell (Fig. 1). In fact, CME is the

most commonly observed endocytic pathway of viruses. One of the best studied enveloped virus, Semliki Forest virus (SFV) has first been shown to use CME as its productive entry pathway (Helenius, Kartenbeck et al. 1980; Mercer, Schelhaas et al. 2010). Since then other viruses could be identified using primarily CME among them are Vesicular Stomatitis Virus (VSV) (Matlin, Reggio et al. 1982; Johannsdottir, Mancini et al. 2009), Denguevirus (van der Schaar, Rust et al. 2008), Hepatitis C virus (Helle and Dubuisson 2008), Adenovirus 2 and 5 (Medina-Kauwe 2003), Avian leukosisvirus (Diaz-Griffero, Jackson et al. 2005) and many more. Some viruses use CME as one of several entry routes, e.g. Influenza A virus (Matlin, Reggio et al. 1981; Sieczkarski and Whittaker 2002).

1.1.2 Caveolae-dependent Endocytosis

Caveolae are membrane indentations devoid of clathrin that contain caveolins as the main structural proteins (Rothberg, Heuser et al. 1992; Anderson 1998). They represent a subgroup of lipid rafts, which are heterogenous plasma membrane microdomains of 10-200nm in size and enriched of glycosphingolipids and cholesterol (Fra, Williamson et al. 1994; Simons and Ikonen 1997; Pike 2006). Caveolae have been implicated in various cellular functions such as endocytosis, transcytosis, potocytosis, calcium signaling, and regulation of diverse signaling pathways (Parton and Simons 2007).

There are three different forms of caveolin, caveolin-1, -2, and -3. Caveolin-1 and 2 are ubiquitously expressed in human cells except muscle cells, neurons, and leukocytes (Anderson 1998), while caveolin-3 is the sole caveolin protein in muscle cells. Cav-1 and 3 predominantly reside in the plasma membrane while Cav-2 is localized primarily to the Golgi and is targeted to the plasma membrane only as hetero-complexes with Cav-1 (Scheiffele, Verkade et al. 1998). Expression of Cav-1 in cells devoid of caveolins is sufficient to induce caveolae formation (Fra, Williamson et al. 1995). In contrast to the clathrin coat caveolins are partially membrane-integrated proteins. They form higher order oligomeric complexes within caveolae. Complex formation starts in the ER, where monomeric Cav-1 molecules assemble into 15-24 oligomers and include molecules of Cav-2 when it is co-expressed. These 8S complexes accumulate in COPII ER exit sites and are trafficked along with GFP-GPI but not VSV-G to the Golgi. There assembly to higher ordered stabile structures of 70S occurs indicated by a loss of diffusional mobility of Cav-1 and -2 (Hayer, Stoeber et al. 2010). Once transported to the plasma membrane assemblies of the caveolin-associated protein PTRF/Cavin-1 is thought to interact with the Cav-1/Cav-2 scaffold either stabilizing or even inducing indentation of the nascent Caveola (Hayer, Stoeber et al. 2010). This is supported by the findings that RNAi against PTRF/Cavin-1 but also other members of the Cavin family led to loss of invaginated caveolae and Cav-1 (Hill, Bastiani et al. 2008; Hansen, Bright et al. 2009; McMahon, Zajicek et al. 2009).

Caveolae are implicated in endocytosis of physiological cargo but also bacterial toxins and viruses. In endothelial cells albumin localizes primarily to caveolae and is transported through these cells mainly by caveolar transcytosis (Lajoie and Nabi 2010). This process could be stimulated by src kinase

activation and dynamin-2 phosphorylation (Shajahan, Timblin et al. 2004). Dynamin-2 is, analog to its role in CCV formation, also important for fission of caveolae from the plasma membrane and localized to the necks of budding vesicles (Oh, McIntosh et al. 1998). Another cargo, lactosylceramide, has been shown to be exclusively internalized via caveolae (Sharma, Choudhury et al. 2003). The insulin receptor is rapidly internalized via caveolae in primary adipocytes (Fagerholm, Ortegren et al. 2009). Toxins such as cholera toxin subunit b and polyoma viruses such as SV40 and mouse polyoma virus are partly endocytosed by caveolae (Parton, Joggerst et al. 1994; Norkin 2001; Pelkmans and Helenius 2003). However, in both cases, recent studies suggest non-caveolae raft-dependent pathways as the major endocytic routes (Damm, Pelkmans et al. 2005; Kirkham, Fujita et al. 2005; Ewers, Romer et al. 2010).

Indeed, several studies question a predominant role of caveolae in raft endocytosis. In contrast to CCPs caveolae are extraordinarily immobile (Thomsen, Roepstorff et al. 2002). Autocrine motility factor (AMF), an exoenzyme secreted from cancer cells that stimulates cell motility, was shown to localize to caveolae and dynamin-2. Its internalization is enhanced in cells that have lower expression of Cav-1 (Le, Guay et al. 2002; Kojic, Joshi et al. 2007). This suggests that Cav-1 has besides its structural role in caveolae formation also a regulatory, in fact inhibitory, role in raft mediated endocytosis (Tagawa, Mezzacasa et al. 2005; Sandvig, Torgersen et al. 2008; Mercer, Schelhaas et al. 2010).

1.1.3 Caveolae-independent Endocytosis by Lipid Rafts

Dynamin-2 dependent formation of smooth vesicles from the plasma membrane occurs in presence but also in absence of Cav-1 (Le, Guay et al. 2002). Indeed, several physiological cargos have been identified that use lipid raft-associated caveolae/Cav-1-independent uptake routes and require both dynamin-2 and cholesterol. Among them are the aforementioned AMF and a fraction of cholera toxin b but also raft-associated interleukin-2 receptors (IL2R) in lymphocytes. IL2R endocytosis occurs constitutively in a dynamin-2 dependent manner and is regulated by small GTPases from the Rho family (Lamaze, Dujeancourt et al. 2001).

Another lipid raft-associated pathway is the so-called CLIC/GEEC pathway (Fig. 1). It stands for clathrin-independent carrier / GPI-anchored protein-enriched early endosomal compartment (Lajoie and Nabi 2010; Mercer, Schelhaas et al. 2010). This pathway is RhoA-independent but requires Arf1, ARHGAP10, and cdc42 (Sabharanjak, Sharma et al. 2002; Kumari and Mayor 2008). It is thought that most of the fluid phase uptake occurs via the CLIC/GEEC pathway (Kalia, Kumari et al. 2006). The role of dynamin in this pathway is controversial. Expression of a temperature-sensitive dynamin mutant that blocks uptake of transferrin has been shown to have no impact on pinocytic fluid phase uptake (Damke, Baba et al. 1994). Also immuno-EM could not find dynamin at early endocytic structures that were assigned to CLICs (Kirkham, Fujita et al. 2005). However, siRNA against dynamin-2 and microinjection of anti-dynamin-antibodies strongly reduce fluid phase uptake that

could be rescued by special splice variants of dynamin-2 (Cao, Chen et al. 2007). The proofs of existence of this pathway are mostly based on perturbations of other pathways. Indeed, physiological cargo that primarily uses CLIC/GEEC has not yet been identified (Doherty and McMahon 2009).

Flotillin or reggie proteins have also been implicated in clathrin- and caveolin-independent endocytosis (Babuke and Tikkanen 2007; Doherty and McMahon 2009). They are ubiquitously expressed and associated to raft microdomains in the plasma membrane that are distinct from caveolae (Glebov, Bright et al. 2006) but also to other organelles such as endosomes, phagosomes, and Golgi (Dermine, Duclos et al. 2001; Gkantiragas, Brugger et al. 2001; Stuermer, Lang et al. 2001). Several physiological functions have been linked to flotillins such as membrane receptor signaling, regulation of cytoskeleton, and raft-mediated endocytosis (Langhorst, Reuter et al. 2005; Glebov, Bright et al. 2006). Their structural homology suggests a similar role in membrane scaffolding than caveolins (Doherty and McMahon 2009). However, in contrast to caveolin-1 and also -3, co-overexpression of flotillins does not lead to plasma membrane indentations (Kirkham, Nixon et al. 2008). It has been shown that CD59 uptake and a portion of cholera toxin b internalization are both dependent on Flotillin-1 (Glebov, Bright et al. 2006; Frick, Bright et al. 2007). Both flotillins apparently cycle between Golgi and plasma membrane (Langhorst, Reuter et al. 2008) and at least flotillin-2 cycling can be stimulated by EGF although it does not colocalize with the EGF receptor nor with GPI anchored proteins such as GFP-GPI (Frick, Bright et al. 2007). To which extent both isoforms colocalize is as yet controversial, probably due to differences in cell lines and expression levels (Langhorst, Reuter et al. 2005; Frick, Bright et al. 2007; Doherty and McMahon 2009). There are hints that flotillin-dependent endocytosis is dynamin-dependent: proteoglycans from the cell surface are internalized in a clathrin and caveolin-independent, flotillin- and dynamin-dependent manner and trafficked to the endosomal system (Payne, Jones et al. 2007).

The small GTPase Arf6 is localized primarily at the plasma membrane and is implicated in clathrin-independent endocytosis. The MHC class I protein and CD59 were shown to co-internalize in vesicles that are arf6-positive but clathrin negative and were apparently distinct from the arf1-dependent CLIC/GEEC pathway. Endocytosis of the Herpes Simplex virus Vp22 protein enters cells in an arf6- and raft-dependent but dynamin-, caveolae- and clathrin-independent manner (Nishi and Saigo 2007). Also cargoes that have roles in cell-matrix interactions, nutrient and ion channels, and hormone receptors depend on arf6 (Eyster, Higginson et al. 2009). However, Arf6 functions in different endocytic pathways. It is important for macropinocytosis but also with clathrin-mediated endocytosis. For example, arf6 can recruit AP-2 to forming clathrin coated pits (Krauss, Kinuta et al. 2003; Paleotti, Macia et al. 2005; Poupard, Fessart et al. 2007). Also arf6 is implicated in a recycling pathway of endocytosed receptors back to the plasma membrane via arf6-positive endosomes indicating complex cellular functions of this small GTPase. This makes it difficult to interpret and assign arf6 phenotypes to the distinct cellular pathways. Therefore, it is questioned whether arf6 defines an independent

endocytic route or represent an arf-dependent variation of an existing clathrin-independent pathway such as the CLIC/GEEC pathway.

Only a few viruses could have been assigned to non-clathrin non-caveolae raft-associated entry pathways yet, primarily because they are poorly defined and lack clear marker proteins. So far, viruses that use these pathways comprise rotavirus and Influenza A Virus (FLU). FLU can use CME and a clathrin- and caveolin-independent pathway for productive infection with similar efficiency (Sieczkarski and Whittaker 2002; Rust, Lakadamyali et al. 2004). It has been shown that FLU infection is almost not affected when a dominant-negative mutant of Eps15 is expressed or cells were pre-treated with chlorpromazine (Sieczkarski and Whittaker 2002); both perturbants are known to strongly reduce CME (Wang, Rothberg et al. 1993; Benmerah, Bayrou et al. 1999; Schmid, Ford et al. 2006). Also treatment with drugs that diminish cellular cholesterol levels had no effect on infection, and co-tracking of labeled virus particles with caveolin-1 showed very little overlap (Rust, Lakadamyali et al. 2004). Besides these data not much is known about the nature of this pathway. A recent study, however, identifies macropinocytosis as the clathrin-independent entry route of FLU (de Vries, et al. 2011). Rotavirus is a non-enveloped virus that is human pathogenic and causes severe diarrhea. Its uptake seems to be dynamin-2- and raft-dependent and resembles the endocytic pathway of the interleukin 2 β receptor (Lamaze, Dujeancourt et al. 2001) (Lopez, et al. 2004).

To the other raft-dependent non-caveolae-mediated pathways discussed here, CLIC/GEEC, Arf6-, and flotillin-dependent routes, so far no virus could be assigned yet. Rather, there are viruses such as the lymphocytic choriomeningitis virus (LCMV), which do not fit into any of the presented schemes. LCMV, an arenavirus, binds to α -dystroglycan and is internalized via smooth non-coated vesicles (Cao, Henry et al. 1998). For successful infection low pH is necessary but not clathrin, caveolin, Arf6, dynamin-2, and actin. Whether endocytosis is cholesterol- and therefore raft-dependent is controversial (Quirin, Eschli et al. 2008; Rojek, Perez et al. 2008). Since dominant negative Rab7 but not Rab5 affects infection it is thought that LCMV takes an as yet uncharacterized “fast track” from the plasma membrane to late endosomes bypassing early endosomes (Quirin, Eschli et al. 2008).

1.1.4 Macropinocytosis

Compared to micropinocytic uptake pathways macropinocytosis internalizes much more fluid and membranes into huge vacuoles in the cell interior. This process is mostly extracellularly induced and bases upon actin-dependent membrane ruffling, which can be morphologically distinguished as lamellipodia, dorsal ruffles, and blebs (Fig. 1) (Mercer and Helenius 2009). Some of the ruffles fold back to the plasma membrane, engulf a varying volume of fluid, and undergo fission, finally leading to macropinosomes (Mercer and Helenius 2009). Although they vary in size macropinosomes are usually bigger than vesicles produced by other endocytic pathways (except phagocytosis, the induced uptake of particles; however, this process is limited to specialized cells such as macrophages).

Polymerization and remodeling of the actin cytoskeleton plays a central role in macropinocytosis. Ruffling depends on local actin polymerization at the membrane, which is initiated by activated Rho GTPases such as Rac, Rho, and cdc42 and synthesis of PI4,5P2 (Gauthier-Rouviere, Vignal et al. 1998; Garrett, Chen et al. 2000; West, Prescott et al. 2000; Brown, Rozelle et al. 2001; Lindmo and Stenmark 2006). Linker proteins bind to patches of these lipids in the membrane, actin, and the Arp2/3 complex that stimulates actin assembly in many motile processes (Innocenti, Gerboth et al. 2005). This leads to directed extensions of existing actin fibers and protrusions of the plasma membrane (Kerr and Teasdale 2009). More than 14 different actin-associated proteins have been identified so far (Mercer and Helenius 2009). Their requirement overlaps mostly for lamellipodia and dorsal ruffles but differs for retracting blebs especially regarding factors for actin nucleation. For example, blebs apparently do not contain the Arp2/3 complex (Mercer and Helenius 2009).

Besides dendritic cells, in which macropinocytosis occurs constitutively, this uptake process requires extracellular signals such as binding of growth hormones to receptor tyrosine kinases (RTK). It is thought that RTKs activate ras, which in turn transduces the signal through three different pathways. Downstream of ras the small GTPase Rac1 has been identified as a trigger for activation of all three types of membrane ruffling (Ridley, Paterson et al. 1992). Indeed, microinjection with anti-ras antibodies inhibits surface ruffling (Bar-Sagi, McCormick et al. 1987). Rac1 functions as the central node that activates factors for actin polymerization and stabilization as well as myosins. Apart from Ras, Rac1 can be activated by src and Arf6. Arf6 has many functions in membrane trafficking and endocytosis (see above). Indeed, Arf6 stimulation has been shown to lead to protrusions of the plasma membrane (Radhakrishna, Klausner et al. 1996) and activates uptake by macropinocytosis (Brown, Rozelle et al. 2001). It seems that Arf6 is able to activate rac without the need of ras indicating a redundant mechanism to initiate macropinocytosis (Santy and Casanova 2001). Also a role in recycling of rac1 back to the plasma membrane has been suggested. Another small GTPase, Rab5, is well-known for its role in early endosomal function (Zerial and McBride 2001) but can also be found at circular ruffles and on macropinosomes (Schnatwinkel, Christoforidis et al. 2004). It recruits a Rab5 effector, RN-tre, that cross-links actin fibers (Lanzetti, Palamidessi et al. 2004).

Kinases play also an important role in macropinocytosis. The p21-activated kinase 1 (PAK1) is an effector of Rac1 and cdc42 and implicated in many processes that require cytoskeleton dynamics and cell motility, cell cycle progression, and death and survival signaling (Puto, Pestonjamas et al. 2003). Activation of PAK1 induces circular dorsal membrane ruffles similar to those appearing in macropinocytosis while inhibition blocks growth factor-induced macropinocytosis (King, Gardiner et al. 2000). Also PAK1 is important for closing the macropinocytic cup. It recruits CtBP/BARS (Liberali, Kakkonen et al. 2008), which works as a fission protein analogue to dynamin-2 in dynamin-independent macropinocytic pathways (Bonazzi, Spano et al. 2005) such as lamellipodia-mediated uptake (Cao, Chen et al. 2007). Together with myosin light chain kinase (Araki, Hatae et al. 2003), PAK1 activates myosins that provide contractile forces at closing membrane ruffles

(Dharmawardhane, Schurmann et al. 2000). Other forms of macropinocytosis, such as PDGF-induced circular dorsal ruffling, seem to depend on dynamin-2 (Schlunck, Damke et al. 2004). Class I PI3-kinases are involved in subcortical actin reorganization, a central process in macropinocytosis (Stephens, Ellson et al. 2002). They are also implicated in completion of macropinosome formation (Araki, Johnson et al. 1996). Members of the protein kinase C family have long been implicated in macropinocytosis, however, their exact role is still unclear (Mercer and Helenius 2009). PKC are activated during RTK signal transduction but also independently via PI3 kinases. Direct activation of PKC by phorbol esters induces fluid phase uptake and macropinosome formation without growth hormone activation (Swanson 1989). C-src, a non-receptor tyrosin kinase, induces membrane ruffling and macropinocytosis (Kasahara, Nakayama et al. 2007) and promotes activation of Arp2/3, rac1, and PI3 kinase (Amyere, Payraastre et al. 2000; Bougneres, Girardin et al. 2004).

Many pathogens employ macropinocytosis to enter cells. Intracellular pathogenic bacteria such as *Yersinia enterocolitica* and *Shigella flexneri* trigger membrane blebbing and cause cytoskeletal rearrangements (Young, Falkow et al. 1992; Niebuhr, Giuriato et al. 2002) during uptake into their host cells. Vaccinia virus (VACV) was shown to require rac1, actin rearrangement, myosin, cholesterol, PAK1, PKC, and PI3-kinase but not dynamin. Moreover, virus particles cause blebbing and are internalized adjacent to the retracting blebs (see part 1.3.6). Adenovirus 3 is a human pathogen that infects epithelial cells of the eye, the respiratory and digestive tracts. Virus entry occurs by rac1-mediated macropinocytosis, is accompanied by fluid phase uptake, and depends on PI3-kinases, low pH, sodium-proton-exchangers, PAK1, and CtBP/BARS (Hayashi and Hogg 2007; Amstutz, Gastaldelli et al. 2008). Some viruses use macropinocytosis as alternative entry routes to their common pathways. HIV-1 is a retrovirus and enters cells by direct fusion with the plasma membrane without the need of endocytosis. However, apart from this canonical pathway, it has been reported that HIV enters some cell types such as macrophages by macropinocytosis (Marechal, Prevost et al. 2001). Ebola virus, an enveloped filamentous filovirus that causes severe hemorrhagic fever, has first been implicated with clathrin-mediated (Bhattacharyya, Warfield et al. 2010) or caveolae-mediated endocytosis (Empig and Goldsmith 2002). However, recent data show that the virus can also enter cells independent of clathrin or dynamin but dependent on rac1, PAK1, PI3-kinase and cdc42. Internalized particles enhanced fluid phase uptake and induced membrane ruffling, all criteria for macropinocytic uptake (Saeed, Kolokoltsov et al. 2008; Nanbo, Imai et al. 2010; Saeed, Kolokoltsov et al. 2010).

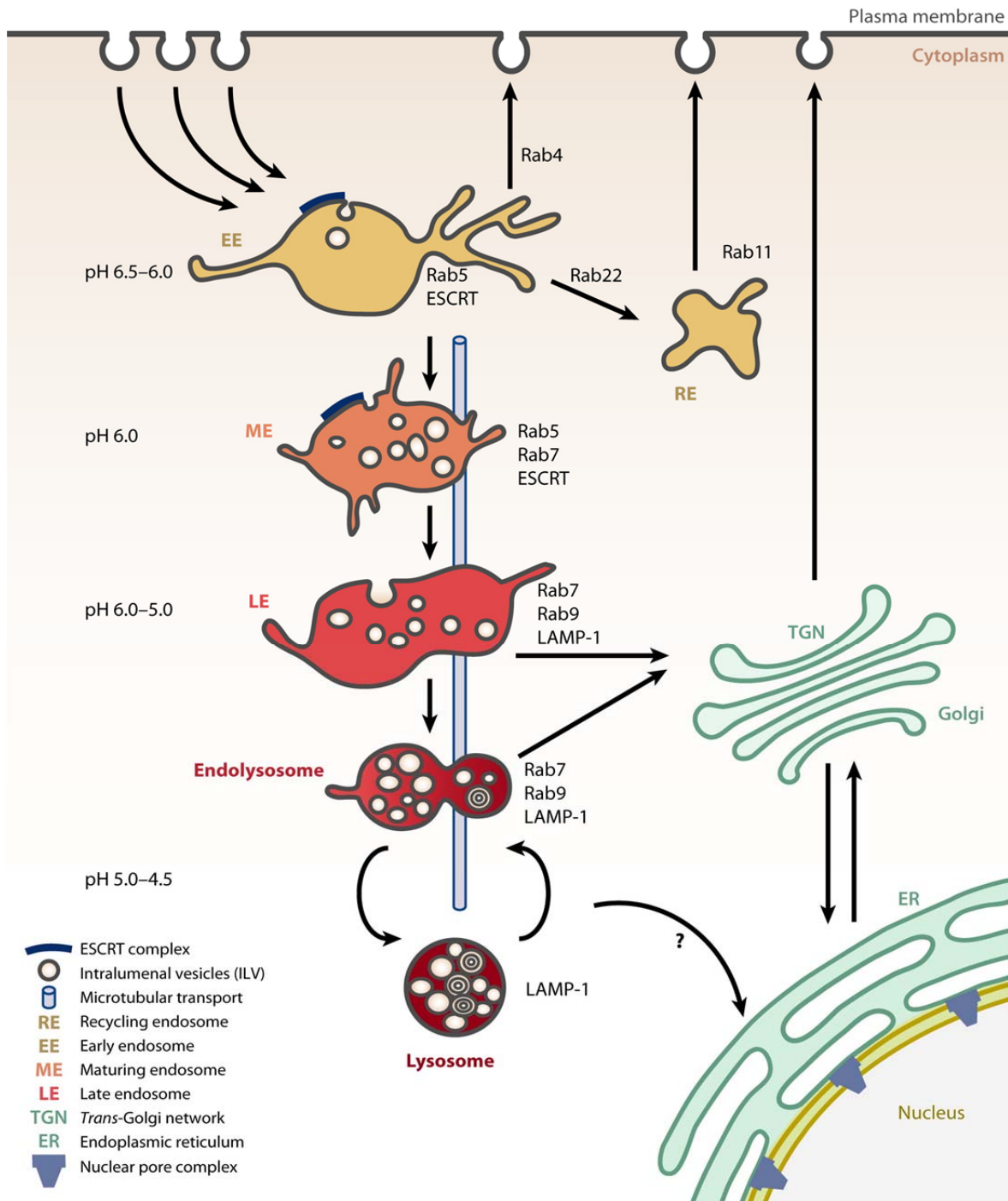
1.2 Endosomes

The endocytic vesicles that were formed by fission at the plasma membrane by one of the aforementioned pathways are finally trafficked to the endosomal compartment. This vesicular compartment can be further separated in early, maturing, late, and recycling endosomes as well as (endo)lysosomes. Early endosomes are the first compartment for incoming cargo. From there several routes go either back to the plasma membrane using recycling pathways, or into the degradative pathway leading from maturing endosomes (ME), multi vesicular bodies/late endosomes (MVB/LE), to endolysosomes. Also there is exchange with the trans Golgi network (TGN) (Bonifacino and Rojas 2006) (Fig. 2). Endocytosed membrane, fluid, and many surface receptors are mostly recycled back to the plasma membrane via early endosomes and recycling routes. 50-180% of the plasma membrane per hour is usually internalized into early endosomes and recycled back to the surface indicating that recycling is the primary pathway and entering the degradative pathway requires a sorting machinery (Steinman, Mellman et al. 1983). Early endosomes therefore are seen as the central sorting station of endocytic cargo (Huotari et al, 2011).

1.2.1 Early Endosomes

It is not completely clear how early endosomes (EE) are generated but incoming endocytic vesicles that undergo homotypic fusion are probably the main source of membrane and volume (Huotari Helenius). They are morphologically diverse with smaller, more mobile vesicles in the periphery and bigger vesicles towards the center of the cell. The individual vesicles have a vacuolar and a tubular portion (Mellman 1996). From tubular parts cargo is sorted into recycling routes to the cell surface or recycling endosomes. Also transport to the trans-Golgi network takes place from there. Cargo destined for degradation accumulates in the vacuolar part and is sorted into LE/MVB (Maxfield and McGraw 2004). This spatial differentiation within EEs is caused by the limiting membrane, which is a mosaic of functionally separated subdomains defined by cytosolic membrane-binding proteins (Geuze, Slot et al. 1987; Schmid, Fuchs et al. 1988; Mayor, Presley et al. 1993; Gruenberg 2001; Zerial and McBride 2001). They comprise Rab proteins such as Rab5, Rab4, Rab11, Rab7; Arf1 and COPI; retromer components such as sortin nexins 1 and 2; and caveolae (Vonderheit and Helenius 2005; Bonifacino and Rojas 2006; Hayer, Stoeber et al. 2010) (Fig.2).

Key proteins that define early endosomal identity and hence serve as canonical markers for this compartment are Rab5, EEA1 (early endosomal autoantigen 1), and class III PI3-kinase also known as hVps34. Rab5 is the key component that binds to phosphatidylinositol-3-phosphate (PI3P), a phospholipid which is primarily synthesized in early endosomes by hVps34 (Behnia and Munro 2005). Both factors, Rab5 and patches of PI3P, form a binding platform for many early endosomal factors such as the tethering factor EEA1 (Zerial and McBride 2001). Early after fission Rab5 binds to the incoming endocytic vesicle and follows early endosomes through their maturation process into LE/MVBs (Huotari 2011).




 Mercer J, et al. 2010.
Annu. Rev. Biochem. 79:803–33

Figure 2

Schematic overview of the endosomal compartments and its interactions with other organelles. Vesicles from different endocytic routes fuse with Rab5-positive early endosomes from which different sorting pathways start. Recycling occurs by a Rab4-dependent fast route, and a Rab22 and Rab11-dependent slow route via the recycling endosome. The degradative branch involves sorting of membranes and ubiquitinated receptors from vacuolar parts of early endosomes into intraluminal vesicles dependent on the ESCRT complex. In a maturation process in which Rab5 is replaced by Rab7 the vacuolar part dissociates and moves towards a perinuclear region mediated by microtubules. The ME continues to acidify by the activity of vesicular ATPases and ion pumps. Late endosomes possess a pH below 6.0 and are devoid of Rab5. They fuse with each other and with lysosomes to form endolysosomes. In (endo)lysosomes degradation by acidic hydrolases occurs. From (Mercer, Schelhaas et al. 2010).

Nutrients such as iron or low density lipoprotein (LDL) bind their receptors at the cell surface, are endocytosed, and reach early endosomes. Here, receptors are sorted into the tubular part for recycling to the plasma membrane while their ligands remain in the vesicular part of EEs and proceed to the degradative pathway. The trigger for ligand release is the weakly acidic pH of 6.8-5.9 in early endosomes (Yamashiro and Maxfield 1987). Acidification is enforced during maturation of EE to LE/MVB and finally lysosomes, and primarily performed by vacuolar ATPases (V-ATPase) that pump protons into the vesicular lumen. Diverse ion channels such as sodium-potassium channels or chloride channels, which neutralize the electric current (Jentsch 2007), act as regulators, as do several identified proton leakage pathways (Huynh and Grinstein 2007). Separating transmembrane receptors from soluble ligands is presumably performed by geometry-based sorting. Tubules have a much higher membrane-to-volume ratio so that membrane-associated proteins are enriched while the soluble fraction is partitioned in the vacuolar part of the EE (Roth 2006; Saraste and Goud 2007).

Cargo and membrane fractions destined for degradation are sorted into intraluminal vesicles (ILV), which are invaginated from the limiting membrane of EEs during maturation. A special posttranslational modification on cargo molecules, monoubiquitination, serves as a signal for the sorting machinery to route them into ILVs (Hurley and Emr 2006). Ubiquitination is done by E3 ubiquitin ligases such as CBL, which was first described as important for sorting of the EGF receptor (Dikic 2003). ILV formation takes place at special membrane domains of the vacuolar part containing a clathrin coat and components of the endosomal sorting complex required for transport (ESCRT) machinery. Clathrin serves as a scaffold and recruits HRS (ESCRT 0) to these subdomains (Raiborg, Wesche et al. 2006), which subsequently recruits the rest of the ESCRT complex (TSG101 alias ESCRT I; ESCRT II, and III). ESCRTs main function is to sort monoubiquitinated cargo, but depletion of ESCRT components also inhibited ILV formation (Razi and Futter 2006). Inward invagination occurs by the ATPase VPS4 by inducing negative membrane curvature after the ESCRT complex has dissociated. However, ESCRT III components have also been shown to support ILV formation (Hanson, Roth et al. 2008; Woodman and Futter 2008). Besides its role as an ESCRT component HRS is implicated in homotypic fusion of early endosomes (Sun, Yan et al. 2003).

1.2.2 Endosomal Recycling Pathways

While entering the degradative pathway is a positive sorting process that requires special signals such as ubiquitination (Woodman and Futter 2008) trafficking through recycling pathways does not require specific signals in non-polarized cells. Rab proteins are important for the different recycling routes: Rab4 is the marker for the “fast track” from EEs directly to the plasma membrane, while Rab11, 21, and 22 are implicated in the slow recycling pathway, which includes sorting into the endosomal recycling center (ERC), and trafficking to the plasma membrane (Maxfield and McGraw 2004)(Fig. 2).

The ERC is a mildly acidic collection of tubular organelles and localized in most cell types in a perinuclear region around the microtubule-organizing center (Hopkins 1983; Yamashiro, Tycko et al. 1984). Export of cargo from ERC to the plasma membrane has been shown to depend on microtubules (Lin, Gundersen et al. 2002). Transferrin receptors are the most studied cargo for endosomal recycling. Once endocytosed by CME they recycle from EEs via both recycling routes back to the surface. Those receptors that entered the ERC returned to the cell surface within about 10 minutes. Truncation of cytoplasmic domains led to reduced endocytosis but did not impair ERC exit kinetics indicating that export from ERC to the plasma membrane does not require special signals (Jing, Spencer et al. 1990).

Recycling endosomes /ERC have additional functions to shipping receptors back to the cell surface. They are crucial to maintain epithelial polarity (van and Hoekstra 1999; van Ijzendoorn 2006). Apical recycling is controlled by several Rabs such as Rab11a that interacts with Rip11/Rab11FIP5 and myosin Vb. Rab11b is implicated in basolateral recycling (Hales, Vaerman et al. 2002; Hoekstra, Tyteca et al. 2004). Also they play roles in cytokinesis and cell fate specification (van Ijzendoorn 2006).

1.2.3 Degradative Pathway

Sorting of proteins destined for degradation takes already place in EEs during formation of ILVs (Fig. 2). The tubular portion containing cargo to be recycled is gradually leaving the vacuolar part of the EE, which accumulates ILVs is accompanied by the generation of Rab7 domains. Accumulation of Rab7 is dependent on Rab5 and leads to a temporary Rab5/Rab7 compartment, called maturing endosome (ME) (Del Conte-Zerial, Bruschi et al. 2008; Huotari 2011). Rab5 is continuously removed and replaced by Rab7 domains while the numbers of ILVs increase. When no Rab5 domains are left the maturation process reaches multi vesicular bodies (MVB) or late endosomes (LE) (Rink, Ghigo et al. 2005). Another model of sorting to MVB/LE was proposed from Gruenberg et al (Gruenberg and Stenmark 2004). He suggested that EEs and LEs are two stable compartments with endosomal carrier vesicles (ECV) forming from Rab7 domains at EEs and transporting cargo and ILVs to LEs, where it fuses with the limiting membrane. Our lab found proofs for this model by following sorting of fluorescently labeled SFV particles: SFV leaves EEs with Rab7 domains while Rab5, Rab4, and Arf1 signals remain back (Vonderheit and Helenius 2005). Consistently, dynamin-2 was proposed to play a role in this fission event (Mesaki, Tanabe et al. 2011).

LEs are defined morphologically by their round or oval appearance harboring many ILVs (more than 30). The membrane contains typical protein markers such as LAMP1 (lysosome-associated membrane protein 1), Rab7, Rab9, and the cation-independent mannose-6-phosphate receptor. Acidification proceeds during maturation, and LEs typically have a pH in the range of 4.9-6.0 (Maxfield and Yamashiro 1987). LEs traffic microtubule-depend further to the perinuclear area (Luzio, Pryor et al. 2007). Acidic hydrolases are transported from TGN to the degradative pathway during maturation. These digestive enzymes reach full activity at pH of endolysosomes, pH 5.0-5.5. ILVs and other

luminal cargo are susceptible for hydrolysis while the limiting membrane of LEs and lysosomes are protected by a layer of glycoproteins such as the LAMP proteins (Barriocanal, Bonifacino et al. 1986; Fukuda 1991). ILVs also contain special phospholipids. Lyso-bisphosphatidic acid (LBPA) is present in late compartments and implicated in lipid hydrolysis and, by its negative charge, recruitment of positively charged acidic hydrolases (Kolter and Sandhoff 2010). LBPA also controls cholesterol levels in the cell. A LBPA-binding protein, Alix, plays a role in sorting to ILVs, their fission and fusion; the number of ILVs is reduced upon Alix depletion (Falguieres, Luyet et al. 2009).

LEs fuse with lysosomes to endolysosomes, which are considered the final compartment of the degradative pathway (Kornfeld and Mellman 1989). The pH in (endo)lysosomes is below 5.5. Already in LEs but mostly in the more acidic (endo)lysosomes digestion of macromolecules and export of the resulting catabolites into the cytosol takes place. Responsible for that are diverse transporters in the membrane of LEs and lysosomes specific for dipeptides, inositol, inorganic ions and many more and driven by the proton gradient (Kolter and Sandhoff 2010). Cholesterol accumulates at LE and lysosomes due to digestion of LDL and ILVs. It is thought to be trafficked to the ER, where main parts of the cholesterol biosynthesis occur (Sobo, Le Blanc et al. 2007; Hayer, Stoeber et al. 2010). Lysosomes appear electron dense in EM images and contain amorphous material in different stages of degradation, and multilamellar membranes. The limiting membrane resembles the membrane of LEs in the presence of Rab7 and LAMP1. Rab9 and CI-M6PR are absent from lysosomes (Lombardi, Soldati et al. 1993; Maxfield and McGraw 2004).

1.3 Viruses

1.3.1 Semliki Forest Virus

Semliki Forest Virus (SFV) is a linear (+)-single stranded RNA virus of the alphavirinae subfamily of the togaviridae family. It belongs to the group of arthropode-borne viruses (arboviruses), which use insects as vectors. SFV is not a human pathogen but causes encephalitis in mice. Avirulent variants are used in gene therapy to transduce neurons and other cells.

SFV is one of the best studied enveloped viruses, and consists of three envelope proteins E1, 2, and 3, one capsid (C) protein, and a 42S RNA genome, which comprises two open reading frames. The first encodes four non-structural proteins required for replication, while the second contains the code for the four structural proteins. The genome contains a 5' cap and a 3' poly(A) tail and the same coding polarity as mRNA, rendering it capable to be translated on ribosomes. The capsid protein encapsulates the genome by 240 copies in hexamers and pentamers in a spherical icosahedral symmetry. The triangulation number of the capsid is T=4 (Strauss and Strauss 1994).

Infection of the virus occurs after binding to an as yet unidentified receptor and internalization by clathrin-mediated endocytosis. Several classes of potential receptors have been proposed.

Proteoglycans such as heparin sulfate have been identified for other alphaviruses such as Sindbis virus as attachment receptors, and for tissue adapted SFV similar results were found. Also DC-SIGN was implicated in binding of arboviruses such as SFV (Strauss and Strauss 1994; Smit, Waarts et al. 2002; Klimstra, Nangle et al. 2003; Zhu, Wang et al. 2010). After internalization SFV is sorted to the endosomal compartment where the envelope proteins fuse with the limiting membrane of the vesicle and release the capsid to the cytosol (Helenius, Kartenbeck et al. 1980). The trigger for fusion is an acid-dependent dissociation of E1 from E2, E1 insertion into the endosomal membrane, and formation of a fusogenic E1 homotrimer (Kielian, Chanel-Vos et al. 2010).

Replication occurs after ribosome-mediated uncoating of the genome (Singh and Helenius 1992). Initially, a polyprotein of the first ORF encoding the four non-structural proteins (nsP's) is translated. From this precursor of a viral replicase an auto-catalytic protease located at the C-terminus of nsP2 cleaves subsequently all four nsP's from the precursor, which remain in an enzymatic protein complex but change their catalytic activity and specificity towards their substrates. The first cleavage releases nsP4, a RNA-dependent RNA polymerase that synthesizes a (-)-stranded template of the genome.

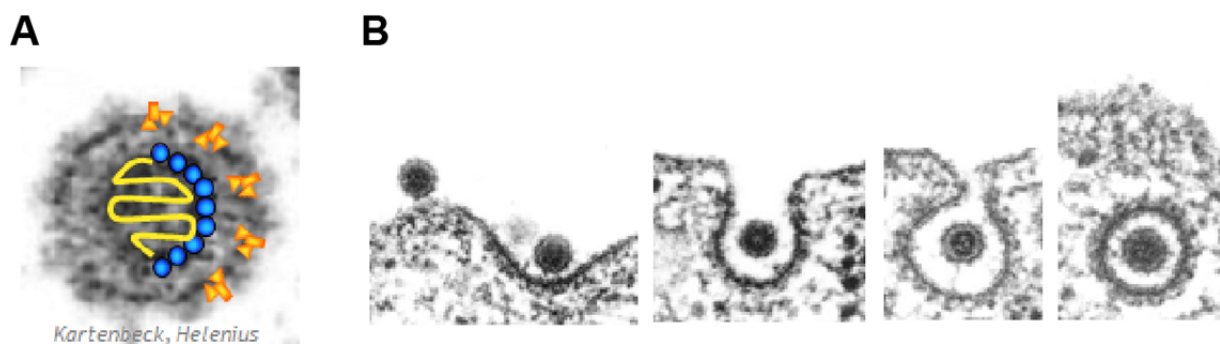


Figure 3

Electron microscopic images of SFV particles. (A) A single SFV virus particle is shown with schematic localizations of the envelope proteins (orange symbols), capsid protein (blue circles), and the RNA genome (yellow). (B) Different steps of SFV internalization are shown: binding to the cell surface, invagination of clathrin-coated pits filled with a virus particle, and a clathrin-coated vesicle. Note the electron-dense coat of the plasma membrane underneath the virus. From J. Kartenbeck and A. Helenius.

Secondly, nsP1 is released from the remaining polyprotein. This event shifts the polymerase activity towards the newly synthesized template to produce (+)-stranded genomes. Helicase, capping, and poly(A) polymerase activities in the nsP proteins support and finalize replication. The final cleavage splits nsP2 and 3 apart, and initiates the late phase of infection since this step shifts the activity of the polymerase complex towards a subgenomic promoter on the (-) strand template, which starts transcription of the structural polyprotein. Once translated the capsid protein cleaves itself from the nascent polyprotein. This autocleavage exposes a signal for ER entry of the precursor of the envelope proteins, p62. After transport of this transmembrane polyprotein and cleavage in part by the host cell protease furin in a post-Golgi compartment (Jain, DeCandido et al. 1991) the envelope proteins reach the plasma membrane, where they accumulate and recruit nucleocapsids that have been formed by self-assembly of cytosolic capsid proteins and genome RNA. The final step is budding of the new

virus generation from the host cell (Garoff, Sjoberg et al. 2004). In mature viruses E1 proteins form dimers with E2, and these are ordered to trimers (E1-E2)₃. The third envelope protein E3 is non-covalently associated with E1/E2.

1.3.2 Simian Virus 40

SV40 is a 50nm small member of the polyoma virus family. It is non-enveloped and consists of a virion with icosahedral symmetry ($T = 7$). The viral coat is made by 360 copies of the virus protein 1 (VP-1). The other structural proteins VP-2 and -3 are buried within the VP-1 proteins in the coat. VP-1 forms 72 pentamers of which 60 are coordinated in pentamers and 12 in hexamers. The pentamers are linked and stabilized by protein-protein interactions, calcium, and covalent disulfide bonds from cysteines (Liddington, Yan et al. 1991; Schelhaas, Malmstrom et al. 2007).

The 5kb circular DNA genome is double-stranded and associated with 21 nucleosomes (Varshavsky, Nedospasov et al. 1977). Besides the structural proteins regulatory proteins are expressed: the large and the small T-antigens, the agnoprotein, 17k T, and small leader protein (Fiers, Contreras et al. 1978; Ahuja, Saenz-Robles et al. 2005). Active T antigens are required for successful infection. They control transcription of late viral proteins such as the structural proteins, are important for viral DNA replication, and play roles in assembly. SV40 induces neoplastic transformations in cells, which are primarily caused by functional T antigens (Eddy, Borman et al. 1962). The transforming capacity of the T-antigens is associated with their binding to tumor-suppressor proteins. While the large T binds to p53, members of the retinoblastoma (Rb) family, and the heat shock cognate 70 (hsc70), the small T interacts with the PP2a protein phosphatase. All four interactions have been shown to contribute to transformation. Noteworthy, in permissive cells in which successful replication takes place the virus induces cell lysis to release the virions. Only a certain percentage of non-permissive cells are transformed. In these cells the viral genome has been inserted into the cellular genome most likely by a non-homologous recombination event (Ahuja, Saenz-Robles et al. 2005).

Virus entry begins with binding of VP-1 proteins to GM1 (Tsai, Gilbert et al. 2003). GM1 is a ganglioside that possesses a GPI-anchor that inserts in the outer leaflet of the plasma membrane. GPI-anchored proteins (GPI-APs) predominantly accumulate in cholesterol- and sphingolipid-enriched membrane domains such as caveolae. Cholesterol depletion from the membrane disrupts caveolae and has been found to reduce SV40 internalization. EM studies found SV40 in tight-fitting uncoated indentations of the plasma membrane. Immunogold staining revealed caveolin-1 associated to the virus. Over time of internalization an increasing number of viruses colocalized with cav-1 indicating an uptake mechanism based on caveolae (Anderson, Chen et al. 1996; Stang, Kartenbeck et al. 1997). This was supported by Chen et al, who found virus entrapped in caveolae after treatment of cells with Genistein, a tyrosin kinase inhibitor, which blocks SV40 infection (Chen and Norkin 1999). Time lapse imaging of labeled SV40 particles and Cav1-EGFP revealed 90% co-localization of virus and Cav1, and both virus and Cav-1 spots, indicating vesicles, moved together. siRNA against Cav-1

moderately reduced infection by 40% (Pelkmans, Burli et al. 2004). Recently, however, it was shown that SV40 VP-1 induces membrane indentations and tubules in the absence of Cav-1 but depending on sphingolipids and long acyl chains of the GPI anchor (Ewers, Romer et al. 2010). This suggests that SV40 uses two pathways for entering a host cell, a Caveolae-dependent and a clathrin- and caveolin-independent route that most likely does not require cellular scaffold proteins. Consistent with this, SV40 is able to internalize and infect Cav-1-knock out cells (Damm, Pelkmans et al. 2005).

SV40 infection was found to be dynamin-2 dependent. Dynamin-2-EGFP was recruited to bound SV40 on the cell surface, while dominant negative dynamin inhibited infection (Pelkmans, Puntener et al. 2002). Entry in Cav-1 knock out cells, in contrast, did not depend on dynamin (Damm, Pelkmans et al. 2005). Actin cytoskeleton was showed to be required for entry and infection. Actin together with Cav-1 was recruited to internalizing virus particles. Inhibitors of tyrosine and ser/thr kinases reduced SV40 entry and infection while drugs against tyrosin phosphatases inhibited infection but promoted entry (Pelkmans, Puntener et al. 2002).

Pelkmans et al found that internalized SV40 is trafficked to caveolin1-GFP-positive organelles, so-called “caveosomes”, close to the plasma membrane. By fluorescein quenching of FITC-labeled SV40 they determined the pH of the “caveosomes” as neutral. Time-lapse imaging showed viruses leaving these organelles, and trafficking along microtubules. SV40 did not colocalize with several markers of endosomes such as transferrin or SFV after 1hr post-warming indicating a non-endosomal post-internalization pathway. However, recent data from our lab show that “caveosomes” are not independent organelles but rather modified lysosomes that contain Cav-1-EGFP and are enlarged due to overexpression of this construct (Hayer, Stoeber et al. 2010). Therefore the pathway of SV40 from the plasma membrane to the ER is unclear.

1.3.3 Vesicular Stomatitis Virus

Vesicular stomatitis virus (VSV) is an enveloped, nonsegmented, (-)-strand RNA virus of the *Rhabdoviridae* family. The viral genome is encapsulated by the N protein and associates with a viral RNA-dependent RNA polymerase to a ribonucleoprotein (RNP) complex. The RNPs are associated with the matrix protein (M) and form condensed structures called skeletons (Newcomb, Tobin et al. 1982). These skeletons consist of a helix surrounded by a layer of M proteins that attach the RNPs to the membrane. The outermost layer of the virion is formed by trimers of the VSVG protein that is a transmembrane protein and mediates receptor binding of the virus to the host cell and acid-triggered fusion within endosomes. The RNP finally reaches the cytosol where replication occurs (Matlin, Reggio et al. 1982; Mire, White et al. 2010).

VSV uses CME and sorting to the endosomal compartment as the entry route. VSVG binds to cell surface receptors that possess negative charge. Virus is internalized in coated vesicles as shown in EM, and this process depends on Eps15 and functional clathrin and dynamin-2 but not AP-2

(Johannsdottir, Mancini et al. 2009). Recently, it was found that VSV enters cells in incompletely closed clathrin coats due to its bullet-shape. Actin seems to play a prominent role in propelling vesicle budding dependent on the particle size (Cureton, Massol et al. 2009; Cureton, Massol et al. 2010).

Delivery to endosomes was found to be Rab5 dependent but Rab7 independent (Sieczkarski and Whittaker 2003). VSVG changes its conformation at a pH of 6.2, which resembles the pH of Semliki E1/E2 envelope proteins (White, Matlin et al. 1981). Unlike SFV, recent data suggest that VSV fuses with internal luminal vesicles (ILVs) and is transported to LEs/MVBs. Exit of the capsid from this compartment is thought to be mediated by back-fusion of ILVs with the limiting membrane of the LE/MVB (Le Blanc, Luyet et al. 2005). However, this is in contradiction to the very rapid internalization and fusion process of VSV and its independence of Rab7, which was found by several studies (Sieczkarski and Whittaker 2003; Johannsdottir, Mancini et al. 2009).

1.3.4 Influenza A Virus

Influenza A virus (FLU) belongs to the class of Orthomyxoviridae. Virus particles are pleomorphic in shape, consisting of both spherical (100nm) and filamentous forms (over 300 nm). The genome of these viruses is composed of a segmented, negative sense single stranded RNA (Palese and Shaw 2006). The virus consists of 10 different genes encoded on 8 RNA segments. The lipid envelope harbors the two viral spike-like glycoproteins hemagglutinin (HA), and neuraminidase (NA) as well as the M2 ion channel. The matrix protein (M1) lies just beneath the lipid bilayer and is attached to the viral ribonucleoproteins (vRNPs). Each vRNP consists of an RNA segment enwrapped in viral nucleoprotein (NP) and one copy of each of the polymerase genes: PA, PB1, and PB2. Influenza A virus has also two additional non-structural proteins: NS1 and NS2. NS1 plays a role in inhibiting host innate immune responses. NEP/NS2 (nuclear export protein/nonstructural protein 2) is required for nuclear export of newly synthesized vRNPs (Palese and Shaw 2006).

The viral HA glycoprotein is responsible for cell surface binding and acid-triggered fusion. It was thought that sialic acid residues on plasma membrane glycoproteins and –lipids are the receptors of HA (Skehel and Wiley 2000). However, FLU can infect cells that are de-sialylated (de Lima, Ramalho-Santos et al. 1995; Stray, Cummings et al. 2000), although at a much lower efficiency. Hence, it was proposed that sialic acid residues serve as attachment factors, while the actual internalization-inducing receptor(s) are as yet unknown (Nunes-Correia, Ramalho-Santos et al. 1999; Ablan, Rawat et al. 2001; Chu and Whittaker 2004). HA fusion with endosomal membranes occurs at pH 5.5, a pH significantly lower than that required for SFV and VSV. The other envelope glycoprotein, neuraminidase (NA), facilitates release of progeny viruses from the host cell membrane, by hydrolyzing interactions between sialic acids and HA. Apart from this function, NA inhibitors reduce infection suggesting an additional role ahead of egress (Matrosovich, Matrosovich et al. 2004; Ohuchi, Asaoka et al. 2006).

FLU has been shown to enter via CME and an additional clathrin- and caveolin-independent pathway by EM data and the insusceptibility of virus infection to diverse inhibitors of CME and Caveolin-1 (Matlin, Reggio et al. 1981; Sieczkarski and Whittaker 2002). These pathways exist in parallel, leading to infection with similar efficiency (Rust, Lakadamyali et al. 2004). Upon internalization, the virus traffics to early endosomes and is further sorted into maturing endosomes and MVB/LEs (Matlin, Reggio et al. 1981; Sieczkarski and Whittaker 2003), consistent with the low pH 5.5 required for fusion. Moreover, VPS4, a component of the ESCRT complex required for sorting of ubiquitinated cargo into the degradative pathway, is necessary for entry and infection. Proteasomal inhibitors also block entry and accumulate virus particles in enlarged endosomes, consistent with previous findings that proteasome activity is required for proper trafficking of cargo to lysosomes (van Kerkhof, Alves dos Santos et al. 2001; Longva, Blystad et al. 2002; Khor, McElroy et al. 2003)

Additional molecular requirements for FLU infection have been revealed. Besides requirement for PI3-kinase, Protein kinase C β II (PRKCG) was shown to be important for infection at the level of endosomal sorting. FLU accumulated upon inhibition of PRKCG in LEs. Since acidification was unchanged another step during endosomal maturation might be affected (Sieczkarski, Brown et al. 2003; Ehrhardt, Marjuki et al. 2006).

1.3.5 Uukuniemi Virus

Uukuniemi virus (UUK) belongs to the family bunyaviridae, which contains several human pathogenic viruses such as Hantavirus and rift valley fever virus. Most bunyaviruses are arboviruses, i.e. transmitted by arthropods. They are enveloped, segmented, (-)-stranded RNA viruses that replicate in the cytosol of the host cell. In EM images viruses appear as roughly spherical and 80-140 nm small particles with spike-like extensions. The spikes consist of two glycoproteins that mediate host cell binding. At their C-termini they are connected with the ribonucleoproteins (RNPs) in the interior of the virus, which consist of viral RNAs and the N protein (Overby, Pettersson et al. 2008; Lozach, Mancini et al. 2010).

UUK entry was until recently poorly characterized. Lozach et al found that the virus internalizes cells with coated and uncoated vesicles indicating several entry routes. Infection depends on Rab5-mediated transit to early endosomes, and UUK is further sorted into the degradative pathway and colocalizes with Rab7- and LAMP1-positive late endosomes. Fusion of the envelope with membranes occurs at pH 5.4 indicating late endosomes/lysosomes. Recent data show that UUK and other bunyaviruses use DC-SIGN (dendritic cell-specific intercellular adhesion molecule 3-grabbing nonintegrin) a C-type lectin expressed primarily by dendritic cells as receptors for attachment and internalization (Lozach, Kuhbacher et al. 2011).

1.3.6 Vaccinia Virus

Vaccinia virus (VACV) is a poxvirus that has been used for vaccination against smallpox caused by the human pathogen variola virus. VACV is a large, enveloped virus that partly fuses directly at the host cell plasma membrane but mostly enters cells in culture by macropinocytosis (Huang, Lu et al. 2008; Mercer and Helenius 2008). Virus particles have been shown to induce transient blebbing once they attach at the plasma membrane, and it is thought that they internalize adjacent to retracting blebs (Mercer and Helenius 2008). Analysis by small compound inhibitors showed that internalization depends on *rac1* and actin rearrangement, PAK1, PKC, and PI3-kinase. Also sodium-proton exchangers, which have been long implicated in macropinocytosis, cholesterol, and myosin II are required for infection. Consistently with the view of macropinocytosis as a largely dynamin-independent process, this small GTPase indeed seems not to play a role in VACV infection. Interestingly, endocytosis strictly depends on the lipid phosphatidylserine that is enriched in membranes of the virus but also in so-called apoptotic bodies that are cleared by many cells using macropinocytosis. Hence, VACV seems to exploit this physiological process by mimicking apoptotic bodies (Mercer and Helenius 2008; Mercer and Helenius 2010)

1.4 RNA Interference

RNAi is based on small double-stranded RNAs to silence genes that possess a complementary sequence. Although endogenous gene silencing operates through multiple mechanisms, including mRNA cleavage, inhibition of translation, and epigenetic modifications of chromatin, mRNA cleavage is the most efficient mechanism (Tuschl 2001).

Small RNAs, either exogenous small interfering RNAs (siRNAs) or endogenous microRNAs, are taken up by a cytoplasmic RNA-induced silencing complex (RISC), which cleaves one strand, leaving the remaining unpaired guide strand to search for mRNAs showing complementary sequences. Once recognized, if the target site on the mRNA has nearly perfect complementarity to the guide siRNA, the mRNA is cut by an endonuclease called Argonaute in the RISC and then degraded. This silences the protein it encodes, i.e. typically, protein expression is reduced but not completely eliminated. RNAi seems to be a ubiquitous feature of all cells, where it is used to regulate the expression of key genes involved in cell development, differentiation, and survival. Small interfering RNAs can nowadays be readily designed to target any gene, being an endogenous host gene or foreign viral gene (Dykxhoorn and Lieberman 2006)

1.5 Image Analysis Software

Advanced imaging technologies such as automated microscopes have become important to virologists to study host-virus interactions at high-throughput scale using cell-biological screening techniques. Usually these techniques are based on viral infection assays with relatively simple read-outs such as expression of fluorescently tagged viral proteins or fluorescent antibody staining of expressed viral proteins. Automated microscopes allow up-scaling of the number of conditions per experiment, such as perturbing drugs or siRNA, by using multi-well plates, while down-scaling the amount of virus, cells, and chemicals per condition.

However, this trend led to a new problem, formerly only known to image analysts and computer scientists: how to automatically and reliably extract virological information from the pixels of images acquired from automated microscopes. Image analysis software automatically extracts objects i.e. groups of adjacent pixels from such a pixel matrix based on so-called homogeneity criteria. Based on these criteria, e.g. pixel intensity exceeding a certain threshold and neighboring (x,y) positions, pixels are identified and grouped into objects. These objects are then classified into biological entities such as nuclei, cell bodies, or areas of cells defined by expression of a protein by object classification criteria such as area/size, average intensity, shape etc. This process is called *image segmentation*. Automated image analysis software has implemented suitable image segmentation algorithms for the kind of images the user might be faced with. It has to deal with raw images that vary in quality within the image and from one to the other, i.e. homogeneity of illumination, background, sample contaminations etc, and has to either filter out these influences, or identify and classify them as “non-objects”. Finally, mathematical and/or statistical operations are applied to the classified objects and given out as results in a way that allows the user to easily access and further process the data with other software. An overview of the image segmentation process is shown in Fig. 4.



Figure 4

Overview of a segmentation process used for image analysis. After recording images can be pre-processed e.g. background-corrected before segmentation and object detection occurs. Objects are classified according special criteria such as “infection” versus “non-infection”.

There are several ways of segmentation dependent of the kind of signal, its strength, variation, and quality. They can be classified into edge-, pixel-, and region-oriented segmentation. In a pixel-oriented segmentation the software decides for each pixel based on criteria such as intensity or surrounded pixels if it is part of an object or not. Mostly, a threshold intensity-based method is used for pixel-oriented segmentation, i.e. each pixel is “positive” if it is above or below a certain global intensity threshold. In a second step, adjacent positive pixels are usually combined to an object when additional object criteria are fulfilled such as size, shape etc. This approach is very easy to realize since programming complexity is usually very low. However, microscopy images often possess uneven

illumination within the image, which alters overall background and object intensities and would lead to over- and/or undersegmentation in some regions of the image. To solve this problem, image corrections are applied before segmentation in a step called *preprocessing*. A very common method is background correction or removal using e.g. flat field correction algorithms.

Another segmentation approach, which is often more robust in images with uneven illumination, is *edge-oriented segmentation*. Several algorithms for edge detection have been published such as Prewitt, Sobel, Canny etc algorithms (Prewitt 1965; Pingle 1969; Canny 1986). In principle, all algorithms define edges as magnitudes of the intensity gradient of an image i.e. the local maximum values of the first derivative of the image intensity function. The Canny algorithm is in general more robust against noise especially in detecting weak edges than the other mentioned algorithms (Canny 1986; MathWorks 2010).

1.5.1 Canny Edge Detection

Edges are defined as discontinuities of the two-dimensional brightness within a gray-level image. Edge detection algorithms try to represent these discontinuity patterns in the two dimensional image by a set of one-dimensional curves. The earliest approaches such as the Sobel and Prewitt operators focused on detecting those points within an image that represent high gradient magnitudes i.e. the first derivative of the image intensity. Introduction of so-called multi-scale techniques improved the quality of edge detection also by special preprocessing filters. Canny et al described a smoothing filter, which minimizes as a preprocessing step noise and other interfering fine-scale structures before the actual differentiation occurs (Canny 1986; Lindeberg 1998). This avoids misdetection of background intensity steps as edges at the cost of possible poor localization and resolution of the “correct” edges. Canny et al showed that such a smoothing filter can be well approximated by the first order derivative of a Gaussian kernel. He also introduced the principles of non-maximum suppression and hysteresis thresholding (Lindeberg 1998).

Typical implementations of Canny edge detectors in image processing software to detect edges possess five subsequent steps: (1) Image smoothing by convolution of the original image with a Gaussian function of width specified by the user (“*sigma*”); (2) Differentiation of the smoothed image by convolution with the first derivative of a Gaussian function and detecting local maxima (or with the second Gaussian derivative and detecting zero-crossings); (3) Non-maxima suppression to get rid of those local maxima that are not in continuity of an extended contour; (4) Edge thresholding by hysteresis deletes edges weaker than a lower user-specified value („*sensitivity*“), and accepts those above a higher value. Edge values in-between are checked whether they are in continuity of already accepted edges (Doms, Lamb et al. 1993).

1.6 Objective of the PhD Thesis

In this PhD thesis we aim to

- Develop a siRNA screening strategy for six different viruses to identify new host cell proteins and pathways
- Compile a “cherry picked” siRNA library containing selected genes that play roles in diverse endocytic pathways, membrane trafficking, cargo sorting, signaling, and secretion
- Develop a image analysis software that extracts virological information (infection index, number of cells) from screening images and can be used by non-computer experts
- Analyze the primary siRNA data and extract hits for each virus
- Validate selected hits and viruses to verify screening outcome
- Unravel new proteins and pathways for selected viruses

2 RESULTS

2.1 Development of an Image Analysis Software

2.1.1 Rationale

Some tools for image analysis have been developed over the last years, e.g. CellProfiler based on MATLAB, or some plugins of the Java-based image analysis software ImageJ. However, their usage often requires advanced computer and/or image analysis knowledge. Therefore, they are not optimized for the day-by-day work of the “standard virologist”.

Based on previous work from Katharina Quirin and Stefan Moese a MATLAB code was developed to easily detect and count cells and classify them into non-infected and infected groups. For both features, cell detection and classification of infection, it requires two microscopy channels, one for fluorescently labeled nuclei, the other for a tagged or fluorescently labeled viral protein expressed in the cytosol and/or nucleus of cells. The software is able to process images acquired from practically any kind of automated and non-automated microscope, and from any kind of assay format. Either single sets of images can be loaded and analyzed or image montages of different wells in many multi-well plates – a setup that is usually used in siRNA- and drug experiments. For an easy usability a graphical user interface (GUI) was developed that should allow everyone to analyze even larger screens, not only computer scientists. Moreover, due to its simple concept, it is possible to run the program virtually on every PC or Mac, even in several instances, and thus use it for “day-by-day” experiments. This led us to develop a software, which we called *InfectionCounter*.

2.1.2 Working Principle of *InfectionCounter*

InfectionCounter is a graphical user interface (GUI)-based single window software written in the technical language MATLAB (The MathWorks). The GUI was developed in the GUI development environment (GUIDE) that is provided by MATLAB. *InfectionCounter* is adapted to Windows operating system but was also tested in a Mac OS X environment. It is in the meantime widely used in the lab for counting virus infection in several cell lines and with different viruses.

The software analyses infection of cells based on microscopy images from two channels: the first, also referred to as the nucleus channel, represents cells by nucleus staining and is utilized to determine the position and number of nuclei in the images. The second channel, referred to as “infection channel”, depicts the intensity of a virus-specific expressed protein. Its intensity at those areas that have been defined as nuclei based on the first channel classifies the fate of a cell as being “infected” or “non-infected”.

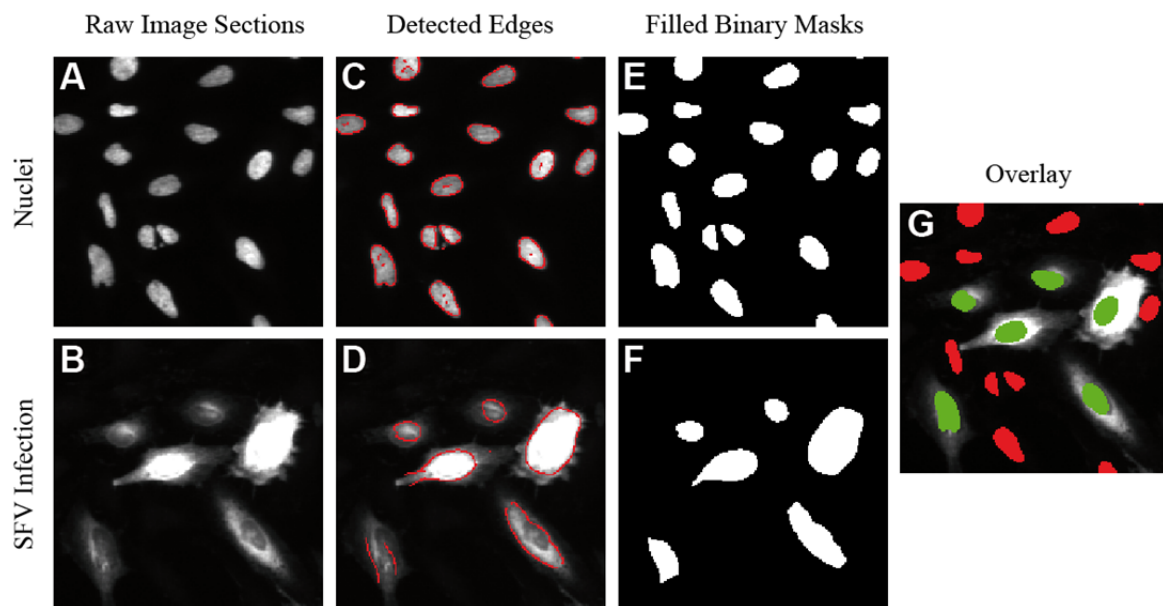


Figure 5

Illustration of the working principle of InfectionCounter using SFV-infected HeLa cells. The upper images (A, C, E) refer to a nucleus image, while the lower images (B, D, F) refer to images showing the corresponding infection. (A, B) Example raw image sections recorded from an automatic widefield microscope (BD Pathway 855) with 10x objective. Cells were stained with Hoechst 33258 for nuclei (A), and with primary antiserum “Lady Di” against SFV E1/2 proteins and secondary antibody goat-anti-rabbit-AF488 (B). (C,D) Image segmentation with identified edges as red lines overlaid to the raw images for nuclei (C) and infection areas (D). Note that the edges in D do not necessarily follow visible edges in the raw image since they are calculated from a strongly smoothed intermediate image (not shown). (E, F) Binary masks showing nuclei (E) or infection zones (F) after edge closure, in (F) after Edge End Analysis, and binary filling of the closed edge objects. (G) Overlay of binary nucleus mask and raw infection image after classification of nuclei as non-infected (red) and infected (green) cells. A threshold of at least 5% of nuclei pixels from (E) that overlap with white areas in (F) was applied for classifying a nucleus as infected. All infected cells represented by green nuclei were classified correctly by visual inspection.

Figure 5 illustrates the working principle of *InfectionCounter*. Objects, i.e. nuclei and infected zones, are detected from the corresponding raw images (Fig. 5A ,B) by the limiting edges of their intensity areas(Fig. 5C and D) using a modified and extended Canny edge detection function (Canny 1986) that is implemented in the MATLAB command `edge()` (MathWorks 2010). The user has influence on the edge detection process by two parameters, *sigma* and *sensitivity*, representing the smooth width of the Gaussian kernel and the lower hysteresis thresholding limit (see 1.5.1). The upper limit is fixed since tests with microscopy images that possessed a large range of signal-to-noise did not show significant differences in edge detection and analysis speed when changing the upper limit parameter (not shown).

Once edges have been detected they are either filled in case of closed edges, or their both ends are first closed by a line, and then filled (Fig. 5E and F). These filled binary masks, independently calculated for nuclei and infection images of the same cell population, are then overlaid and the percentage pixel overlay of each nucleus is determined. If this parameter is above a user-specified threshold (*Overlap Nucleus/Infection*) the cell - represented by its nucleus - is classified as “infected” (green in Fig. 5G); if it is below this threshold the cell is classified as “non-infected” (red in Fig. 5G). The results of the analysis, the number of nuclei per image, the number of classified infected cells per image, the percentage of infected cells per image, and the time of analysis are written to user-specified results files, and given out during run time in the *Run Window* of the GUI. Based on the user settings on the

montage type used for microscopy imaging the results per well are calculated from those of each image file and saved in a separate results file. Details are in the instruction manual.

The instruction manual of *InfectionCounter* is located in the chapter Supplemental Information as well as on the accompanying CD to the thesis. It describes the start of the software, the description of the input and output regions of the GUI, their functions, the analysis parameters, the output files and their interpretation as well as a step-by-step protocol to use the GUI for an analysis.

2.1.3 Special Features of the Program

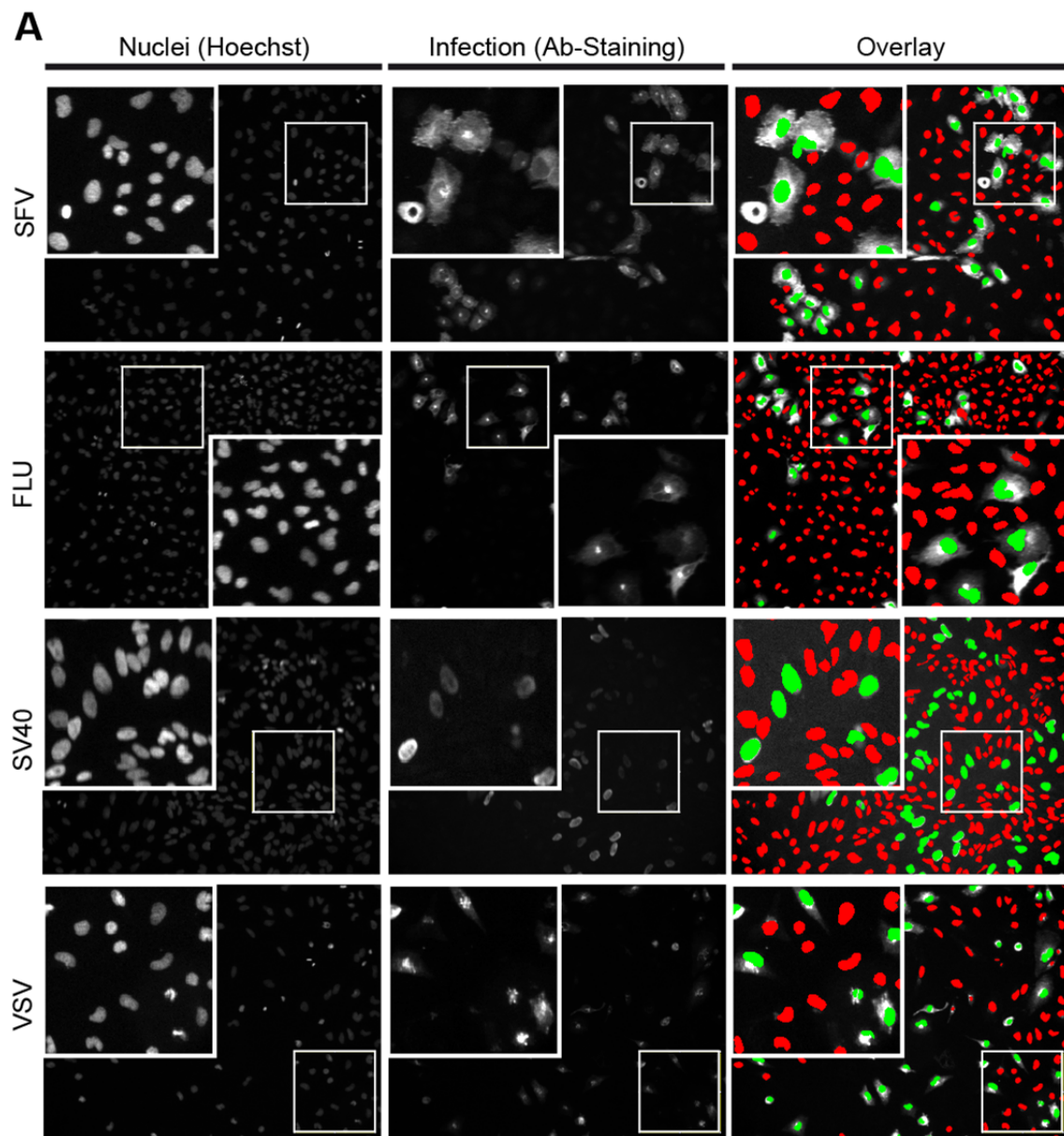
Besides its core feature to detect cells and virus infection, *InfectionCounter* was developed with high priority on user friendliness. Therefore the following features allow non-professional users a simple handling:

- All necessary settings are present on a graphical user interface
- Different colors indicate groups of parameters that have to be set by the user
- A GUI evaluation ahead of analysis prevents wrong parameter inputs and allows changing of settings
- Error message are easily to understand and mostly accompanied by red blinking of the GUI field that corresponds to the wrong parameter.
- A file name parser (i.e. syntax analyzer) allows building hierarchical file name lists based on counter definitions. Automated imaging often creates a lot of image files whose names encode information about the experiment, plate, well, and site, to which the image belongs. Usually this is realized by character- or number-based identifiers that continuously change, e.g. “...Well A01..., ...Well A02..., ...Well A03...” etc. The parser interprets curly brackets such as “Well A0(1-3)” within a file name as counter definitions and creates as many file names as these definitions imply. See Supplementary Information for details.
- File lists can be sorted according to the counter definitions.
- Single files can be added or deleted from file lists.
- Results files are text files that can be read by any text editors.
- Ongoing analysis can be supervised by graphical output of the current images, edge detection, and final cell classification using overlays with special color codes.
- Cell classification overlays (red “nuclei” = non-infected cells; green “nuclei” = infected cells; both overlaid over the corresponding raw infection images) are routinely saved and can be opened by any graphics software to control and evaluate the counting process.

2.1.4 Test of the Program

Analysis of different viruses and cell lines

The software should be able to detect different cell lines and expression of different virus proteins. To assess this capability we used two HeLa cell lines (ATCC and CNX) as well as the lung epithelial cell line A549 and Semliki Forest virus (SFV), Influenza A virus (FLU), Vesicular Stomatitis virus (VSV), Vaccinia virus (VacV), Simian virus 40 (SV40), Human Papilloma virus 16 (HPV16). SFV, VSV, FLU, and SV40 infection was visualized by immunofluorescence using antibodies or antisera against viral protein. HPV is a recombinant pseudovirus that expresses mRFP upon uncoating while VacV is engineered to express a GFP-tagged viral protein.



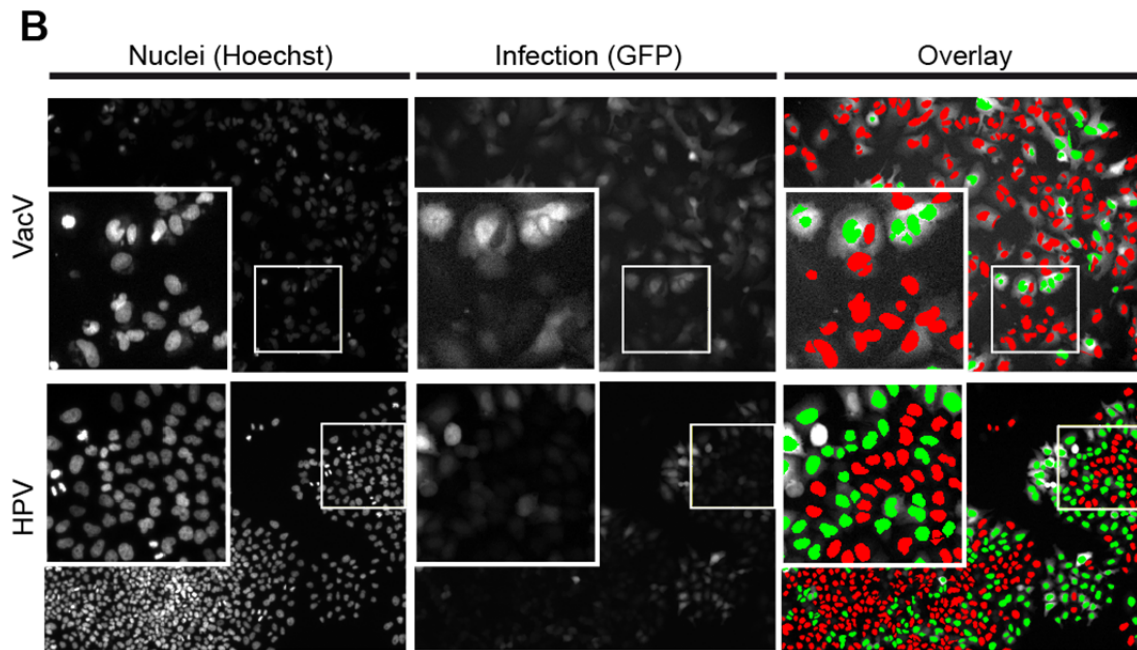


Figure 6

InfectionCounter recognizes infection of several different viruses. Cells from different cell lines are correctly detected over a broad range of cell densities. The software can handle different infection read-outs such as antibody staining of viral proteins as well as GFP or mRFP expression. (A) Example images for Hoechst 33258-stained nuclei and their corresponding infection images for Semliki Forest virus (SFV, HeLa ATCC cells), Influenza A virus (FLU, A549 lung epithelial cells), Simian virus 40 (SV40, HeLa CNX), and Vesicular Stomatitis virus (VSV, HeLa ATCC). Infection was visualized by antibody staining against the envelope proteins E1 and E2 (SFV; “Lady Di” antiserum), against the HA antigen (FLU), against the T-antigen (SV40; 1605 antibody), and against VSVG (VSV; F-14 antiserum). See M&Ms for cultivation details. (B) Example images for recombinant viruses expressing GFP -tagged viral proteins or mRFP. Upon infection with Vaccinia virus (VACV) HeLa ATCC cells express GFP. Human Papilloma virus 16 pseudovirion (HPV) infected HeLa CNX cells express mRFP.

For infection with SFV, VSV, and VacV HeLa cells from ATCC were used, while another HeLa cell line, called CNX (Cenix AG, Dresden), was used for SV40 and HPV infection. FLU efficiently infects lung epithelial cells therefore we chose the A549 cell line. To perform infection we grew 2’200 cells per well of 96 well plates for all viruses except SV40. SV40 only infects HeLa CNX cells at low density. Therefore, 1’200 cells were seeded per well. For the detailed protocols for infection of each virus see M&Ms. For staining of nuclei Hoechst 33258 was used in presence of detergent either as part of the secondary antibody buffers (SFV, VSV, SV40, FLU), or as an additional step (HPV, VacV).

Figure 6A shows one example for each virus with antibody-staining while Figure 6B shows examples for the fluorescent protein-expressing HPV and VacV. All grey scale images are raw i.e. not brightness-corrected. The images on the left represent nucleus stainings and show relatively homogeneous signal intensities. In the middle of Figure 6A antibody-stainings of example cells are shown, while Figure 6B depicts raw images of cells infected with viruses that express GFP. On the right of Figure 6A and B overlays of the classification process described above on the corresponding infection images indicate a precise and robust detection of nuclei and classification of non-infected versus infected cells when compared with the raw images in the middle section.

Nuclei as well as infection images in Figure 6 are in raw status, and have not been preprocessed before Canny edge detection. While all nuclei images show relatively homogeneous intensity the infection signals relative to the background differ significantly between the viruses. Among those examples tested GFP-expressing virus images possess relatively high background intensities while signal-to-noise ratios seems higher in case of antibody-stained examples (compare middle images in Figure 6B with those in Figure 6A). Nonetheless, the software handled all examples with less than 10% error (qualitative inspection) as the overlays (Fig. 6 right) show.

Simulation of low signal-to-noise ratio images

We next simulated too little exposure or poor signal-to-noise ratio due to improper microscopy settings or poor object fluorescence. We artificially introduced random pixel noise in an example image of nuclei and used *InfectionCounter* to detect and measure the number of nuclei. HeLa ATCC cells were stained for Hoechst 33258 and processed as for Figure 6 for analysis with *InfectionCounter*. Figure 7 shows that the error of detection is acceptably low even at a quite poor image quality.

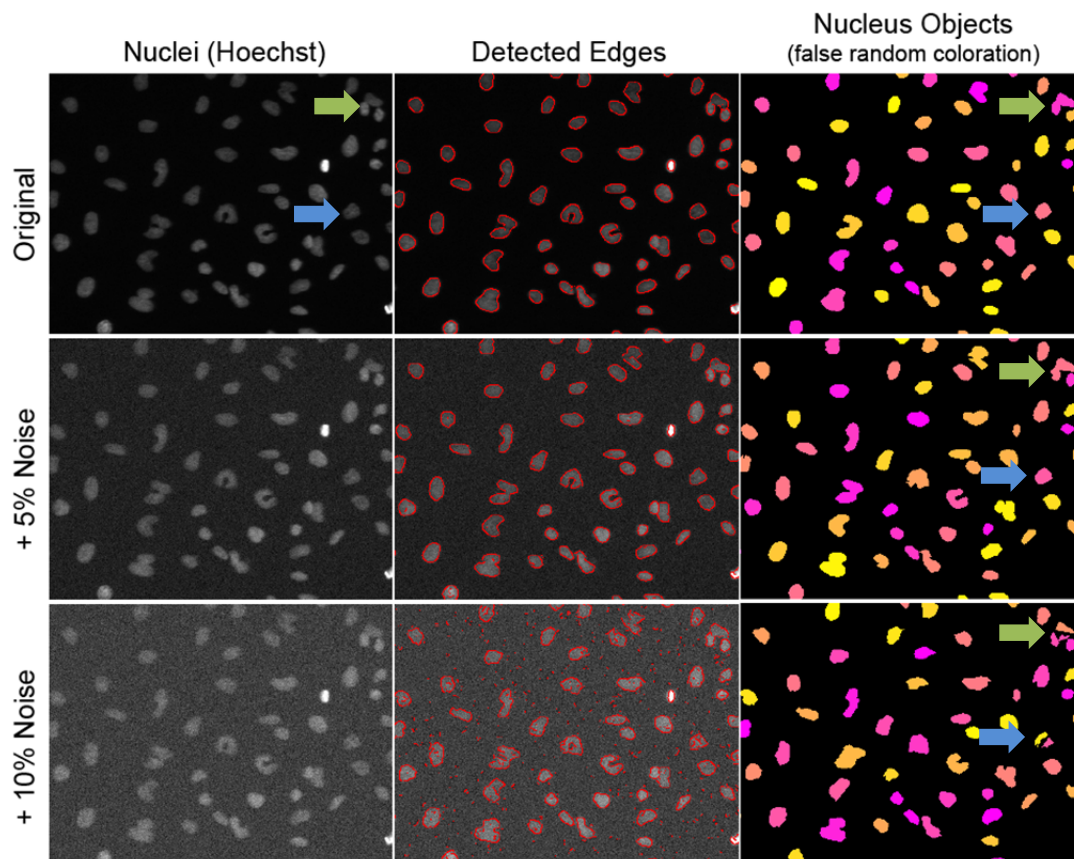


Figure 7

Artificially added random pixel noise did not have a strong influence on object detection capabilities up to a standard deviation of 10% of the averaged object pixel intensity. Example raw image “Original” shows Hoechst 33258-stained HeLa ATCC cells imaged by a Pathway 855 automated microscope (Beckton Dickinson) using a 10x objective. For the “+ 5% Noise” and “+ 10% Noise” images “Original” images were processed by the “Add Specified Noise...” function of ImageJ. Pixelated random noise of a standard deviation of 5% (10%) of the average signal intensity (375 intensity units; 12 bit image) of non-saturated nuclei pixels were added to the corresponding images and analyzed with *InfectionCounter* using the same settings of *Sigma* (1.2) and *Sensitivity* (3.2). Counted nuclei: 55 (Original), 55 (+ 5% Noise), and 56 (+ 10% Noise). Note that some very adjacent nuclei (green arrow) cannot be resolved reliably while dimmer nuclei containing inner edges become

oversegmented and are split into two objects (blue arrow). Nuclei objects in the right column have false random coloration to separate adjacent nuclei from each other. Brightness of the figure was enhanced for presentation.

Simulation of out-of-focus images

Out-of-focus errors happen frequently during an automated imaging run e.g. due to mechanical errors on the bottom of the microplate (scratches, drops, crystals etc.) or due to varying microplate thickness and, hence, varying focusing distances. We simulated such out-of-focus errors by adding Gaussian blurring with increasing filter kernel size to a maximum radius of 4 pixels (average object size: 158.5 square pixels). Figure 8 shows that the software is able to correctly detect objects from even strong out-of-focus images or image areas with the same *Sigma* and *Sensitivity* settings than used for the original image. The number of open edges increases indicating undersegmentation but the embedded correction functions close open edge ends. However, extreme out-of-focus causes object splitting and, if the sizes of the object parts are below the *Min Size* criterion set by the user, also removal from the finally detected objects.

Test by different users

To test how different users and their settings would influence a screening outcome we used a data set of an siRNA-mediated silencing experiment. One plate with sample siRNA in the inner 60 wells (27 different siRNA in duplicates, 4 negative controls (AllStarNegative) and two transfection controls (positive control for cell number, Hs_KIF11_6)) and medium without cells in the outermost wells to avoid edge effects was prepared and imaged on a BD Pathway 855 automated microscope. Three different users determined the best settings for analysis by *InfectionCounter*, and analyzed the plate.

Although one user chose settings that under-segment the nucleus channel, the differences of infection indices between the three users were very low (supplementary information).

Based on the successful tests we conclude that *InfectionCounter* has proven the capability to analyze automated images in lab-scale RNAi screens.

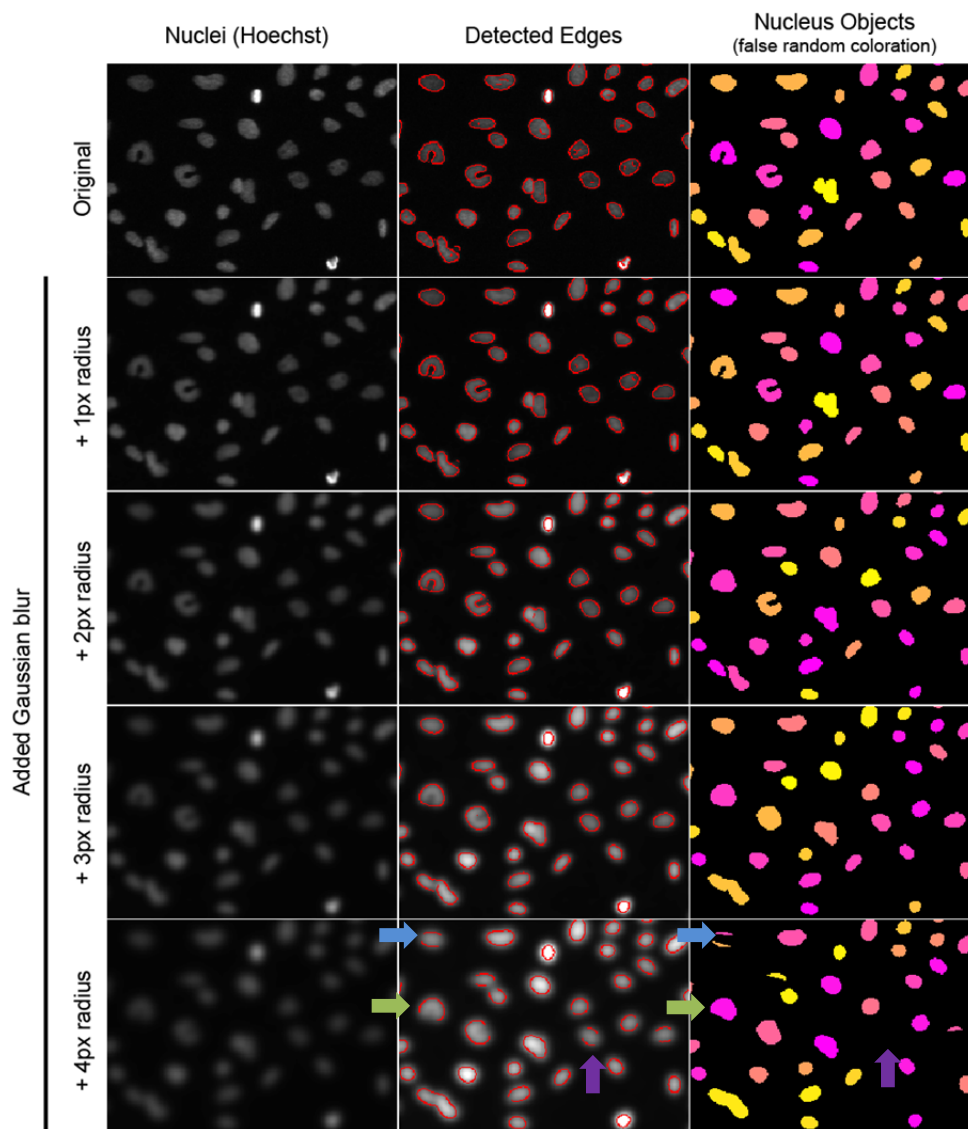


Figure 8

Simulation of out-of-focus imaging by increased Gaussian blurring before object detection by *InfectionCounter*. ImageJ was used to apply a Gaussian blurring filter to the “Original” image. The filter width radius is 1 pixel up to 4 pixels. Most of the nuclei objects are correctly detected even after a 4-pixel-Gaussian blurring. Analysis by *InfectionCounter* was performed using the same settings throughout each blurring condition. Increasing blurring radius causes object edges to be less steep compared with those in the “Original” image. Using the same *Sigma* and *Sensitivity* settings in *InfectionCounter* results in increasing undersegmentation (arrows) and non-closed edges, which are correctly (green arrow) or incorrectly (blue arrow) closed during the object detection process leading to splitted nuclei. Some of these splitted objects are below the *Min Size* criterion and are excluded (lilac arrow). Counted objects: 36 (Original), 35 (+ 1px, +2px), 34 (+3px, +4px). Figure was brightness-enhanced for presentation.

2.2 RNAi Screening for Host Cell Factors Important for Virus Infection

2.2.1 Introduction

RNA interference (RNAi) is a relatively new technology that allows silencing of specific proteins on the mRNA level in a sequence-specific manner by transfecting cells with a short double stranded RNA probe (siRNA) that has the same sequence than the mRNA of interest. SiRNAs are about 21-25 nucleotides in length and are substrates for the RISC (RNA-induced silencing complex) possessing a ribonuclease activity. SiRNAs bound to RISC guide this protein complex to sequence-homolog mRNAs and cleave these in the region of homology (Hannon 2002; Meister and Tuschl 2004).

We took advantage of RNAi technology to knock-down single proteins within cell arrays and measured the influence of this perturbation on virus infection. Infection was monitored either by staining against viral proteins or GFP expression.

We performed siRNA-mediated gene silencing screens of virus infection targeting a small set of characterized cellular proteins (108 genes, so-called “Usual Suspects”) to test the developed cell and infection detector software, *InfectionCounter*, and to find new cellular proteins involved in the viruses’ life cycle. Besides SFV five other viruses infecting different cell lines were involved in the screens to be able to classify genes as virus-specific or general hits.

2.2.2 General Screening Procedure

For all screens a common general protocol for siRNA transfection of cells in 96 well micro titer plates, imaging of the virus-infected, fixed, and stained plates, image recording and analysis, and hit determination was developed, which is schematically depicted in Fig. 9 and described in detail in Materials and Methods. Virus-specific protocols for preparation of virus stocks, screening-adapted virus infection assays, and infection staining if applicable were developed and applied by each user (see M&Ms for SFV in detail, for other viruses in brief). siRNA were represented in duplicates per plate, and in three siRNA sets targeting all 108 genes of the screen. In general, every screen was repeated three times (UUKV four times) but not all replicates passed the quality control during analysis (Fig. 10C). A negative control siRNA was used in 4 wells per plate (AllStars Negative siRNA, Qiagen; “ASN”), and Hs_KIF11_6 siRNA was used as transfection control (positive control for cell number)

siRNA Transfection

Transfection of siRNA was performed by a screening-adapted lipid complex-based reverse transfection strategy, which has been tested for each virus and cell line ahead of screening. Shortly, siRNA diluted in DMEM (buffered with 20 mM HEPES pH 7.2; DMEM/H) was mixed with the pre-

diluted transfection reagent, Lipofectamine RNAiMAX (LIPO), in DMEM/H for 30 min to allow lipid complex formation. A virus- and cell line-dependent number of cells suspended in full medium was mixed with the lipid-siRNA complexes and incubated for 72 hrs. The final concentration of siRNA was 20 nM per 96 well plate and the dilution of LIPO was 1:1000.

Analysis with InfectionCounter

After transfection virus-specific infection assays were performed, and all plates were fixed, stained for nuclei by 1:10'000 Hoechst 33258 and (except VACV) immunostained for virus-specific proteins (details described in M&Ms). Imaging occurred on an automated widefield microscope station. Images were analyzed by *InfectionCounter*, which resulted in two parameters, Infection Index (II) and Cell Number (CN) per well. Due to oversampling (one to three replicates, three siRNA per gene, and each siRNA in duplicates per plate) a single gene was represented by 6 to 18 wells. Those wells that contained less than 400 cells in all images were not considered for the analysis. All plates that were contaminated or showed no appropriate cell death in the positive control wells (ratio “averaged cell number in ASN wells” : “averaged cell number in positive control wells” ≥ 7) were discarded, contaminated wells were flagged and removed from analysis.

Cell-Density Correction

The efficiency, with which a cell is infected, is often susceptible to the local cell density (Snijder, Sacher et al. 2009). Since siRNA on-target and off-target effects can influence cell growth and cell death and, hence, cell density, we applied a cell density correction procedure to the infection index of each well for those viruses that were susceptible to cell density changes over the range of screening. Except for VACV, which is relatively independent of cell density ((Snijder, Sacher et al. 2009) and data not shown), we determined a correction function with checker boards that allowed us to correct the raw II of each sample well for siRNA-mediated changes of cell density in that particular well. The general procedure and cell-/virus-dependent correction functions can be found in Materials and Methods.

Normalization and Significance Scoring

Density-corrected II were normalized against the negative controls on each plate and subjected to two different analysis methods using z-score calculation and a ranking algorithm to be able to apply a significance criterion, which filtered out those siRNA that did not reduce or increase infection significantly better than the population of negative controls.

An effect of a sample siRNA is designated here as “significant” when the likelihood is very low that its reducing or increasing effect on virus infection is only random. We defined for the sample siRNA to be significant a bandwidth of 5x the standard deviation of the negative control wells of the whole screen (z-scoring method) or of 2.5x the standard deviation of each individual replicate (ranking

method). Although both methods base on the distribution of the negative control infection indices they treat sample outliers differently and are differently susceptible to larger changes of the screening parameters between replicates such as different absolute percentages of infection or different dynamic ranges of the knock-down effects. Individual siRNA scores were calculated to quantify the effect of a significant siRNA on infection using the z-score of infection in the z-scoring method and the rank distance to the negative control population in the ranking method.

Hit definition

A gene became a primary hit for each virus, cell line, and significance scoring method when at least two out of three siRNAs targeting the same gene were significant (“2/3 criterion”). In some screens a few siRNA weakly but significantly increased virus infection. However, these effects were exclusively limited to one siRNA per gene, and filtered out by the 2/3 criterion. Hence, genes in the primary and final hit lists all reduced infection.

For each virus a final hit list was determined by applying overlap criterions to the primary hit lists. Genes were considered “final hits” when they were primary hits with at least one significance scoring method in both cell lines (for screens with one cell line: primary hits with both methods). To be able to compare and summarize primary hit lists created by different scoring methods we normalized them by ranking the primary hit scores from 1 (weakest) to 10 (strongest) and summarize them to achieve final hit scores. The final hit score is the higher 1) the more frequently a gene appeared in any of the primary hit lists; 2) the more siRNAs were considered as significant; 3) and the stronger a siRNA impaired virus infection compared to the negative controls.

2.3 Usual Suspects Miniscreens of Six Different Viruses

We selected 108 genes that have been characterized to play a role in endocytosis, receptor signaling, vesicle trafficking and fusion, cytoskeleton re-arrangement, ER-/Golgi- mediated secretion, and selected phosphoinositide-modifying enzymes (Fig. 10A and B; gene information and siRNA sequences see supplementary information on CD) based on two similar approaches ((Kolokoltsov, Deniger et al. 2007); Greber U unpublished) as well as on published literature to cover as many potential virus entry and sorting pathways as possible. Due to this biased approach and since several pathways are much better studied than others there is an overrepresentation of genes involved in clathrin-mediated endocytosis, endosomal sorting, Rac/Rho/cdc42-related pathways, and ER/Golgi-mediated secretion (Fig. 10A, B). Six different viruses infecting one or two out of three different cell lines, chosen based on the susceptibility to the corresponding virus, were used in the Usual Suspects project (Fig. 10C).

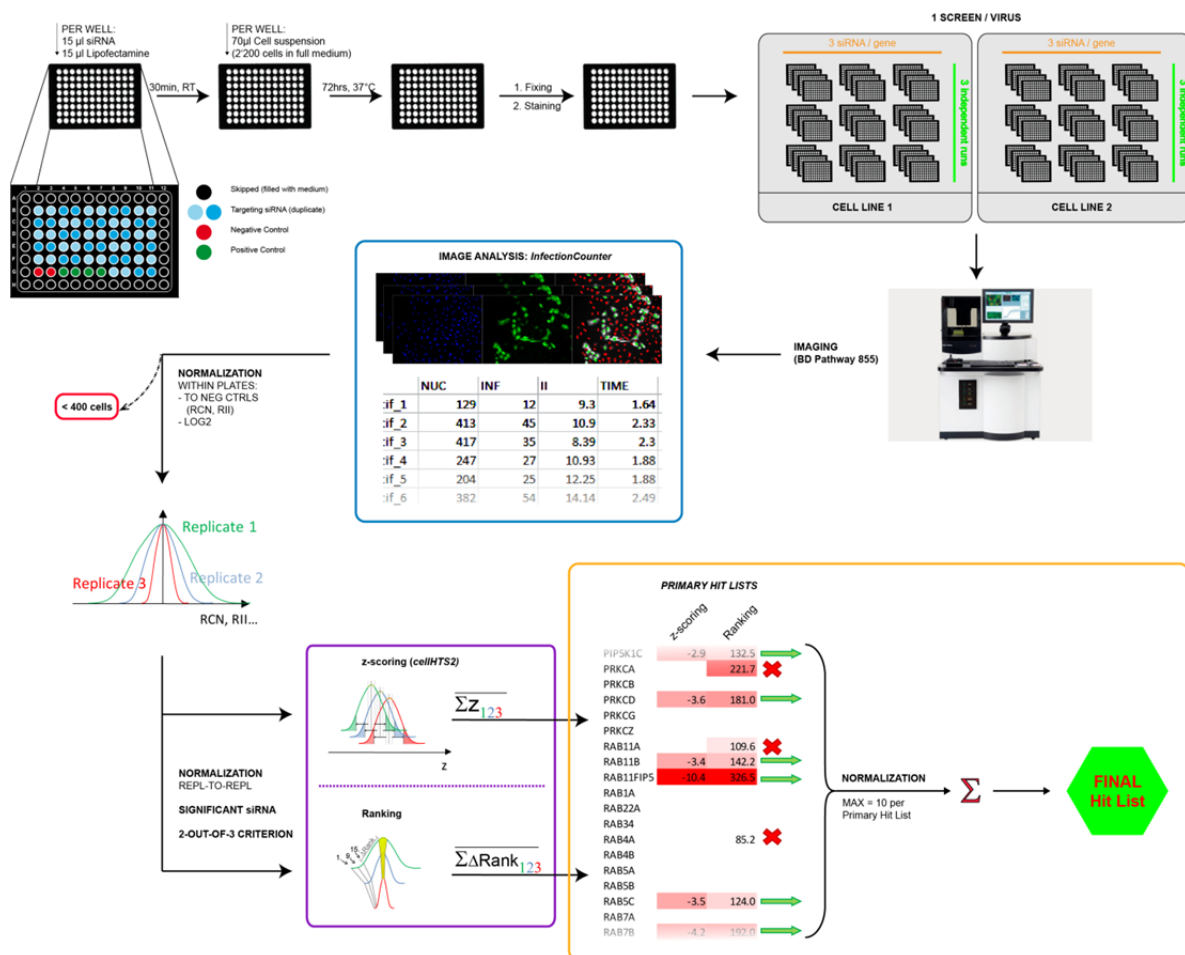


Figure 9

Schematic overview of the general screening workflow from transfection of 96-well plates to the final hit list. For all screens the inner 60 wells of 96 well plates were transfected with siRNA at a final concentration of 20nM using Lipofectamine RNAiMAX at a final dilution of 1:1000 in a reverse transfection setup. After 72h transfection medium was replaced by virus suspension and the cells were infected according to screening-adapted and virus-specific protocols (see Materials and Methods). After fixation and, for some viruses, IF staining plates were imaged with an automated widefield microscope (BD Pathway 855) and the images were analyzed by *InfectionCounter* using virus- and cell-specific settings. The raw infection indices per well were cell-density corrected using a pre-determined polynomial function and normalized to the within-plate negative control wells. Replicate-to-replicate normalization and significance scoring of each siRNA were performed using both, a z-scoring and a ranking algorithm, based on the screening-wide (z-scoring method) or on replicate-wide (ranking method) negative control standard deviations. Primary hit lists of genes for both methods were determined from the siRNA scores when at least 2 out of 3 siRNA targeting the same gene were significant. Overlaps of the method-specific and cell line-specific primary hit lists led to the final hit list for a virus.

2.3.1 Screening of Semliki Forest Virus (SFV)

We performed the screening of SFV in three independent replicates per cell line and used two HeLa cell lines, ATCC and CNX. The MOI needed to infect both HeLa cell lines at a percentage of infection of 20-40% was titrated using checker boards as described in M&Ms. In HeLa ATCC, compared to HeLa CNX, an about ten times higher MOI of SFV was needed to lead to the same percentage of infection.

The results of the SFV screens done for two cell lines and with both significance scoring methods are shown in Table 1. A sorted list of the final hits for SFV according their strength is depicted in Fig. 11A. For HeLa ATCC 18 genes were identified as hits decreasing SFV infection using the z-scoring method versus 22 genes using the ranking method, with an overlap of 14 genes common for both

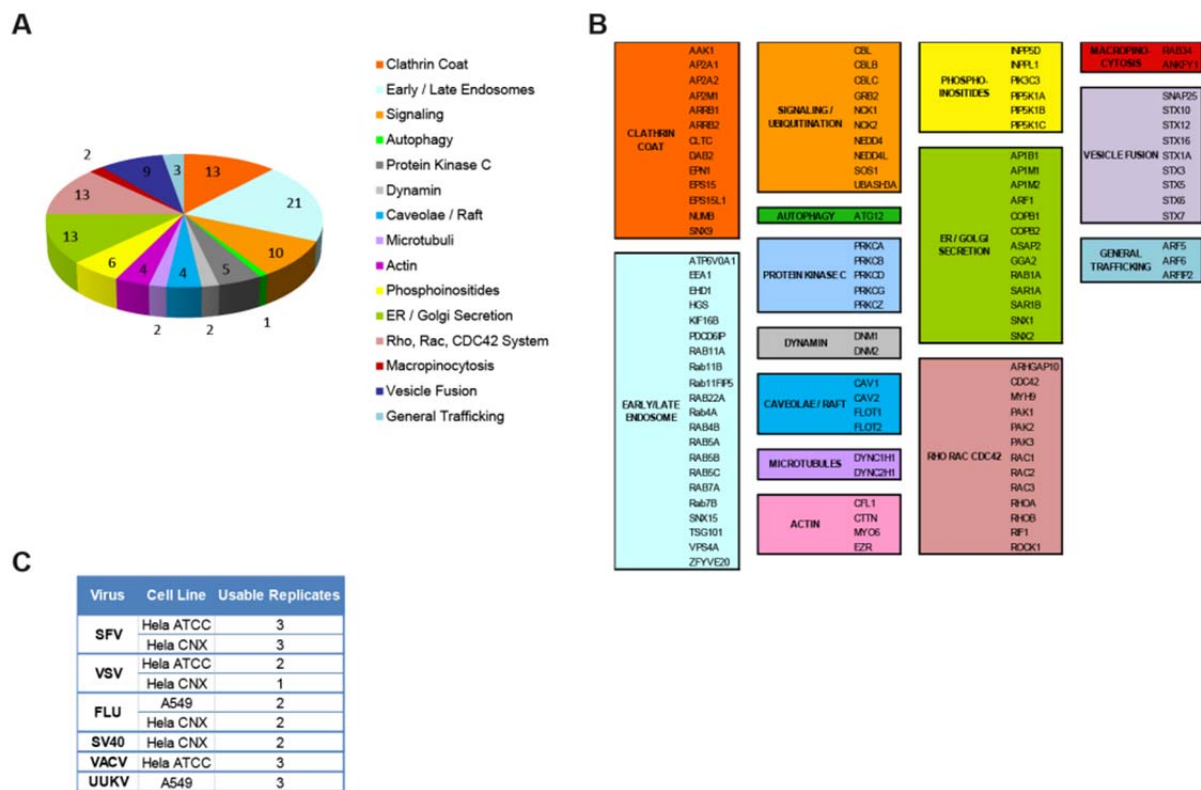


Figure 10

108 genes chosen for Usual Suspects Screens and categorized according their major functions. (A) Pie chart of the functional groups covered by the screen. (B) List of all 108 genes used in the screen (names correspond to the official Entrez Gene Symbols at GeneBank). (C) Viruses involved in Usual Suspects screening with the corresponding cell lines and the number of replicates that have passed the quality control for the screening analysis

methods. In case of HeLa CNX the z-scoring method resulted in 38 hits, whereas the ranking method showed 34 hits, with 30 genes in common (see Table 1 cell line- and method-specific columns as well as column “COMBINED”). Both methods resulted in mostly identical hits (HeLa ATCC: on average 71 %; HeLa CNX: on average 84 % identity) and showed more hits for HeLa CNX than for HeLa ATCC.

This difference between the cell lines might partly be due to differences in knock-down levels for particular genes and cell line-specific differences of the genes in cellular physiology. Other factors might be screening variations, especially differences in the spreading of negative control infection indices based on which the significance threshold for the sample siRNA is calculated in both methods. Also replicate-to-replicate variations in virus titer and cell density have different impacts on both methods. Therefore, those genes with lower scores corresponding to weaker hits showed higher variance among the primary hit lists.

To calculate a final hit list comprising genes, which are hits in either of the cell lines, determined with either of the methods, we combined the primary hit lists and overlapped and ranked their primary hit scores to a final score (Table 2, Fig. 13A). Of those 34 final hits almost half (16) appeared in both cell

Gene Symbol	Gene ID	Hela ATCC			Hela CNX			FINAL HIT	Gene Symbol	Gene ID	Hela ATCC			Hela CNX			FINAL HIT
		z-scoring	ranking	COMBINED	z-scoring	ranking	COMBINED				z-scoring	ranking	COMBINED	z-scoring	ranking	COMBINED	
AAK1	22848								NUMB	8650							
ANKFY1	51479								PAK1	5058	3.3	3.9	7.3	6.3	7.1	13.4	20.7
AP1B1	162								PAK2	5062							
AP1M1	8907								PAK3	5063							
AP1M2	10053								PDCD6IP	10015	5.7						
AP2A1	160								PIK3C3	5289							
AP2A2	161								PIP5K1A	8394		0.8					
AP2M1	1173	2.4	2.0	4.4				PIP5K1B	8395					3.9			
ARF1	375							PIP5K1C	23396	2.8	3.0	5.8	4.7	5.8	10.4	16.2	
ARF5	381				5.3	6.4	11.7	PRKCA	5578		5.0		3.3	3.6	6.9	11.9	
ARF6	382				3.6	3.5	7.1	PRKCB	5579								
ARFIP2	23647	3.6						PRKCD	5580	3.4	4.1	7.5	6.4	5.8	12.1	19.6	
ARHGAP10	79658				3.0	3.5	6.5	PRKCG	5582								
ARRB1	408							PRKCZ	5590				3.2				
ARRB2	409					2.6		RAB11A	8766		2.5		2.9	2.7	5.6	8.1	
ASAP2	8853							RAB11B	9230	3.3	3.2	6.5	6.2	7.5	13.7	20.2	
ATG12	9140							RAB11FIP5	26056	10.0	7.4	17.4	10.0	9.2	19.2	36.5	
ATP6V0A1	535							RAB1A	5861				4.1	4.3	8.4	8.4	
CAV1	857							RAB22A	57403								
CAV2	858				4.5	3.1	7.6	RAB34	83871				5.8				
CBL	867	3.5	3.6	7.1	4.7	5.5	10.2	RAB4A	5867		1.9						
CBLB	868				3.4			RAB4B	53916				6.2	7.1	13.2	13.2	
CBLC	23624							RAB5A	5868				2.7	2.3	5.0	5.0	
CDC42	998							RAB5B	5869								
CFI1	1072							RAB5C	5878	3.4	2.8	6.2	4.4	5.0	9.4	15.5	
CLTC	1213				5.7	6.2	11.9	RAB7A	7879								
COPB1	1315							RAB7B	338382	4.1	4.3	8.4	6.9	8.4	15.3	23.7	
COPB2	9276							RAC1	5879					2.3			
CTTN	2017							RAC2	5880				2.2	2.4	4.6	4.6	
DAB2	1601							RAC3	5881								
DNM1	1759				4.3	5.4	9.7	RHOA	387				2.8	1.6	4.5	4.5	
DNM2	1785							RHOB	388								
DYNC1H1	1778							RNF34	80196								
DYNC2H1	79659							ROCK1	6093								
EEA1	8411							SAR1A	56681								
EHD1	10938		5.0					SAR1B	51128								
EPN1	29924							SNAP25	6616				2.9				
EPS15	2060							SNX1	6642		3.8						
EPS15L1	58513		2.8		5.0	4.1	9.1	SNX15	29907								
EZR	7430							SNX2	6643								
FLOT1	10211							SNX9	51429								
FLOT2	2319				6.0	7.5	13.5	SOS1	6654								
GGA2	23062				3.7	3.1	6.8	STX10	8677	5.3	3.3	8.6				8.6	
GRB2	2885				2.9			STX12	23673				5.2				
HGS	9146	3.8			7.9	9.4	17.3	STX16	8675								
INPP5D	3635							STX1A	6804								
INPPL1	3636	3.9	3.3	7.2	5.0	5.8	10.9	STX3	6809				2.2				
KIF16B	55614							STX5	6811	10.0	10.0	20.0	9.5	10.0	19.5	39.5	
MYH9	4627				3.5	4.0	7.5	STX6	10228								
MYO6	4646							STX7	8417								
NCK1	4690		2.4					TSG101	7251	3.9	4.2	8.1	4.4	4.1	8.5	16.6	
NCK2	8440							UBASH3A	53347	3.0	2.6	5.6	2.8			8.9	
NEDD4	4734				3.6	2.6	6.2	VPS4A	27183								
NEDD4L	23327							ZFYVE20	64145	2.3				3.2		5.5	

Table 1

Results of the Usual Suspects screening of SFV. From all SFV screens each gene was analyzed with two significance scoring methods (z-scoring and ranking) in two cell lines (HeLa ATCC and CNX) and designated as “primary hit” when at least two out of 3 siRNA were “significant” according to the method-specific definitions in the Materials and Methods. The siRNA scores were summed up to primary hit scores (shown in the corresponding method/cell line columns) and combined to a method-independent score for each cell line (columns “COMBINED”). Genes that appeared as primary hits in either of the cell lines were considered “final hits”. Genes that appeared at least 3x in primary hit lists are shown in yellow. These stringent final hits were used to compare SFV with other viruses in section 2.3.3.

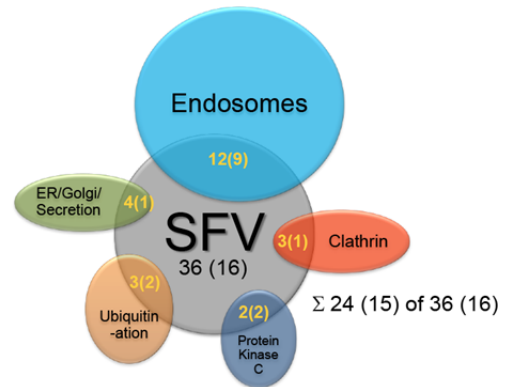
lines, with the first 12 being the strongest hits judged by their hit scoring (Fig. 11A, orange background).

The final hit list contains primarily hits that are essential for endosomal function (12 hits from either of the cell lines, 9 of them appearing in both cell lines: 12(9)), clathrin mediated endocytosis (CME) (3(1)), Protein Kinase C members (2(2)), ubiquitination pathways (3(2)), and ER/Golgi-associated secretion pathways (4(1)). CME and endosomal pathways are represented together in almost half (15) of the 36 hits from both cell lines, of those are 10 out of 16 (62%) cell line-independent hits.

A

Gene Symbol	Gene ID	Gene Name	FINAL HIT SCORE
STX5	6811	syntaxin 5	39.5
RAB11FIP5	26056	RAB11 family interacting protein 5 (class I)	36.5
RAB7B	338382	RAB7B, member RAS oncogene family	23.7
HGS	9146	hepatocyte growth factor-regulated tyrosine kinase substrate	21.1
PAK1	5058	p21 protein (Cdc42/Rac)-activated kinase 1	20.7
RAB11B	9230	RAB11B, member RAS oncogene family	20.2
PRKCD	5580	protein kinase C, delta	19.6
INPPL1	3636	inositol polyphosphate phosphatase-like 1	18.1
CBL	867	Cas-Br-M (murine) ecotropic retroviral transforming sequence	17.3
TSG101	7251	tumor susceptibility gene 101	16.6
PIP5K1C	23396	phosphatidylinositol-4-phosphate 5-kinase, type I, gamma	16.2
RAB5C	5878	RAB5C, member RAS oncogene family	15.5
FLOT2	2319	flotillin 2	13.5
RAB4B	53916	RAB4B, member RAS oncogene family	13.2
CLTC	1213	clathrin, heavy chain (Hc)	11.9
EP515L1	58513	epidermal growth factor receptor pathway substrate 15-like 1	11.9
PRKCA	5578	protein kinase C, alpha	11.9
ARF5	381	ADP-ribosylation factor 5	11.7
DNM1	1759	dynamain 1	9.7
STX10	8677	syntaxin 10	8.6
RAB1A	5861	RAB1A, member RAS oncogene family	8.4
UBASH3A	53347	"similar to ubiquitin associated and SH3 domain containing, A; ubiquitin associated and SH3 domain containing, A"	8.3
RAB11A	8766	RAB11A, member RAS oncogene family	8.1
CAV2	858	caveolin 2	7.6
MYH9	4627	myosin, heavy chain 9, non-muscle	7.5
ARF6	382	ADP-ribosylation factor 6	7.1
GGA2	23062	golgi associated, gamma adaptin ear containing, ARF binding protein 2	6.8
ARHGAP10	79658	Rho GTPase activating protein 10	6.5
NEDD4	4734	neural precursor cell expressed, developmentally down-regulated 4	6.2
ZFYVE20	64145	zinc finger, FYVE domain containing 20	5.5
RAB5A	5868	RAB5A, member RAS oncogene family	5.0
RAC2	5880	ras-related C3 botulinum toxin substrate 2 (rho family, small GTP binding protein Rac2)	4.6
RHOA	387	ras homolog gene family, member A	4.5
AP2M1	1173	adaptor-related protein complex 2, mu 1 subunit	4.4

B



C

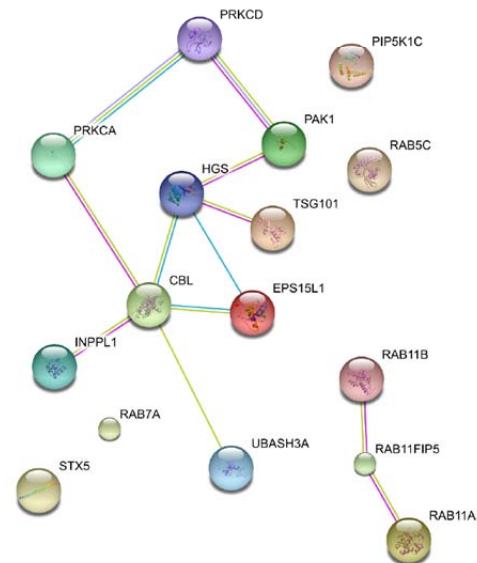


Figure 11

Final hits from the SFV screening. (A) Final hit list of SFV sorted according to the final hit scores. 34 genes were identified as hits in either of two cell lines, HeLa ATCC and CNX. Of those 16 genes were hits in both cell lines (indicated with orange background). Each gene is listed with its official gene symbol, ID, and name according to Entrez Gene Bank. Final hit scores were calculated by summation of the primary hit scores for each significance scoring method. Only those genes were considered final hits that were primary hits in at least two lists (see Table 2). (B) Blow chart of the primary cellular functions and pathways that are present in the final hit list of SFV. The yellow numbers represent the number of genes from the hit list in (A) that belong to the corresponding functional group, while the number in brackets are cell line-independent hits (orange in (A)). (C) STRING analysis of interactions between 16 final cell line-independent hits (orange in (A)).

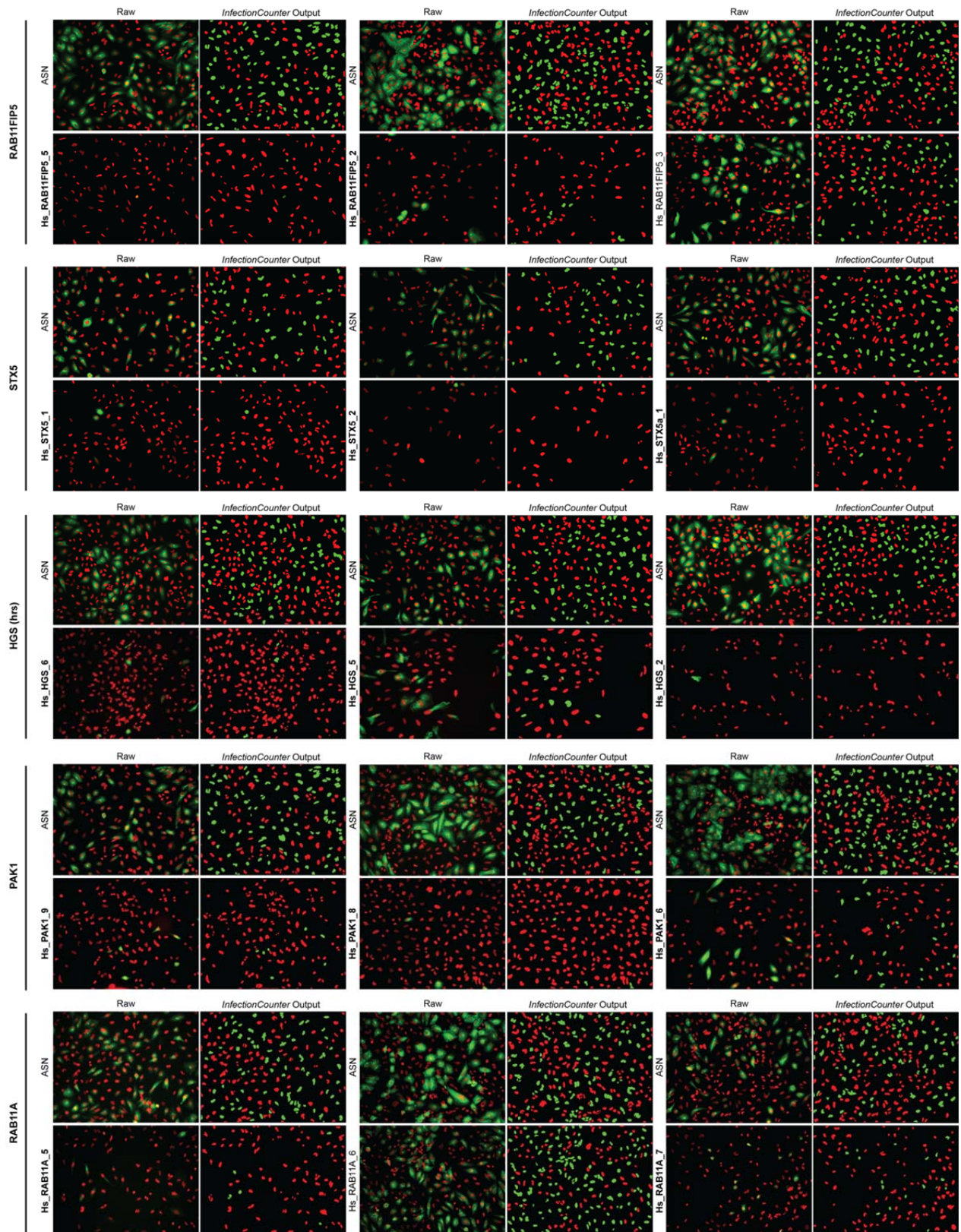


Figure 12

Selected images of hits from the SFV screen. Five example hits of the SFV Usual Suspects screen are shown with 3 targeting siRNA each as raw image and binary red/green image to show *InfectionCounter* analysis from the raw images. “Raw” RGB images were created by merging one of 16 gray-scale images per well of a replicate showing staining for SFV envelope (green) and Hoechst 33nuclei (red). Those siRNA that were identified as significant are indicated by bold siRNA names (Hs_xxxx_n; “Hs” indicates the species Homo sapiens, “xxxx” represents the gene symbol as in (A), and “n” an siRNA identifier given by the vendor Qiagen).

2.3.2 Screening of Simian Virus 40, Vesicular Stomatitis Virus, Vaccinia Virus, Uukuniemi Virus, and Influenza A Virus

Simian Virus 40 (SV40)

The Usual Suspects Screening of SV40 was performed in three independent runs, of which two passed the quality control (minimal infection in negative controls to be 10%), using one cell line (HeLa CNX). HeLa CNX was tested before to be the only cell line suitable for RNAi that is susceptible to SV40 infection. The screen was set up and analyzed with *InfectionCounter* essentially as described for SFV. For SV40 infection the virus stock was diluted 1:1 with a minimal Infection Medium buffered to pH 6.8 with 20mM HEPES and incubated at 37°C for 2 hrs with siRNA-transfected HeLa CNX. Medium was replaced by full medium containing FCS for additional 22 hrs until fixation. We used staining against the T-antigen (Pelkmans, Fava et al. 2005) to identify infected cells besides Hoechst 33258 to identify nuclei. To determine hits we first calculated z-scores of infection and ranking hit scores, and searched for those primary hits that overlapped in both lists (Table 2). In contrast to SFV, the ranking method produced almost twice (59) the hits of the z-scoring method (30) but 26 genes of each list were overlapping (see Fig. 14). Hence, the z-scoring list is almost completely included in the ranking hit list, the latter representing essentially a hit list with less stringent filtering than the first.

Vesicular Stomatitis Virus (VSV)

We used HeLa ATCC and HeLa CNX cell lines for screening of VSV. Of 5 replicates of VSV screens with HeLa CNX only one passed the quality assessment (mostly transfection control, AllStarsDeath siRNA, did not reduce cell number below 20% of the average cell number of the negative control wells), while two of three HeLa ATCC replicates could be analyzed. VSV was prepared as described in the Materials & Methods. A dilution factor from the stock leading to about 25% absolute infection under screening conditions was determined by checker boards that also served to calculate the cell density correction function. VSV infection was detected by expression of the viral envelope protein VSV-G using an antibody (F-14). The virus, diluted in minimal Infection Medium (RPMI) buffered with 20 mM HEPES to pH 6.8, was applied to the transfected cells and incubated 5 hrs at 37°C before fixation and staining. Plates were prepared for microscopy and image analysis with *InfectionCounter* and cellHTS2 (z-scoring method) as well as Excel calculations (ranking method) to extract the final hit list.

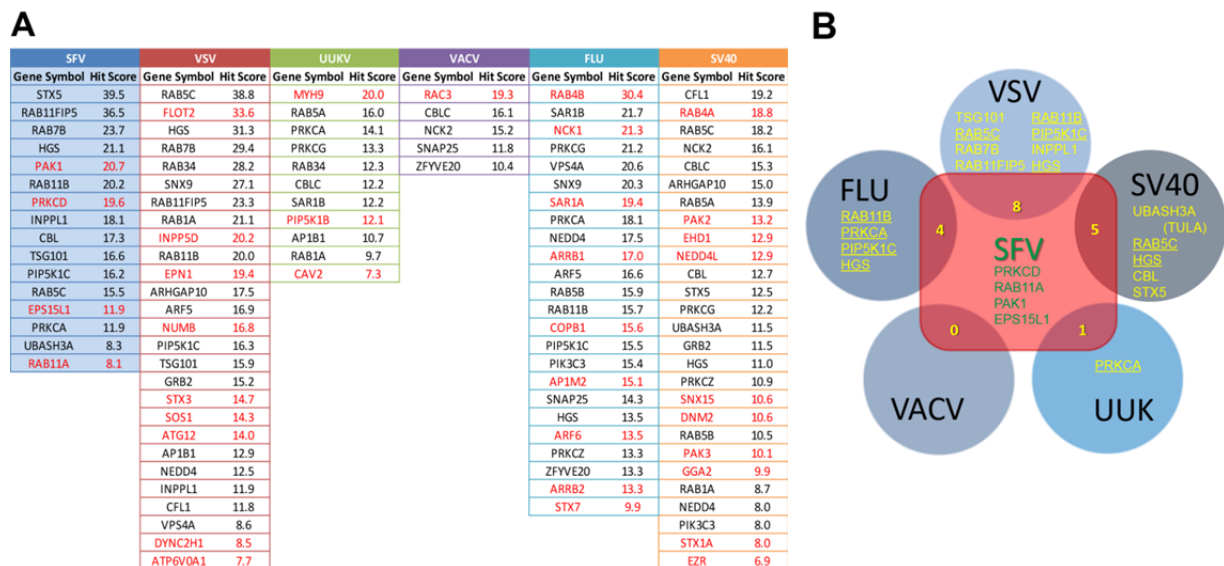


Figure 13

Final hits from Usual Suspects screening of SFV in comparison with other viruses. (A) Final hits of SFV (first column) and five other viruses from Usual Suspects screening with final hit scores and Entrez Gene Symbol (NCBI Gene Bank). Red names indicate unique hits for the corresponding virus. (B) SFV screening resulted in 16 genes, of those 4 genes (PRKCD, Rab11A, PAK1, EPS15L1; names in green) are unique to SFV. SFV shares hits with all other viruses except VACV (yellow numbers). The gene names (according to Entrez Gene Bank database) of the overlapping hits of SFV with the corresponding viruses are depicted in yellow. Those genes that are underlined indicate SFV hits overlapping with more than one virus.

Uukuniemi Virus (UUK), Influenza A Virus (FLU), Vaccinia Virus (VACV)

We used one cell line (FLU: two) for the other viruses: A549 ATCC (UUK and FLU), HeLa ATCC (VACV), and HeLa CNX for FLU. Virus preparations, development and performance of screening-adapted infection assays, preparation for and performance of imaging were done by lab members (brief protocols see Materials and Methods).

For all virus screens 3 replicates (UUK: 4) were performed. Image analysis was done by *InfectionCounter*. Checker board test plates were used to determine cell density correction except for VACV, which shows very low cell density-dependent variations (Mercer, personal information and (Snijder, Sacher et al. 2009)). Quality assessment finally led to 3 (FLU: 2 for both cell lines) usable replicates for hit definition (Fig. 10C).

Primary hit lists from z-scoring and ranking methods for each virus were calculated as described for single cell line screens (UUK and VACV) and two cell line screens (FLU) before. Primary hits are listed in the supplemental material on the CD, the final hits are shown in Fig. 13A and Table 2.

Gene Symbol	Gene ID	SFV	VSV	UUKV	VACV	FLU	SV40	COUNT	Gene Symbol	Gene ID	SFV	VSV	UUKV	VACV	FLU	SV40	COUNT
AAK1	22848							0	NUMB	8650	16.8						1
ANKFY1	51479							0	PAK1	5058	20.7						1
AP1B1	162		12.9	10.7				2	PAK2	5062					13.2		1
AP1M1	8907							0	PAK3	5063					10.1		1
AP1M2	10053					15.1		1	PDCD6IP	10015							0
AP2A1	160							0	PIK3C3	5289					15.4	8.0	2
AP2A2	161							0	PIP5K1A	8394							0
AP2M1	1173							0	PIP5K1B	8395			12.1				1
ARF1	375							0	PIP5K1C	23396	16.2	16.3			15.5		3
ARF5	381	16.9				16.6		2	PRKCA	5578	11.9		14.1		18.1		3
ARF6	382					13.5		1	PRKCB	5579							0
ARFIP2	23647							0	PRKCD	5580	19.6						1
ARHGAP10	79658	17.5				15.0		2	PRKCG	5582			13.3		21.2	12.2	3
ARRB1	408					17.0		1	PRKCZ	5590					13.3	10.9	2
ARRB2	409					13.3		1	RAB11A	8766	8.1						1
ASAP2	8853							0	RAB11B	9230	20.2	20.0			15.7		3
ATG12	9140	14.0						1	RAB11FIP5	26056	36.5	23.3					2
ATP6V0A1	535		7.7					1	RAB1A	5861		21.1	9.7		8.7		3
CAV1	857							0	RAB22A	57403							0
CAV2	858			7.3				1	RAB3A	83871		28.2	12.3				2
CBL	867	17.3				12.7		2	RAB4A	5867						18.8	1
CBLB	868							0	RAB4B	53916					30.4		1
CBLC	23624			12.2	16.1	15.3		3	RAB5A	5868			16.0			13.9	2
CDC42	998							0	RAB5B	5869					15.9	10.5	2
CFL1	1072		11.8			19.2		2	RAB5C	5878	15.5	38.8				18.2	3
CLTC	1213							0	RAB7A	7879							0
COPB1	1315					15.6		1	RAB7B	338382	23.7	29.4					2
COPB2	9276							0	RAC1	5879							0
CTTN	2017							0	RAC2	5880							0
DAB2	1601							0	RAC3	5881					19.3		1
DNM1	1759							0	RHOA	387							0
DNM2	1785					10.6		1	RHOB	388							0
DYNC1H1	1778							0	RNF34	80196							0
DYNC2H1	79659		8.5					1	ROCK1	6093							0
EEA1	8411							0	SAR1A	56681					19.4		1
EHD1	10938					12.9		1	SAR1B	51128			12.2		21.7		2
EPN1	29924	19.4						1	SNAP25	6616				11.8	14.3		2
EPS15	2060							0	SNX1	6642							0
EPS15L1	58513	11.9						1	SNX15	29907					10.6		1
EZR	7430					6.9		1	SNX2	6643							0
FLOT1	10211							0	SNX9	51429		27.1			20.3		2
FLOT2	2319	33.6						1	SOS1	6654		14.3					1
GGA2	23062					9.9		1	STX10	8677							0
GRB2	2885	15.2				11.5		2	STX12	23673							0
HGS	9146	21.1	31.3			13.5	11.0	4	STX16	8675							0
INPP5D	3635		20.2					1	STX1A	6804					8.0		1
INPPL1	3636	18.1	11.9					2	STX3	6809		14.7					1
KIF16B	55614							0	STX5	6811	39.5				12.5		2
MYH9	4627		20.0					1	STX6	10228							0
MYO6	4646							0	STX7	8417					9.9		1
NCK1	4690					21.3		1	TSG101	7251	16.6	15.9					2
NCK2	8440				15.2	16.1		2	UBASH3A	53347	8.3				11.5		2
NEDD4	4734	12.5				17.5	8.0	3	VPS4A	27183	8.6				20.6		2
NEDD4L	23327					12.9		1	ZFYVE20	64145				10.4	13.3		2

Table 2

Comparison of the final hit list of Usual Suspects screening of SFV with those of five other viruses. 108 genes with gene name and gene ID are shown in rows that were screened for decrease of infection of each virus (columns). SFV (VSV, UUK, VACV, FLU, SV40) screening resulted in 16 (27, 11, 5, 24, 27) final hits. Hits are specified with their final hit scores, the color code indicates the relative strength of a hit (white – weakest; dark red – strongest hit of a particular virus). The “COUNT” column shows the number of viruses, whose infection is impaired by siRNA of the particular genes. SFV hits are highlighted with light green background

2.3.3 Comparison of hit lists from different viruses

Besides SFV and SV40 we screened four other viruses with the Usual Suspects screening protocol: Vaccinia Virus (VACV), Uukuniemi Virus (UUKV), Influenza A Virus (FLU), and Vesicular Stomatitis Virus (VSV).

For SV40, UUKV, and VACV the hit definition procedure had to be adapted (see Materials and Methods) since only one human cell line could be used due to limited susceptibility of human cell lines to the viruses (SV40, UUKV) or poor quality of the screen (VACV in HeLa CNX).

As for SFV and SV40 screening, those siRNA were skipped that decreased cell number below 400 per imaged part of a well. Both significance scoring methods together with the 2-out-of-3 siRNA criterion were applied to get two primary hit lists per cell line and virus. The final hit list for each virus was determined as the overlap hits of the primary hit lists (Figure 13A and Table 2).

Figure 14 indicates that both significance scoring methods only converge to a similar hit list in case of SFV and VACV screens. Usually one method hit list contains almost all hits of the other method hit list plus additional hits that have primarily low scores. Hence, the differences in both methods mostly reflect different stringencies with which significant siRNA were determined. Indeed, a strong dissimilarity between methods occurs only in one case, FLU screen in HeLa CNX. Here, the number of overlapping genes is only about 25% (compared to z-scoring method) and 30% (compared to ranking method), respectively. In summary, most of the strong hits of almost all viruses appear always in the hit lists, independently on the data analysis method used. Mostly they differ at the weak scoring part of the lists in that more or less many weak hits are included in the final list.

To determine robust hits that are independent of the significance scoring method used and, for VSV and FLU, are also independent of the two cell lines used, all primary hit lists were overlapped as described previously for SFV and SV40. These final hits of all six viruses are shown in Table 2. Out of 16 cell line-independent SFV hits four are unique among the viruses tested: Rab11A, EPS15L1 (Eps15 like-1), PAK1 (p21 protein [Rac1/cdc42]-activated kinase 1), and PRKCD (protein kinase C delta). Fig. 13A shows unique hits for all viruses tested, and Figure 13B depicts unique and overlapping SFV hits with the hits of the other viruses.

Most of the unique hits, however, belong to cellular pathways that are represented by other yet related members in other virus hit lists. Among the most frequent pathways appearing in most of the virus hit lists are 1) endosomal proteins; 2) protein kinase C subfamily members; and 3) ubiquitination-related genes:

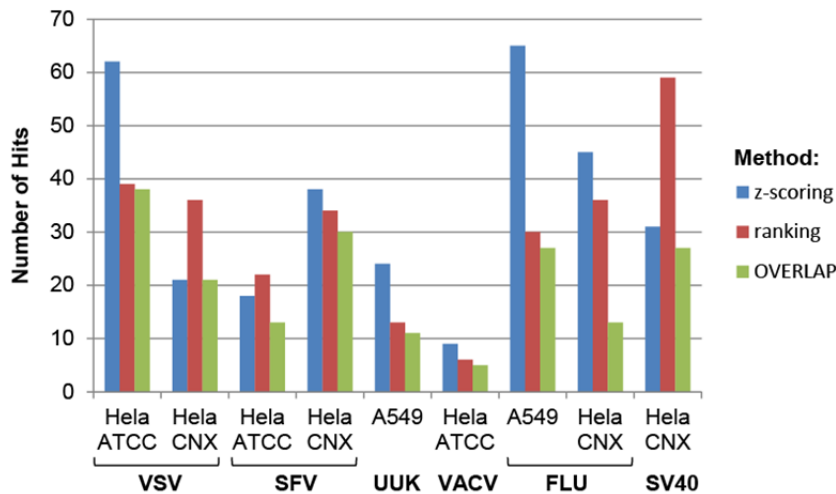


Figure 14

Diagram showing number of primary hits calculated by two different methods to score for significant siRNA for each screen. z-scoring is shown in blue bars while ranking method hits are depicted in red bars. The number of identical primary hits of both methods (hit list overlaps) is indicated by green bars for each screen. In most screens (except FLU in HeLa CNX) the hits of either of both methods were also part of the hit list of the other method, i.e. a subset of the other. Hence, both methods differed in most cases only in the stringency with which hits were identified.

1) endosome-related genes can be further separated in early / sorting endosomal genes such as the small GTPases Rab5A (hit in UUKV and SV40), Rab5B (FLU and SV40), and Rab5C (SFV, VSV, and SV40); in genes of the recycling pathway such as the Rab11 family (Rab11A in SFV, Rab11B in SFV, VSV, and FLU), the Rab11/Rab5 interactor RAB11FIP5 (strong hit in SFV and moderate hit in VSV) and the Rab4 family proteins (Rab4A in SV40 and Rab4B in FLU); and in genes of the degradative pathway (Rab7B in SFV and VSV, hrs/HGS in SFV, VSV, FLU, and SV40, tsg101 in SFV and VSV, VPS4A in VSV and FLU).

2) All viruses except VACV were susceptible to siRNA against one or more PKC family members such as PKC alpha (PRKCA; SFV, UUKV, and FLU), PKC delta (PRKCD; SFV), PKC gamma (PRKCG; UUKV, FLU, and SV40), and PKC zeta (PRKCZ; FLU and SV40), while PKC beta did not appear as a hit for any virus.

3) At least one ubiquitination-related gene was part of the hit lists of all viruses (CBL in SFV and SV40, CBLC in UUKV, VACV, and SV40, NEDD4 in VSV, FLU, and SV40, and NEDD4L in SV40), while CBLB appeared in no hit list.

2.4 Analysis and Validation of Screening Hits

We focused primarily on two viruses for analysis and validation of the screening hits, Semliki Forest Virus (SFV) and Simian Virus 40 (SV40). We compared viral hit lists and applied bioinformatic tools to identify cellular pathways that are over- and underrepresented in the hit lists of these viruses.

Several tests for validation of the hits were performed: measuring knock-down efficiency of siRNA, validating the effects of siRNA on virus infection by FACS, applying non-siRNA perturbants such as small compound inhibitors and dominant negative mutants. We also validated siRNA by virus binding assays, virus internalization and replication assays to further define the location of block within the virus life cycle.

2.4.1 Western Blot Analysis to Quantify Knock-down efficiency

To validate knock-down of the siRNA used in the Usual Suspects screen we selected seven hits for at least one virus and a non-hit and determined protein knock-down with SDS-PAGE (Figure 15).

We tested cofilin (CFL; hit for SV40 and VSV), Dynamin-2 (DNM2; hit for SV40), ezrin/villin-2 (EZR; hit for SV40), hrs (HGS; hit for SFV, VSV, FLU, and SV40), NEDD4L (hit for SV40), Rab4a (hit for SV40), Rab5a (SV40, and UUKV), and Caveolin-1 (hit for none of the viruses). All siRNA showed knock-down of the corresponding protein by at least 39%, while 15 of 23 (65%) siRNA caused depletion of the target protein by more than 70%.

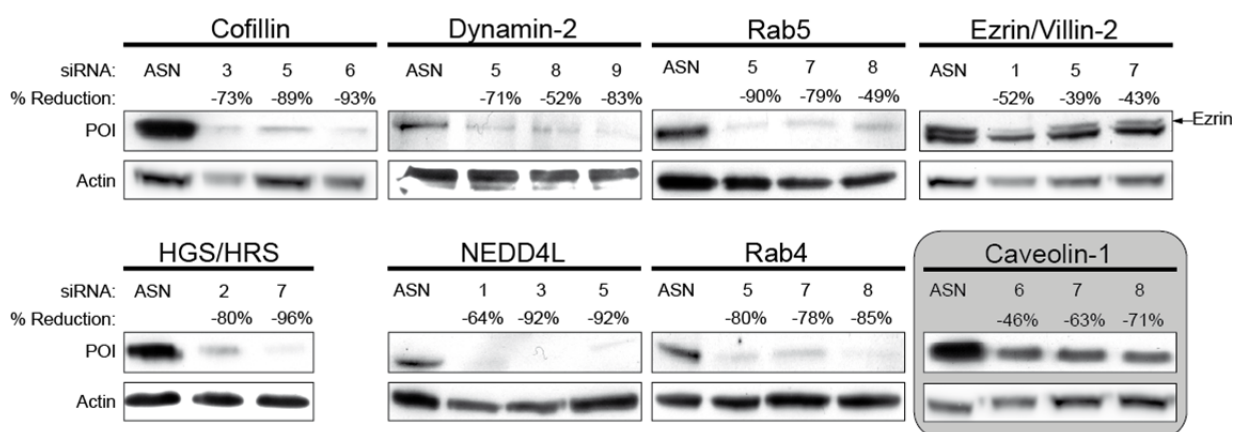


Figure 15

Western Blots to verify protein knock-down of siRNA from eight genes of the RNAi screen. SiRNAs to knock-down cofilin, dynamin-2, ezrin, HGS, NEDD4L, Rab4, Rab5, and caveolin-1 were transfected into HeLa cells. Seventy-two hours after transfection cells were lysed and subjected to Western Blot analysis. Actin was stained as a loading control. Knock-down efficiency is indicated as „% Reduction“ normalized to AllStarsNegative (ASN) control siRNA and to the corresponding actin loading control. The second band in the Ezrin western blot corresponds to Moesin, which the antibody also recognizes. The grey background of the Caveolin-1 box indicates a non-hit for all viruses.

2.4.2 Screening of Semliki Forest Virus (SFV)

2.4.2.1 FACS Validation of SFV Hit siRNA

First, we confirmed the effects on SFV infection of the best siRNA of some of the hit genes from the screen using a non-image based analysis method. We chose FACS analysis and adapted transfection and SFV infection protocols from the screen to FACS scale. HeLa ATCC cells were reverse-transfected with siRNA in 12 well format according to an scale-adapted transfection protocol from screening (see Materials & Methods). For transfection reagent and siRNA the same concentrations than under screening conditions were used.

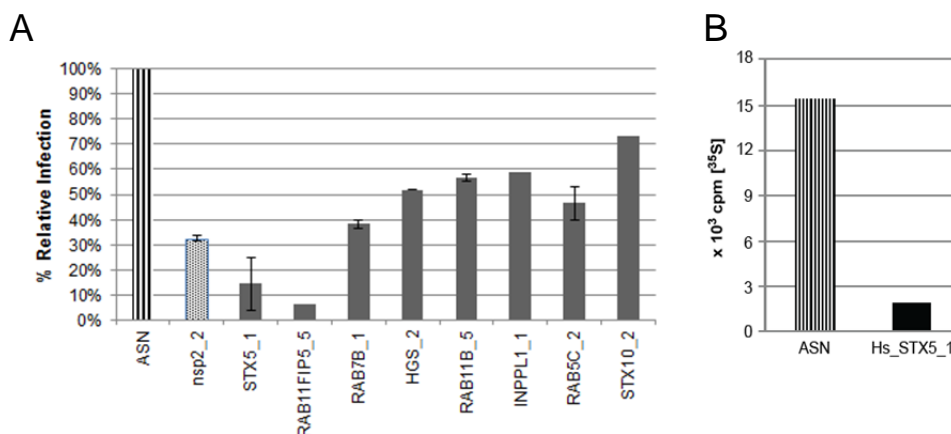


Figure 16

Validation of some of the hits from SFV screen. (A) siRNA targeting some of the hits of the SFV screen that gave the strongest reductions of infection were transfected into HeLa ATCC cells using the screening protocol adapted to 12 well plates. After 72 hrs incubation medium was replaced by SFV with an MOI that led to about 30% absolute infection in the negative control (AllStarsNegative siRNA) and cells were incubated for 4 hrs followed by fixation and preparation for FACS analysis. All sample siRNA were normalized to the negative control, which is set to 100% (“ASN”). siRNA against the non-structural protein 2 of SFV (“nsp2_2”) was used as a positive control. (B) Surface binding of SFV is reduced by more than 85% by siRNA against Syntaxin-5 (STX5). The strongest siRNA targeting STX5, which was used in the Usual Suspects screen (Hs_STX5_1), was transfected to HeLa ATCC according to an adapted transfection protocol used in (A), and incubated for 72 hrs. After washing, cells were incubated with radioactive SFV (200’000 cpm of [³⁵S]-SFV) for 1 hr in the cold. After washing with PBS cells were detached by 20mM EDTA / PBS at 4°C and scraping and prepared for scintillation counting.

Syntaxin-5 (STX5) and RAB11FIP were the strongest hits for SFV in both HeLa cell lines with a hit scoring of almost 40 (Table 2, Figure 13A). Rab7B, hrs (HGS), Rab11B, Ship2 (INPPL1), and Rab5C were hits in both cell lines with a scoring between 23.7 and 15.5, while syntaxin-10 (STX10) did only appear as a primary hit in the HeLa ATCC screen (score 8.6) but not in the final hit list. Figure 16A shows a similar siRNA effect on SFV infection of HeLa ATCC determined by FACS analysis than determined by image-based analysis (compare Fig 16A with hit scores of Table 2). While STX5 and RAB11FIP5 siRNA led to more than 85% reduction of infection, the hits with half of the maximal screen showed reductions of about 40-60%, and the most effective siRNA Hs_STX10_2 of the weak hit syntaxin 10 could reduce infection only by about 30%. Interestingly, both strongest hits reduced infection more efficiently than the positive control (“nsp2_2”), a siRNA against the non-structural protein 2 of the virus. Taken together, FACS-based validation of a selection of SFV hit siRNA essentially confirms their effects on infection determined by the image-based screening method.

2.4.2.2 SFV infection requires clathrin-mediated endocytosis and endosome function

Three important proteins for CME appear as hits in the SFV screen: CLTC (clathrin heavy chain) and AP2M1 (μ 1 subunit of AP2) in HeLa CNX and PIP5K1C (phosphatidylinositol-4-phosphate-5-kinase I, subtype gamma) in both cell lines (Fig. 17). For clathrin as well as the clathrin adaptor complex AP2 it was shown that siRNA-mediated knockdown is difficult unless cells are double-transfected with siRNA (Motley, Bright et al. 2003; Johannsdottir, Mancini et al. 2009), which is not applicable in screening experiments. Therefore, their low hit score and appearance in only one cell line does not surprise. PIP5K1C is yet another essential factor for CME upstream of clathrin: it synthesizes patches of the lipid phosphatidylinositol-4,5-bisphosphate (PIP₂) in the plasma membrane, which initiate clathrin and AP2 accumulation around cargo receptors, finally forming clathrin coated pits (see Introduction; (Conner and Schmid 2003; Bairstow, Ling et al. 2006)).

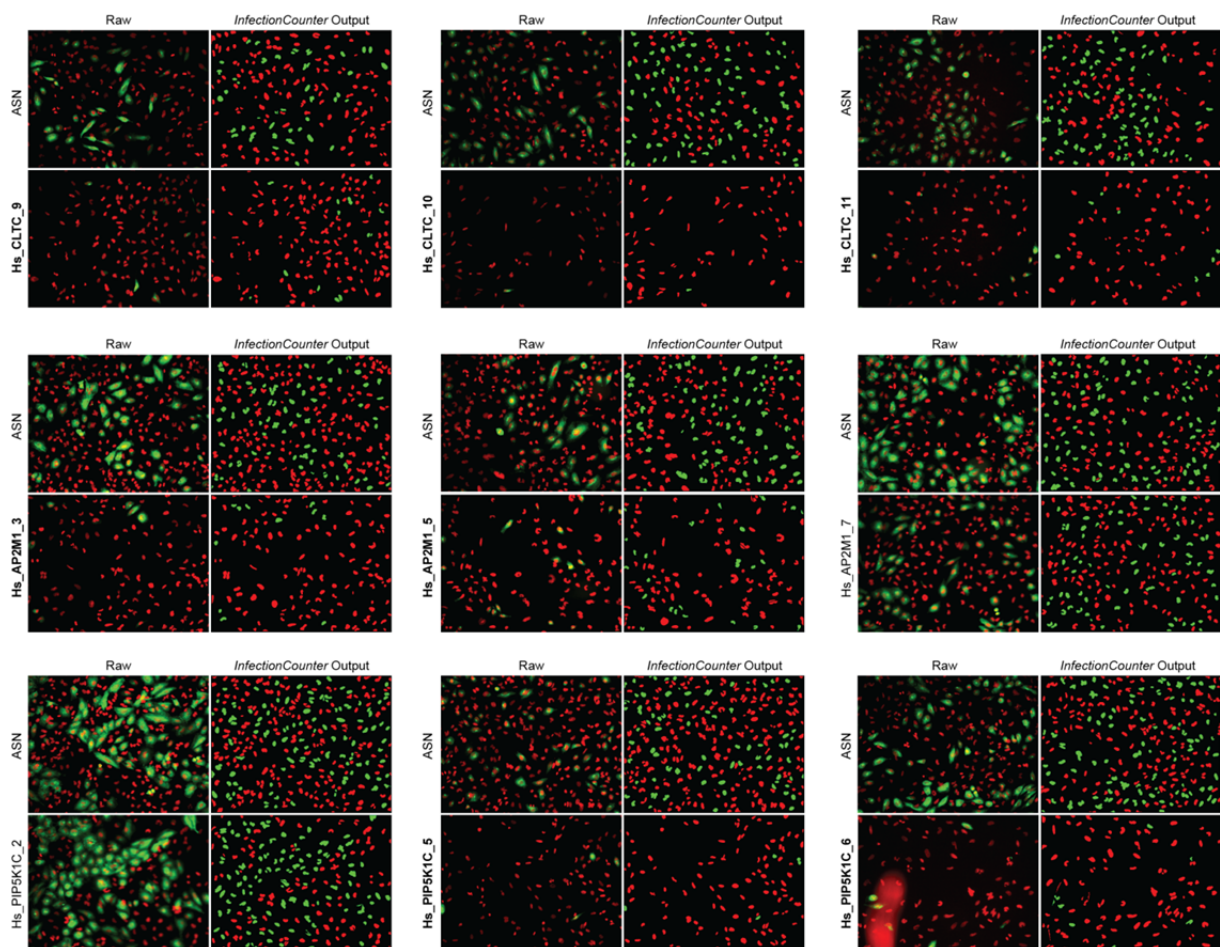


Figure 17

Hits of clathrin-mediated endocytosis identified for SFV. Effects on infection of the three siRNA used in the screen against Clathrin-heavy chain (CLTC), Adapter Protein -2 μ 1 subunit (AP2M1), and phosphatidylinositol-5-kinase class I gamma (PIP5K1C) are shown by representative IF-stained images (“Raw”) and the corresponding *InfectionCounter* analysis (“*InfectionCounter* Output”). “Raw” RGB images were created by merging gray-scale images showing staining for SFV envelope (green) and Hoechst 33258 nuclei (red). Binary red/green overlap images (*InfectionCounter* Output) show all identified nuclei belonging to non-infected cells (red) or infected cells (green). Significant siRNA are indicated by bold siRNA names. Hs_AP2M1_7 does not significantly reduce infection while Hs_PIP5K1C_2 slightly increases it. Significance was calculated from averaged, normalized, and cell density-corrected z-scores and ranks, while the images shown are selected example images from one of the three replicate screens to show the principle. For all siRNA at least 400 cells per 16 images per well (averaged over all replicates) were detected.

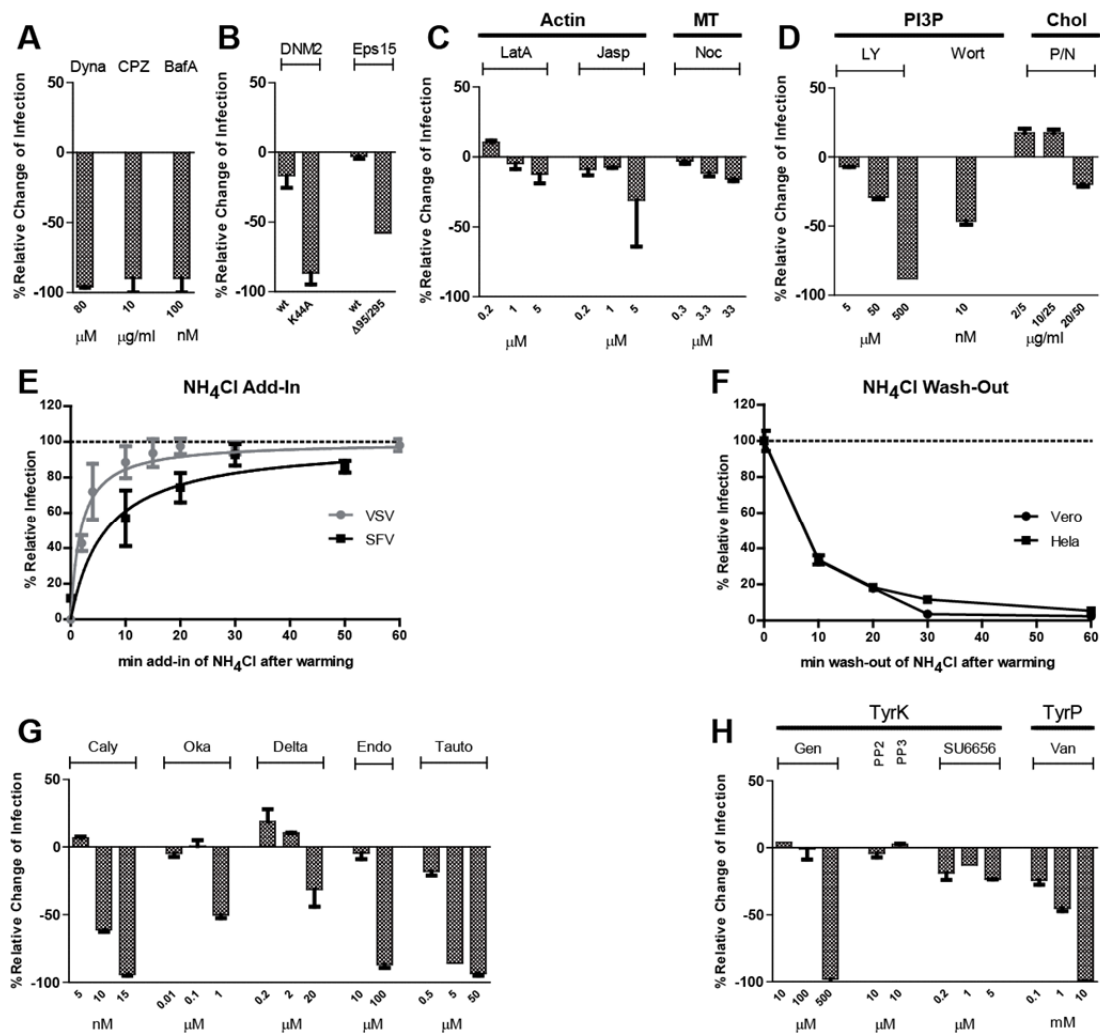


Figure 18

Drug profiling of SFV infection using FACS infection assay. Relative changes of infection are normalized against the negative control samples. For all experiments, SFV infection occurred in total for 4 hrs at 37°C. After washing cells were detached by Trypsin/EDTA treatment, fixed with 4% HCHO, stained against E1-3, and prepared for FACS analysis. Values are percentage of infection relative to negative (no drug) control if not stated otherwise (A) Cells were pre-incubated with drugs for 30 min at 37°C, followed by infection in the presence of the drugs for 4 hrs. (B) Expression of wild-type (*wt*) or dominant-negative mutants of dynamin-2 (*DNM2*; *K44A*), and Eps15 (*Δ95/295*). Expression vectors carrying *wt* and mutant cDNA tagged with EGFP, and pEGFP-N1 as a negative control were transfected into Vero cells, incubated for 12hrs, and infected. (C, D) as described for (A) except for cholesterol depletion (Chol; D): To distinguish between cholesterol in the viral membrane and cellular cholesterol, cells were treated with progesterone together with nystatine (*P/N*) in the indicated concentrations overnight but not during infection. (E) NH₄Cl add-in during SFV infection. SFV was bound to the cell surface for 30 min at 4°C, washed with PBS, and incubated with pre-warmed infection medium to start infection. At the indicated time-points medium was replaced by pre-warmed 20mM NH₄Cl in infection medium and further incubated until trypsinization and fixation. Regression curves were fitted assuming Michaelis-Menten-Kinetics and 0% infection at time-point (TP) 0 min. VSV data are modified from (Johannsdottir, Mancini et al. 2009). (F) NH₄Cl wash-out during SFV infection in HeLa ATCC and Vero cells. SFV was bound to cells at 4°C and washed and replaced by pre-warmed infection medium (TP: 0 min) or 20mM NH₄Cl. For the other TPs the drug was replaced by 37°C infection medium at the corresponding TP. Total incubation was 4 hrs before fixation and FACS preparation. Abbreviations: Dynasore (Dyna), Chlorpromazine (CPZ), Bafilomycin A (BafA), Latrunculin A (LatA), Jaspokinolide (Jasp), Nocodazole (Noc), LY294002 (LY), Wortmannin (wort), Calyculin (Caly), Okadiac Acid (Oka), Deltamethrin (Delta), Endothall (Endo), Tautomycetin (Tauto), Genistein (Gen), Van (o-Vanadate).

No other protein came up in the screen that is known to be important for non-clathrin endocytosis pathways such as Arf6, Caveolins, and Flotillins.

Experiments using other perturbants than siRNA, namely small compound inhibitors as well as dominant-negative constructs against essential proteins of CME, supported the primary role of this pathway for SFV entry: 1) Chlorpromazine (CPZ), a well-known drug that perturbs recycling of clathrin and AP2 to the plasma membrane and, thus, blocks new formation of clathrin-coated pits and –vesicles (Wang, Rothberg et al. 1993), blocked infection of SFV by 90% as quantified by a FACS-based infection assay (see Fig. 18A and Materials and Methods); 2) the Eps15 deletion mutant, *eps15*(Δ 95/295), which lacks the EH domains of Eps15, inhibits internalization of physiological cargo such as EGFR and transferrin (Benmerah, Lamaze et al. 1998; Benmerah, Bayrou et al. 1999; Sigismund, Woelk et al. 2005) but also the clathrin-dependent Vesicular Stomatitis Virus (VSV) (Sun, Yau et al. 2005). SFV infection is reduced by more than 50% (Fig. 18B).

Infection of *eps15*(Δ 95/295)-EGFP-positive cells was reduced by almost 60% (57.9%) compared to EGFP, while expression of Eps15-wt-EGFP had no effect on SFV infection (Fig. 18B). 3) dynasore, a specific inhibitor of dynamins (DNM1, 2, and Drp1; (Macia, Ehrlich et al. 2006)), almost completely blocked infection (-96.0%, Fig. 18A) in a concentration, which efficiently blocks the uptake of transferrin, a cargo that exclusively employs CME (Macia, Ehrlich et al. 2006). Moreover, the DNM2 dominant-negative mutant DNM2-K44A (Damke, Binns et al. 2001) reduced infection by 86.6% in FACS compared to control cells that have been transfected with EGFP only (Fig. 18B).

Most of the SFV hits are endosome-related (see Fig. 11B). Endosomes are essential for successful infection of the virus since their acidic interior serves as the trigger for fusion of the viral envelope membrane with that of endosomal vesicles. Indeed, inhibitors of the vacuolar proton pump (V-ATPase) such as Bafilomycin A (BafA, Fig. 18A) or buffering compounds such as Ammoniumchloride (NH₄Cl; Fig. 18E, F) block infection almost completely (Helenius, Kartenbeck et al. 1980). SFV infection experiments with NH₄Cl add-in and wash-out at certain time points are useful to determine the half time of sensitivity to an acidic environment of the virus. Fig. 18F shows wash-out experiments for SFV in HeLa and Vero cells and implicates a cell line-independent early time point of less than 10 min after synchronous start of infection by warming to 37°C (time point 0min). To further quantitate the half time, we performed an NH₄Cl add-in experiment for SFV in comparison with VSV (modified from (Johannsdottir, Mancini et al. 2009), Fig. 18E), another virus that depends on CME and acid-mediated fusion in the endosomal compartment (ref). By Michaelis-Menten-based curve fitting the approximated half times of SFV (5.5 min) versus VSV (1.6 min) could be determined, which confirms previous findings in other cell lines (Kielian, Marsh et al. 1986; Schmid, Fuchs et al. 1989).

Cargo endocytosed by CME is trafficked to and fuses with early endosomes (EE) in a Rab5-dependent manner (Gorvel, Chavrier et al. 1991; Bucci, Parton et al. 1992; Zerial and McBride 2001). There are

three isoforms of Rab5, “a”, “b”, and “c”, which share more than 90% of sequence identity (Chen, Kong et al. 2009). All isoforms are part of the Usual Suspects screen, and two of them appear as hits for SFV: Rab5a (HeLa CNX) and Rab5c (HeLa ATCC and CNX) with the “c” isoform being the stronger hit (see Fig. 5). The importance of Rab5a for SFV infection was demonstrated in a previous study by using the dominant-negative mutant of this small GTPase (Sieczkarski and Whittaker 2003) as well as by time lapse microscopy of fluorescently labeled SFV and Rab5 (Vonderheit and Helenius 2005). About the potential role of Rab5c much less is known. Although all isoforms have been localized to the early endosomal compartment (Zerial and McBride 2001) there is growing evidence of differences in their regulatory functions. Phosphorylation sites and affinity to kinases are different *in vitro* among the isoforms (Chiariello, Bruni et al. 1999) and knock-down of Rab5a and b but not Rab5c delays degradation of the EGF receptor while internalization is unaffected (Chen, Kong et al. 2009).

Two members of the ESCRT complex, Hrs (HGS) and TSG101 are strong hits in the SFV screen. The ESCRT complex primarily mediates the formation of intraluminal vesicles (ILVs) within EEs, the initial process of the degradative endosomal pathway that sorts ubiquitinated cargo via LEs to (endo)lysosomes where hydrolysis takes place. It is thought that hrs concentrates ubiquitinated proteins destined for lysosomal degradation on the perimeter membrane of the early endosome (Raiborg, Bache et al. 2002) and recruits Tsg101, which in turn interacts with ubiquitinated proteins (Bishop, Horman et al. 2002); it is required for efficient degradation of EGF/EGFR (Doyotte, Russell et al. 2005).

Depletion of Hrs and especially TSG101 has strong impact on the morphology and function of LEs but also EEs, primarily with regard to lower numbers of ILVs and increased vacuolar size after EGF stimulation (Doyotte, Russell et al. 2005; Razi and Futter 2006). Interestingly, tsg101 depletion causes impaired acidification (Bache, Stuffers et al. 2006). The latter effect might explain why SFV infection is decreased by knock-down of tsg101 (see Table 1). Whether acidification is also impaired in hrs depleted cells is unknown.

Rab7b, another strong hit in the SFV screen, is an isoform to the better characterized marker of late endosomes, Rab7a, which is not a hit in all screens. Although both are localized to late endosomes only Rab7a is involved in EGFR degradation (Progida, Cogli et al. 2010). In contrast to Rab7a, Rab7b is located also on lysosomes as well as Golgi and TGN (Bucci, Bakke et al. 2010). It has been shown that trafficking and maturation of cathepsin D, a lysosomal protease, is impaired upon depletion of Rab7b as well as dominant-negative Rab7b (Progida, Cogli et al. 2010). Maturation of cathepsin D occurs by self-cleavage of its precursor, prepro-cathepsin D and pro-cathepsin D. Since its proteolytic activity is dependent on pH this maturation defect upon Rab7b depletion might directly or indirectly be due to impaired acidification. That RNAi against Rab7a did not appear in any hit list indicates improper depletion.

2.4.2.3 SFV infection requires a functional recycling endosomal compartment

Besides the classical markers for CME and early endosomes, proteins of cellular recycling pathways were enriched in the hit list: Rab11 family interacting protein 5 (class I) (RAB11FIP5) as the second strongest hit in both cell lines (hit score of 36.5 see Table 2; reduced SFV infection by 95% using FACS assay of the strongest siRNA in Fig. 16); the small GTPase isoforms Rab11a and Rab11b in both cell lines; and Rab4b (only in HeLa CNX).

Rab4 and Rab11 are markers for rapid (directly from peripheral endosomes) and slow (perinuclear endosome-dependent) recycling routes and form distinct membrane domains on early or recycling endosomes (Mellman 1996; Maxfield and McGraw 2004). Together with Rab5 they regulate sequential transport steps e.g. of transferrin along the endocytic/recycling pathway (Sonnichsen, De Renzis et al. 2000). RAB11FIP5, or Rip11, is one of eight so-far identified Rab11 interacting proteins, and is localized to peripheral endosomes where it regulates together with Rab11 the sorting of internalized receptors to the slow recycling pathway (Schonteich, Wilson et al. 2008). Recently, Oelke et al found that Rab11a and b can interact with vesicular ATPase, and that Rab11b together with Rab11FIP5 are involved in trafficking of V-ATPase, the endosomal proton pump, in polarized cells (Oehlke, Martin et al. 2011). The number of Rab11 and –interacting proteins appearing as hits and their strong phenotypes on SFV infection implies an important role in infection.

2.4.2.4 Role of ER/Golgi/Secretion Hits in SFV Infection

Syntaxin 5 (STX5A), a SNARE (SNAP receptor) for ER-to-Golgi vesicle transport (Nichols and Pelham 1998; Pelham 1998), is the strongest SFV hit in both cell lines (see Fig. 13A, hit score 39.5) with all three siRNA as being significant (see Fig. 12C). To verify the screening data we used a FACS-based infection assay with transfection of HeLa CNX cells with Hs_STX5_1, the strongest siRNA against STX5 in the screen, in 12 well plates according to a 12 well plate-adapted screening protocol (see Materials and Methods). Hs_STX5_1 decreased infection under these conditions by 85% \pm 10% compared to wells with a negative control siRNA (ASN; see Fig. 16A).

STX5 is the primary tSNARE at the Golgi and is implicated in inner-Golgi-(Fernandez and Warren 1998) and ER-to-Golgi transport (Dascher, Matteson et al. 1994; Hay, Chao et al. 1997) but also in endosome-to-TGN trafficking of bacterial toxins such as shigatoxin (Tai, Lu et al. 2004; Amessou, Fradagrada et al. 2007). Recently, STX5 was identified in an RNAi screen to be essential for constitutive secretion in mammalian cells (Gordon, Bond et al. 2010) and hence thought to be important for the transport of many extracellular and transmembrane proteins to the cell surface, including potential virus receptors. To test whether the decrease of SFV infection is primarily due to reduced binding of virus at the virus receptors on cell surface we used a radiolabeled [³⁵S]-SFV binding assay. 200'000 cpm virus stock was incubated for 1hr at 4°C with HeLa ATCC cells, which were transfected before for 72hrs with Hs_STX5_1 and control (AllStarsNegative) siRNA. Under these conditions virus particles bind to the cell surface but are not endocytosed. After thoroughly washing cells were detached in the cold by incubation with 20mM EDTA / PBS for 30min and

scraping, and pelleted in a centrifuge at 1'000 x g for 5 min. The pellets were resuspended in scintillation liquid and radioactivity was measured with a scintillation counter. Figure 16B shows that SFV binding was dramatically reduced (-87%) compared with negative control. This suggests that the strongly reduced infectivity of SFV in STX5-depleted cells is due to a lack of binding of the virus on the cell surface, presumably due to impaired secretion of the viral receptor(s).

2.4.2.5 SFV Depends on Functional Protein kinase C Isoforms

Protein kinase C family isozymes alpha (PRKCA) and delta (PRKCD) are hits for SFV (Table 2). For each hit two siRNA reduced SFV infection significantly (see Fig. 19A and B) and independently of cell lines (Table 1). While PRKCA is a so-called “classical” PKC i.e. Ca^{2+} - and DAG-dependent, PRKCD is a member of the “novel” PKC subgroup and is independent of Ca^{2+} -signaling but dependent on DAG. The PKC family of isozymes is long known as regulators of receptor endocytosis (Takai, Kishimoto et al. 1977; Constantinescu, Cernescu et al. 1991; Webb, Hirst et al. 2000; Alvi, Idkowiak-Baldys et al. 2007). It has also been implicated in the entry of Adenovirus (Nakano, Boucke et al. 2000) and Influenza virus (Sieczkarski, Brown et al. 2003).

To validate the screening hits we used several more or less specific PKC inhibitors such as staurosporin (Stauro), Calphostin C (CalC), Gö6976 (Gö), and CGP53353 (CGP; see Figure 19C). Stauro strongly inhibits PKC (Tamaoki, Nomoto et al. 1986; Ruegg and Burgess 1989) but also MLCK with similar potency (Gschwendt, Furstenberger et al. 1995). SFV infection was strongly inhibited at moderate (2 μM) and almost blocked at high concentrations (-91.8% at 10 μM ; Fig. 19C). Up to 50% of the cells at the highest concentration detached during the incubation time (4 hrs) presumably since Stauro has a strong pro-apoptotic effect after 2-3hrs incubation in several cell lines (Zhou, Li et al. 1998).

To distinguish between PKC and MLCK effects specific inhibitors of both families were tested. CalC is a specific inhibitor of the PKC isozymes without strong preference to sub-types and blocks Adenovirus 2 (Ad2) escape from endosomes at a concentration of 5 μM (Nakano, Boucke et al. 2000). Already 500nM CalC drastically reduced SFV infection (Fig. 19C) with only a minor effect on viability judged by cell detachment.

A specific inhibitor of the classical PKC isozymes, CGP53353 (CGP) (Chalfant, Ohno et al. 1996), reduced SFV infection concentration-dependently and blocked almost completely infection at 50 μM (-97.3%; Fig. 19C). A derivative of Stauro, Gö6976 (Gö) is also specific to classical PKC (Conner and Schmid 2003) at concentrations up to 30 μM (Gschwendt, Furstenberger et al. 1995; Hofmann 1997; Maddali, Korzick et al. 2005; Matsuo, Hotokezaka et al. 2006; Van Kolen and Slegers 2006). While 30 μM Gö does not affect Vaccinia virus infection (Mercer, Knebel et al. 2010) it completely blocked

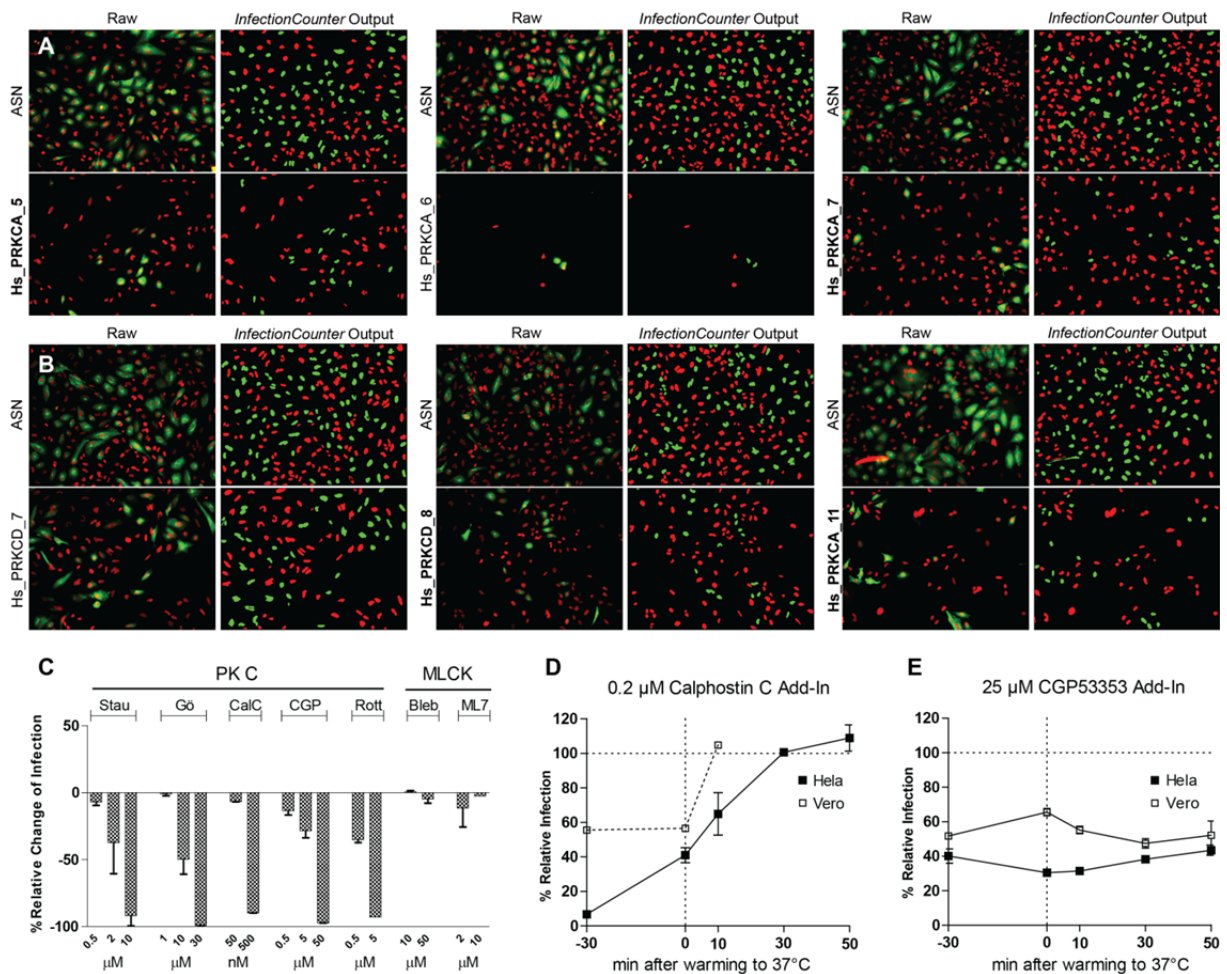


Figure 19

Protein Kinase C plays a role in SFV infection. (A, B) Two PKC hits (PRKCA; PKC alpha and PRKCD; PKC delta) of the SFV Usual Suspects screen are shown with example images from 3 targeting siRNA. “Raw” RGB images were created by merging one of 16 gray-scale images per well of one replicate showing staining for SFV envelope (green) and Hoechst 33258 nuclei (red). Binary red/green overlap images (*InfectionCounter* Output) show all identified nuclei belonging to non-infected cells (red) or infected cells (green). Those siRNA that were identified as significant are indicated by bold siRNA. For all siRNA except Hs_PRKCA_6 at least 400 cells per well (averaged over all replicates) could be detected. Hs_PRKCD_7 does not significantly reduce infection. Significance was calculated from averaged, normalized, and cell density-corrected z-scores and ranks, while the images shown are selected example images to show the principle. (C) PKC inhibitors of different specificity or MLCK inhibitors were applied in the indicated concentrations to Vero cells 30 min before, and during, SFV infection. Drug pretreatment and infection was done in minimal medium (MEM) buffered with 20mM HEPES pH7.2 at 37°C. Virus stock was diluted to reach 30-40% absolute infection. Cells were fixed after 4hrs and prepared for FACS analysis. Infection was detected by antibody staining against the envelope proteins of SFV. (D) Add-in of 200nM Calphostin C to HeLa ATCC or Vero cells at the indicated time points (TP). SFV was bound to the cells for 30min either with (TP -30min) or without the drug at 4°C on ice. At TP 0min cells were washed with 37°C prewarmed infection medium either with the drug (for TP 0min) or without. For TPs +10, +20, and +50min the drug was applied to the medium under thorough shaking. After in total 4hrs cells were detached by trypsin/EDTA treatment for 10 min, fixed (4% HCHO in PBS for 30min) and stained for FACS analysis of SFV infection as described above. (E) analogous to (D) but with 25μM CGP53353 as the drug to be added.

SFV infection (-99.2% at 30 μ M; Fig 19C). This is in contrast to what has been reported for SFV (Mario Schelhaas (not published))(Sieczkarski, Brown et al. 2003) but corresponds to the screening hits for SFV and VACV (Table 2): while PRKCA as a classical PKC is a strong hit for SFV it is not for VACV. In contrast to PKC inhibitors, MLCK-specific drugs such as ML7 and Blebbistatin (Bleb) did not show a significant effect on SFV infection (Fig. 19C).

We then performed drug add-in experiments to temporally localize the inhibitory effect on SFV infection, essentially as described for NH₄Cl. We used CGP and CalC in concentrations that reduced but did not block SFV infection in the infection assay before. Vero and HeLa cells were used to examine whether the PKC effect on SFV infection is cell line-dependent. 200nM CalC reduced SFV infection by 50% in Vero cells and by more than 90% in HeLa cells when added during virus binding in the cold and during the following 4 hrs infection at 37°C (add-in time-point “-30min”). However, the drug showed no effect on infection any more when added after 10min (Vero) or 30min (HeLa) post-warming, respectively (Fig. 19D). 25 μ M CGP, applied for pre-incubation, reduced infection in both cell lines to 40-50% compared with the negative control (DMSO). In contrast to CalC, add-ins of CGP at later time-points until 50min post-warming did not significantly change the inhibitory effect of the drug on infection (Fig. 19E). Compared with the add-in curve for NH₄Cl the inhibitory effect of CalC on SFV infection can be roughly localized to the viral fusion event during entry (Vero) or slightly later (HeLa) while the CGP effect is significantly later.

2.4.3 Screening of Simian Virus 40 (SV40)

2.4.3.1 Introduction

Unlike SFV, SV40 is a non-enveloped polyoma virus that replicates its DNA genome in the nucleus. Virus particles bind to GM1, a ganglioside on the cell surface, and are internalized via caveolae/lipid raft-mediated endocytic mechanisms (Hummeler, Tomassini et al. 1970; Kartenbeck, Stukenbrok et al. 1989; Smith, Lilie et al. 2003; Tsai, Gilbert et al. 2003; Ewers, Romer et al. 2010). Hereafter, the virus spends several hours intracellularly after it is found in ER structures, where it penetrates through ER membranes and transfers its genome to the nucleus (Engel, Heger et al. 2011). It has been proposed that the incoming virus accumulates in so-called caveosomes, defined as large, pH-neutral, endocytic organelles, and primarily bypasses endosomes before it traffics to the ER by unknown mechanisms (Pelkmans, Kartenbeck et al. 2001). Although SV40 had been found in early endosomes by EM and confocal microscopy (Kartenbeck, Stukenbrok et al. 1989; Pelkmans, Burli et al. 2004) it was assumed that these particles used a dead-end pathway. This was based on the findings that 1) the majority of virus particles could not be co-localized with endosomal markers; 2) SV40 infection seemed to be acid-independent since drugs affecting endosomal acidification did not reduce infection; 3) dominant-negative endosomal Rabs had no effect on infection (Pelkmans, Kartenbeck et al. 2001). In contrast to this, our lab recently found that caveosomes are not independent organelles but rather enlarged late endosomes or endolysosomes, in which fluorescently tagged caveolin-1 (Cav1-EGFP) has been accumulated (Engel, Heger et al. 2011).

2.4.3.2 SV40 Hits of Endosomal Compartments are enriched

Interestingly, and in contrast what we expected, almost 60% of the hits (15) were genes that have been associated with endosomal functions. Among those were all three Rab5 isoforms, hrs, phosphoinositide-3-kinase class 3 (PIK3C3), the major PI3P-synthesizing enzyme at early endosomes (Christoforidis, Miaczynska et al. 1999; Murray, Panaretou et al. 2002), Rab4a, a marker for the fast recycling pathway (van der Sluijs, Hull et al. 1992; Maxfield and McGraw 2004), and EHD1, which mediates recycling of molecules such as the transferrin receptor and others (Lin, Grant et al. 2001; Jovic, Kieken et al. 2009). This accumulation of endosome-related genes therefore resembles the hit lists of SFV and VSV, viruses that utilize endosomes for entry and differs from VACV that does not transit through endosomal compartments and, in line with this, also did not produce endosomal hits (Fig. 20A). Moreover, classical representatives of caveolin- and raft-mediated endocytosis, such as Cav-1, 2, Flot1, 2 did not appear for SV40 (Fig. 20A). For Cav-1 this is in accordance with previous findings that SV40 infection in Cav-1-knock out cells is not impaired (Damm, Pelkmans et al. 2005).

2.4.3.3 SV40 Colocalizes with Endosomes

Since the strong representation of endosomal hits is in stark contrast to previous findings and models (Pelkmans, Kartenbeck et al. 2001), in which the infectious route of SV40 bypasses endosomal compartments, we analyzed to what extent incoming viruses enter endosomes. We colocalized fluorescently labeled SV40 particles with diverse constructs of endosomal proteins tagged with fluorescent proteins, which have been transfected by electroporation into CV-1 cells, and used live microscopy to avoid fixation. We recently found that fixation leads to burst and modifies the morphology of late endosomes and endolysosomes. We used CV-1 cells since they are bigger and more suitable for electroporation as well as live cell microscopy than HeLa cells (own observation and (Vonderheit and Helenius 2005)).

First, we colocalized SV40 with hrs and Rab5a. CV-1 cells were transfected with Hrs-EGFP and Rab5a-EGFP plasmids respectively, and infected with SV40 particles labeled with AF647. Hrs is a strong hit in SV40 but also in the SFV screen; it is an early endosomal protein and, as a ESCRT 0 component, important for the sorting mechanism into the degradative pathway. Indeed, in hrs-EGFP-transfected cells we found fluorescently labeled SV40 particles in hrs-positive organelles 145 min after warming (Fig. 20C). Virus colocalized also with another early endosomal marker, EEA1 (early endosomal antigen 1) in bigger, more perinuclear early endosomes (Zoncu, Perera et al. 2009) (shown in (Engel, Heger et al. 2011)). Rab5a is a small GTPase important for homotypic fusion and maturation of early endosomes. Its constitutively active form, Rab5Q, causes enlarged early endosomes and blocks sorting of cargo to late endosomes due to inhibition of endosome maturation (Flinn, Yan et al. 2010; Wegner, Malerod et al. 2010). When CV-1 cells were transfected with Rab5Q-EGFP a day before and infected for 2 hrs with fluorescently labeled SV40, virus accumulated in large vesicles positive of green Rab5Q signal (Fig. 20E).

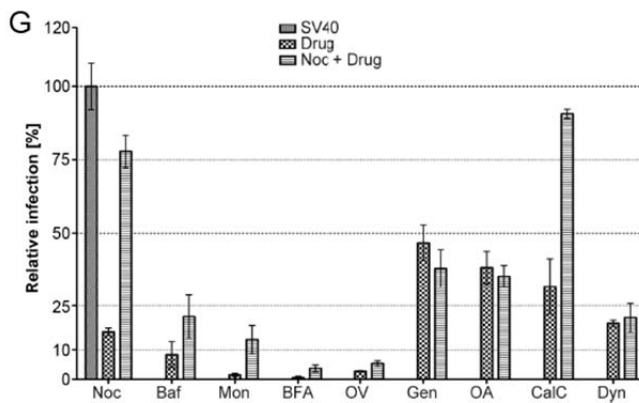
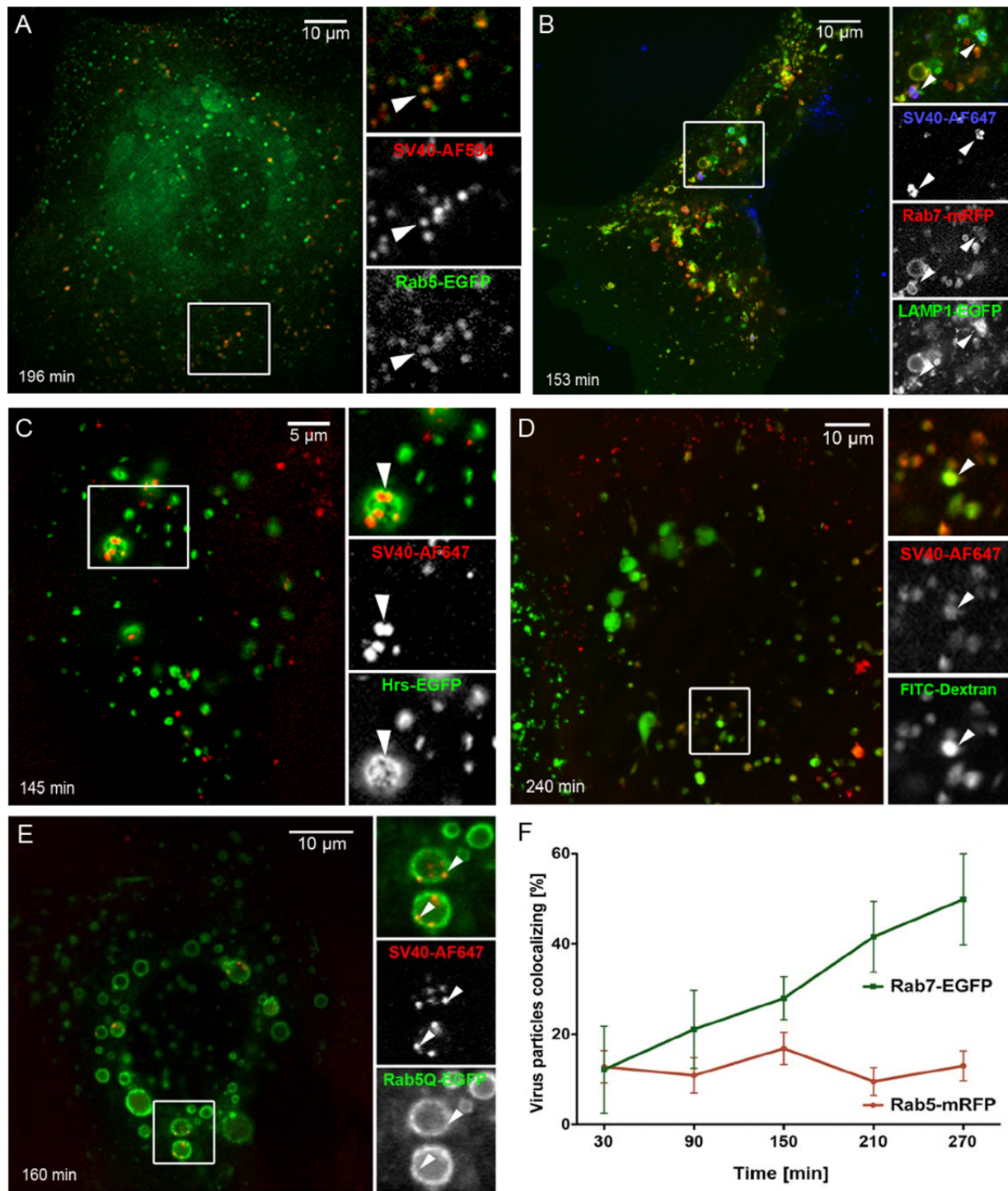


Figure 20

SV40 colocalizes during entry with markers of early and late endosomes. Inhibitors against acidification, dynamin, kinases, phosphatases and Golgi function impair infection at both early and late phases of the entry pathway while PKC inhibitor only affects early entry steps. (A-C) Fluorescently labeled SV40 was added to CV-1 cells transfected with tagged versions of the indicated early and late endosomal proteins. Images were recorded live on a spinning-disc (A, B) or a Zeiss LSM 510 confocal microscope (C) at the indicated time points. (D) CV-1 cells were pulsed for 2hrs with FITC-Dextran, pulsed over night, and incubated with fluorescently labeled SV40 on ice for 2 hrs. Images were recorded after 4 hrs after warming to 37°C on a Zeiss LSM 510 confocal microscope. (E) CV-1 cells were transfected with Rab5Q-EGFP over night and infected with SV40-AF647. Images were recorded 160 min post-warming. (F) Quantification of colocalization of SV40-AF647 with Rab5a-mRFP and Rab7a-EFP. (G) CV-1 cells incubated with 5µM Nocodazole (Noc) were infected with SV40 for 24hrs. The drug was washed out at 8hrs postwarming, or different drugs were added after the washout. Cells were fixed and stained for SV40 T-antigen and prepared for FACS analysis. Infection was normalized to drug-free controls. Shown are means \pm SEM from three independent experiments. Abbreviations: Baf – Bafilomycin A, Mon – Monensin, BFA – Brefeldin A, OV – o-Vanadate, Gen – Genistein, OA – Okadaic Acid, CalC – Calphostin C, Dyn – Dynasore. Modified from Engel, Heger et al.

To quantify colocalization of SV40 with early and late endosomes without perturbation, we double-transfected CV-1 cells with Rab5-mRFP and Rab7-EGFP and infected them with fluorescently labeled SV40 over 4.5 hrs and imaged every 60min using a Zeiss 510 LSM confocal microscope. A MATLAB-based colocalization analysis tool (Peter Horvath, LMC) was used to quantify virus colocalization with early endosomes (Rab5a positive) and late endosomes (Rab7-positive). The percentage of SV40 particles that colocalize with Rab5-mRFP did not change over the experimental time frame (at time point 150 min: 16.8% \pm 3.6%; Fig. 12F), which is in agreement to previously reported observations (20% \pm 6%, from (Pelkmans, Burli et al. 2004)). However, colocalization with Rab7-EGFP increased continuously until almost half (49.9% \pm 10.1%) of the spots colocalized with SV40 (Fig. 20F).

To be sure that transfection and overexpression does not alter SV40 trafficking we visualized late endosomes/endolysosomes by pulse-chasing of fluorescently labeled Dextran. CV-1 cells were pulsed with FITC-Dextran for 2 hours, washed, and incubated in full medium overnight. Four hours before imaging SV40-AF647 was applied to the cells. Fig. 20D shows eminent colocalization of SV40 with FITC-Dextran.

2.4.3.4 SV40 is Sensitive to Inhibitors of Acidification, Dynamin, and Protein Kinase C

Among many other functions microtubules are important for endosomal maturation and fusion with lysosomes (Aniento, Emans et al. 1993; Bayer, Schober et al. 1998; Baravalle, Schober et al. 2005; Driskell, Mironov et al. 2007). Nocodazole is a reversible inhibitor of microtubule polymerization. The fact that the drug blocks SV40 infection due to accumulation of virus particles at the level of maturing endosomes (Pelkmans, Kartenbeck et al. 2001) can be used to divide the entry pathway of SV40 into two parts, early events until maturing endosomes, and late events during which SV40 transits to late endosomes and finally to the ER. To take advantage of the Noc effect we incubated CV-1 cells with Noc for 8hrs and replaced it with several drugs for the remaining time.

We applied drugs that increase endosomal pH such as BafA and Monensin (Mon). Infection was almost blocked in the presence of the carboxylic ionophore Mon and BafA before and after the Nocodazole block (Fig. 20G, “Baf”, “Mon”).

Two PKC isozymes, PRKCG (PKC gamma) and PRKCZ (PKC zeta), are hits in the SV40 screen. Using Calphostin C we found indeed a strong block of infection (Fig. 20G, “CalC”). Fig. 20G shows that CalC did not inhibit virus infection after the Noc block suggesting that there is a PKC-dependent step upstream of maturing endosomes. Since CalC primarily inhibits classical PKC isozymes at the concentrations we used for the experiments it is likely that PRKCG is the target of the drug and causes the block of SV40 infection.

DNM2 (Dynamin-2) is another strong hit of the SV40 screen. A previous study showed reduction of virus infection when cells were transfected with a dominant-negative DNM2 construct. The internalization assay with Nocodazole showed that Dynasore, an inhibitor of dynamins (Macia, Ehrlich et al. 2006; Kirchhausen, Macia et al. 2008), blocked SV40 in a post-Nocodazole step (Fig. 20G, “Dyn”). Similar effects revealed inhibitors of kinases (Genistein, “Gen”), phosphatases (o-Vanadate “OV”, Okadaic Acid “OA”) as well as the Arf protein inhibitor Brefeldin (“Bre”).

Taken together, we could validate important hits for the SV40 screen, and found strong evidence that 1) SV40 is sorted into the endosomal compartment, from early to late endosomes and finally endolysosomes; 2) the endosomal pathway is the infectious pathway of SV40; 3) endosomal acidification and Dynamin are important in multiple steps in infection; 4) protein kinase C inhibitors impair an early step in infection.

3 DISCUSSION

Since its discovery, the broad usage of RNA interference-based screening technology has proven its efficiency and reliability in various fields of cell biology. In this thesis, we present the development and validation of a versatile siRNA screening platform strategy that allows identification of host cell proteins and pathways essential for the entry of viruses. As part of this platform, we developed an image analysis program that is capable of processing images from diverse automated microscopes. We screened six viruses, Semliki Forest virus (SFV), Vesicular Stomatitis Virus (VSV), Simian Virus 40 (SV40), influenza A Virus (FLU), Vaccinia Virus (VACV), and Uukuniemi Virus (UUK). New proteins and pathways could be identified, and for SFV and SV40, some of them were validated and further characterized using small molecules inhibitors, dominant negative variants of cellular proteins, and live cell imaging.

For the screening project we used a siRNA library targeting 108 human genes that are related to several pathways of endocytosis, membrane trafficking, secretion, and signaling. We carefully chose these genes based on several sources: 1) lab-wide expertise on pathway-related proteins; 2) the literature that was available at the time we started the project (2005); 3) a similar approach that identified CME as the entry pathway for respiratory syncytial virus (RSV) (Kolokoltsov, Deniger et al. 2007); 4) a screen with Adenovirus (Jurgeit A, Greber UF; personal communication).

For SFV we found proteins associated to clathrin-mediated endocytosis and endosomal sorting, which we could validate and were consistent to previous findings. Moreover, we identified Syntaxin 5 as important for SFV binding to the cell surface presumably due to a role in secretion of the virus receptor. We showed that different Protein Kinase C isoforms are involved in infection of SFV and SV40 and presumably other viruses. Especially we could identify a classical PKC dependent step on the level of endosomal sorting and maturation of several viruses. Our data furthermore indicate that recycling endosomal proteins are crucial factors for infection of several viruses.

The most important result is that SV40 entry depends on proteins that are associated with the endosomal pathway, whereas caveolin-1 knock-down had only a moderate effect. This led us to revise the former model of SV40 entry that proposed trafficking of the virus through caveosomes, bypassing endosomes. Instead, we propose an endosomal, acidification-dependent route similar to what has been found for the related mouse polyomavirus from the same family (Ashok and Atwood 2003; Liebl, Difato et al. 2006).

We developed a modular screening platform that standardizes the screening process to minimize variances between screens and is flexible enough to allow screening of diverse viruses. We maximally

standardized crucial, non-virus specific steps of the screening protocol such as siRNA library handling, cell transfection, image analysis, data processing, significance calculations of siRNA and hit determination. The screening platform is still flexible enough to simply integrate different virus-specific assays for infection, staining, and imaging.

Standardization within the screening process also includes image analysis. We developed *InfectionCounter* a program that quantifies cell number and infection index from images recorded by automated microscopes. The major criteria were quality and reproducibility in analyzing images, compatibility to diverse viruses and infection assays, computer and microscopy systems, as well as user-friendliness.

We achieved these requirements in several aspects. First, we performed tests to show that our analysis strategy, especially the robust edge detection algorithm, which we implemented to analyze both channels, is relatively unsusceptible to varying image quality and is compatible to diverse virus infection assays. We showed that the error of object detection was less than 5% when considerable artificial noise or Gaussian blur was added to a test image to simulate underexposed and out-of-focus images. The software was able to identify almost all infected cells on test images from six different viruses using infection assays based on immunofluorescence or expression of fluorescent proteins. Also we showed that variability of detected cell numbers and infected cells is very low when different users analyze the same data set with individually adjusted parameters based on subjective impression of optimal segmentation and classification.

Secondly, we developed an ergonomic graphical user interface (GUI), in which all necessary settings, files, and functions can be modified, and the current status of analysis is clearly visible. On an optionally activated second GUI window the current analysis can be supervised. Moreover, the extracted parameters appear in a text field and are saved as overlay images and text files, which are highly compatible to downstream analysis software.

Furthermore, the file import function simplifies loading of large image sets from different microscopy controlling software. It allows encoding the file names of complete image data sets in a single string with user-defined counters representing plate numbers, row, column, and site IDs – without the need of multiple file selections and drag-and-drop.

We successfully integrated *InfectionCounter* in our screening platform and analyzed during this project screens of six different viruses in different cell lines comprising more than 30'000 images. The extracted image information of cell number and infected cells was normalized and subjected to a careful quality control. This comprised checks of transfection efficiency in the positive controls, in which we used siRNA against KIF11, a microtubule motor protein that is responsible for bipolar spindle assembly. Its knock-down leads to mitotic arrest, activation of the spindle check point, and finally apoptosis (Zhu, Zhao et al. 2005; Sarli and Giannis 2006). Cell number reduction should be at

least 7-fold to the negative control. Also we checked for siRNA toxicity and absolute infection levels being in the range of 10-40% to ensure quality of the screens. Since virus infection often depends on its population context such as varying cell density (Snijder, Sacher et al. 2009; Snijder and Pelkmans 2011) we corrected the infection data from those viruses that showed a strong density effect. This was the case for all viruses except VACV, consistent with previous findings (Snijder, Sacher et al. 2009).

From these normalized and corrected raw data hits were determined by a three step filtering based on how strongly the siRNA reduced infection. For that, we filtered significant from non-significant siRNA was whether their effect on infection was stronger than a certain threshold, which was determined from the distribution of the negative controls of each screen. We implemented this criterion into the two different methods to normalize and sum replicate data, one based on z-scoring, the other based on ranking. To determine hits we applied a 2-out-of-3 criterion i.e. at least two siRNA effects related to the same gene must be significant in order to be considered as a hit. Finally, we determined from those primary hits so-called “final hits”, which are independent from cell lines and scoring methods. This allows comparing viruses with each other that were screened with one or two cell lines.

Interestingly, the two methods that we employed to define significant siRNA, one based on z-scoring, the other on ranking, only marginally differed at strong hits while the hit lists showed considerable differences among weak hits. This confirms similar findings in recent systematic tests on different analysis methods by the Swiss InfectX consortium (personal communication).

Indeed, the final hit lists differed in the number of hits: we found 16 for SFV, 27 for SV40 and VSV, 24 for FLU, 11 for UUK, and 5 for VACV. Some of the hits and pathways of SFV and SV40 could be validated and confirmed. In general the hits that we identified reduced infection by 50% and more indicating relatively stringent hit definition. This was confirmed by FACS quantitation of several hit siRNA for SFV.

The stringent hit definition is one explanation why the VACV screen identified only 5 hits whereas for SFV and VSV we could determine 16 and even 27 hits. Another reason is certainly that SFV and VSV depend on pathways that are over-represented in the screening library, namely clathrin-mediated endocytosis and endosomal sorting. VACV, on the other hand, enters cells via macropinocytosis (Mercer, Knebel et al. 2010), a process that is much less characterized on the molecular requirements and therefore under-represented in the library. Another factor is varying dynamic ranges of siRNA effects, which depend on the particular virus infection assay and the underlying signal, antibody staining or fluorescent protein expression, but also the quality of experimentation since the threshold that determines significant siRNA effects is based on the spreading of the negative controls.

We analyzed the hit lists of two viruses, SFV and SV40, in detail and validated several hit siRNA, proteins, and pathways with various methods such as Western blots, small compound inhibitors,

dominant-negative mutants of proteins, FACS-based infection assays, radioactive binding assays, and live cell imaging and colocalization analysis of fluorescent virus and fluorescently tagged proteins during entry of transfected cells.

The knock-down efficiency of 21 hit siRNAs of mostly SV40, but also SFV, UUK, FLU, and VSV, was quantified by Western Blots. The reduction ranged from about 40% until more than 95% and confirmed siRNA effects on the target proteins. For SFV we validated the image-based quantification of siRNA effects on virus infection by an FACS infection assay. Selected hit siRNA reduced infection to a similar level previously shown by the screen, confirming the feasibility of the image-based analysis of siRNA effects.

Most of the hits for SFV are endosome-associated proteins, and factors involved in clathrin-mediated endocytosis (CME). We identified a component of the clathrin coat, clathrin heavy chain, phosphatidylinositol-5-kinase type I gamma, the major enzyme that synthesizes PIP2 on the plasma membrane (Conner and Schmid 2003), and a regulatory subunit of the clathrin adaptor complex AP2 (Nesterov, Carter et al. 1999; Collins, McCoy et al. 2002). It is long known, primarily based on EM data, that SFV is internalized by CME (Helenius, Kartenbeck et al. 1980). This is confirmed by the use of perturbants against important factors of CME: chlorpromazine, a drug that blocks recycling of clathrin and AP2 to the plasma membrane, also blocks SFV infection (Fig. 18). Furthermore, we showed by the specific inhibitor dynasore (Kirchhausen, Macia et al. 2008) and a dominant-negative mutant that SFV infection is dependent on dynamin-2, a small GTPase that is involved in fission of clathrin-coated vesicles from the membrane (Schmid and Frolov 2011). Moreover, a dominant negative mutant of Eps15, known to affect CME of some cargo such as transferrin (Benmerah, Bayrou et al. 1999), reduces infection by 50%. This confirms the core function of CME in SFV infection.

Interestingly, the screen suggests a role of AP2 in SFV entry. This adaptor complex has been long seen as essential for formation of all clathrin-coated pits and vesicles and uptake of cargo. However, recent studies showed that the internalization of transferrin but not EGF receptor or low-density lipoprotein (LDL) receptor are dependent on AP2 (Motley, Bright et al. 2003; Wang, Huang et al. 2003; Robinson 2004). Consistent with this, VSV infection was unaffected or even slightly enhanced upon depletion of the AP2 alpha and mu subunit (Johannsdottir, Mancini et al. 2009), while our data indicate a more important role for SFV. That only one of the four subunits of AP2 is a hit does not surprise since depletion of AP2, but also of clathrin, is known to be difficult probably due to long protein life time (Doherty and McMahon 2009).

Endosomal proteins predominate the hit list with more than 60% of all identified hits in the SFV screen. We found primarily early but also recycling endosomal proteins. That SFV traffics through the endosomal compartment was first shown by EM, and by the sensitivity of the virus to inhibitors of endosomal acidification (Helenius, Kartenbeck et al. 1980). In particular, it was shown that fusion of the viral envelope is activated in mildly acidic environment of pH 6.2 (Marsh, Bolzau et al. 1983), and

that the acid-sensitive step occurs within 1-5 min of internalization (Mercer, Schelhaas et al. 2010) – both consistent with early endosomes as the site of fusion. This was further confirmed by dominant-negative mutants of the small GTPases Rab5 and Rab7, markers of early and late endosomes, respectively. While dn-Rab5 reduced infection by 50%, dn-Rab7 did not impair the virus (Vonderheit and Helenius 2005).

We could confirm these findings in different cell lines and, in part, with endosome-specific acidification inhibitors. Bafilomycin A1 blocked SFV infection, and ammonium chloride wash-out and add-in experiments in HeLa and Vero cells both had identical half times of inhibition, about 5 min after warming. This is later than the half time for VSV, which is about 2 min (Fig. 18), indicating that VSV fuses earlier in time than SFV. This is consistent with previous studies (Johannsdottir, Mancini et al. 2009).

Taken together, we found strong dependence of the virus on clathrin-mediated endocytosis, sorting into early endosomes, and endosomal acidification. This puts the virus in a row with many other viruses that exploit the classical endocytic route and enter the cytosol by fusion in acidic compartments (Mercer, Schelhaas et al. 2010). Alternative hypotheses such as delivery of the viral genome into the cytosol by a channel without the need of endocytosis and acid-dependent membrane fusion are clearly inconsistent to our screening and validation experiments (Kononchik, Hernandez et al. 2011).

Surprisingly, the strongest hit from the screen was syntaxin-5 (STX5), confirmed by FACS to strongly reduce infection by more than 85%. This protein is a t-SNARE responsible for membrane fusion in vesicle trafficking from ER and endosomes to the cis-Golgi (Nichols and Pelham 1998). Silencing of STX5 causes secretion defects of transmembrane proteins destined for the plasma membrane (Gordon, Bond et al. 2010). We showed that SFV binding to the plasma membrane was strongly reduced. These findings propose a role of syntaxin-5 in trafficking of the as yet unknown SFV receptor(s) to the plasma membrane (Fig. 21).

Furthermore, drug profiling revealed that SFV infection depends on Ser/Thr phosphoprotein phosphatases based on strong effects of the inhibitors Calyculin, Tautomycin, and Endothall on virus infection while Okadaic Acid and Deltamethrin showed only moderate inhibition at high concentrations. Also we found tyrosin phosphatases as important for infection based on inhibition by vanadate. Genistein, a tyrosin kinase inhibitor, blocked infection only at high concentrations. Actin and microtubule (MT) inhibitors did not have strong effects on infection in Vero cells. This might be a cell line dependent effect since actin and MT have been shown to play a role in the trafficking of SFV replication complexes from plasma membrane to modified lysosomes in BHK cells (Spuul, Balistreri et al. 2010).

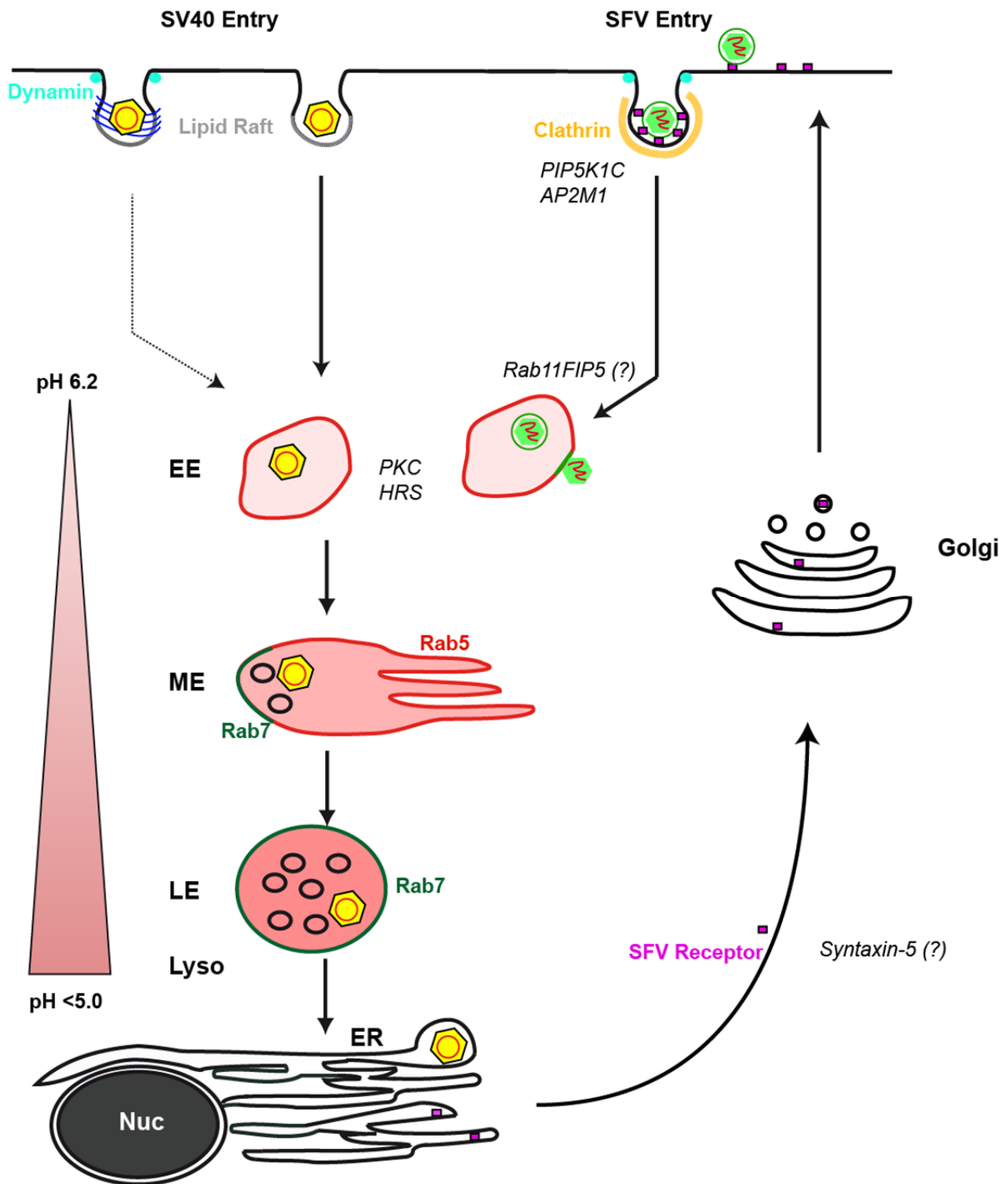


Figure 21

Model of the entry of SV40 and SFV. SFV binds to an as yet unidentified receptor and internalizes dependent on clathrin, dynamin, AP2M1, and phosphatidylinositol-5-kinase Igamma. SFV is sorted into mildly acidic early endosomes, fuses, and releases its capsid to the cytosol. The secretion of the SFV receptor is likely to dependent on syntaxin-5. SV40 enters cells primarily via clathrin- and caveolin-independent routes but to a minor portion also by caveolae. SV40 is sorted into early endosomes and acid-dependent to late endosomes/endolysosomes. From there the virus is trafficked to the ER where release to the cytosol occurs. SFV and SV40 depend on PKC in an early step of their entry routes, presumably at the stage of early endosomes.

The SV40 screen is the second that we further validated. The screen was done with one cell line only since susceptibility to SV40 was limited among the cell lines we used in the screen. Of the 30 preliminary hits that we obtained from the z-scoring method (published in (Engel, Heger et al. 2011)) 27 were also found by the ranking method and thus were designated as final hits. The three hits that fell out of the list were Dab2, Dynein heavy chain (DYNC2H1), and Rab22A; they were among the weakest hits of the z-scoring.

The final hits of the SV40 screen are primarily linked to endosomal protein sorting and vesicle transport pathways; also proteins related to the actin cytoskeleton, protein kinase C, and ER/Golgi-related secretory pathways appear in the hit list for SV40.

Some of the hits are expected: Protein kinase C zeta is known to play a role in SV40 signaling via its small t-antigen (Sontag, Sontag et al. 1997) while another hit, dynamin-2, was shown to reduce virus infection (Pelkmans, Puntener et al. 2002).

Our screen for SV40 showed clear enrichment of endosomal genes and in this point resembled the hit lists of SFV, VSV, and Influenza – viruses that are trafficked through endosomal compartments. We found strong reduction of SV40 infection when any of the Rab5 isoforms (Rab5a, b, and c), Hrs, c-Cbl, SNX15, Rab4b, Rab11b, PIK3C3, EHD1, and β 2-arrestin were depleted by siRNA. All of these proteins play diverse roles in endosomal sorting, regulation, and function.

This was surprising to us since it is in discrepancy to the current model of virus entry (Pelkmans, Kartenbeck et al. 2001). According to this, SV40 enters cells via a caveolin-1-dependent non-endosomal route that brings the virus from the plasma membrane finally to the ER. Furthermore, a new pH-neutral organelle, called caveosome, was proposed through which SV40 should be trafficked on this route, bypassing endosomal compartments (Pelkmans and Helenius 2002; Pelkmans, Burli et al. 2004).

We performed in-depth validations and could confirm several hits and pathways of the screen. We showed that SV40 traffics through the endosomal compartment for productive infection. Moreover, we found that both early and late steps of virus entry are strongly dependent on endosomal acidification. Based on these findings and recent studies in our lab concerning trafficking of Caveolin-1 (Hayer, Stoeber et al. 2010), we abandon the caveosome model and propose a new model in which incoming SV40 particles are sorted first into early endosomes then into late and most likely endolysosomes before they part to the ER.

The RNAi screen identified several early endosomal proteins such as Rab5a, Hrs, and PIK3C3 to be essential for productive infection. For some of them, Rab5a and hrs, we found significant colocalization with incoming virus using live cell imaging.

That the degradative endosomal pathway is involved in SV40 entry we showed by the finding that a majority of SV40 particles colocalized with the late endosomal marker Rab7 and with vesicles positive for FITC-Dextran, a marker for late endosomes and endolysosomes. Moreover, we could show quantitatively that the portion of fluorescently labeled virus colocalizing with Rab7 increased over several hours during entry until it reached about 50%. In the same time the portion of SV40 colocalizing with Rab5 remained constant at about 15%, which is consistent to previous results (Pelkmans, Burli et al. 2004). This speaks for a relatively fast sorting process of a major portion of incoming SV40 from early to late endosomes.

We found that acidification is crucial for entry and successful infection of the virus. Small compounds that neutralize the pH of endocytic vesicles and the endosomal compartment led to strong reduction of internalization. The virus failed to move beyond early or late endosomes, depending on the pH-neutralizing drug used (data not shown but published in (Engel, Heger et al. 2011)).

The mechanism behind this phenomenon is not clear. In contrast to many enveloped viruses that undergo acid-mediated fusion in endosomes, this is not the reason for non-enveloped viruses such as SV40. One possible explanation is the observation from several studies that inhibition of acidification impairs trafficking and maturation of endosomal vesicles (Clague, Urbe et al. 1994; Bayer, Schober et al. 1998; Baravalle, Schober et al. 2005).

That maturation of endosomes might be impaired is further supported by our observation that SV40 infection is strongly reduced upon depletion of hrs, c-CBL, CBLC, NEDD4, and NEDD4L. These proteins are different components of the ubiquitin-dependent machinery that is necessary for formation of intraluminal vesicles (ILV) at the level of maturing endosomes. In addition, virus particles accumulated in enlarged early endosomes in cells that have been transfected with a constitutively active form of Rab5 (Rab5Q). Expression of this mutant has been previously shown to strongly reduce SV40 infection (Pelkmans, Kartenbeck et al. 2001) and is known to block endosomal maturation at the level of the maturing endosome (Flinn, Yan et al. 2010; Wegner, Malerod et al. 2010). Also disruption of microtubules that are important for endosomal trafficking and maturation using the inhibitor nocodazole blocks infection (Shimura, Umeno et al. 1987) at early steps of entry.

Protein kinase C (PKC) has long been proposed to play a role in infection of several enveloped viruses including rhabdoviruses, alphaviruses, poxviruses, and herpesviruses (8). Especially classical PKC isozymes have been related to endosomal sorting and maturation: Sieczkarski et al showed that Flu entry is blocked in late endosomes by the classical PKC inhibitors Calphostin C and Gö6976 and identified PKC betaII (= gamma) as the important isozyme (Sieczkarski, Brown et al. 2003). Adenovirus 2 requires functional classical PKC for vesicle trafficking and release from endosomes (Nakano, Boucke et al. 2000). Our screen identified classical Protein kinase C (PKC) isozymes as hits for SFV (alpha), SV40 (gamma), UUK and FLU (alpha and gamma). For FLU this confirms the previous report (Sieczkarski, Brown et al. 2003). That classical PKC isoforms play a role for SV40

and SFV we could show with inhibitor experiments. In experiments with Calphostin C SFV but also SV40 infection was blocked when the drug was present at the level of (early) endosomal sorting of the viruses. For SV40 we could not see any drug effect after the nocodazole step. For SFV the kinetics of Calphostin C add-in showed a half-maximum less than 10 min after start of virus entry. This resembles the add-in and wash-out kinetics of NH₄Cl in different cell lines. Since NH₄Cl is an indicator for the acid-dependent step during SFV infection, i.e. endosomal fusion, we propose a PKC-sensitive step at endosomal fusion of the virus (Fig. 21). Our findings basically confirm the screening outcome and further support the idea that endosomal function requires classical PKC.

The screen identified also some non-classical PKC isoforms, which are less characterized than the classical group. Nevertheless, two hits could be confirmed: PKC zeta, a weak SV40 hit, was shown previously to be crucial for small t-antigen-induced promoter transcriptional activation (Garcia, Cereghini et al. 2000), which in turn enhanced, besides many cellular proteins, also transcription of early genes of SV40 (Jackson, MacDonald et al. 1990). For the SFV hit PKC delta, a novel PKC isozyme, we found strong reduction of SFV infection upon treatment of cells with the PKC delta inhibitor Rottlerin. That more than one PKC isozyme is involved in SFV infection is further supported by the add-in experiments using the drug CGP53353. In contrast to the Calphostin C add-in CGP53353 reduced infection continuously until almost 1 hr post-warming. This indicates an additional PKC-dependent step post-entry.

With Rab11a, Rab11b, and Rab11FIP5 all proteins from the slow recycling pathway of the siRNA library were also in the SFV hit list. We confirmed the strong effects of siRNA against Rab11FIP5 and Rab11b on infection by FACS, which was -95% for the former and -55% for the latter protein. Interestingly, all viruses except UUK and VACV showed several hits associated with recycling pathways such as Rab4b for FLU being the strongest hit in the screen, Rab4a and EHD1 for SV40, and Rab11b and Rab11FIP5 for VSV. The significance of these findings is as yet speculative. Many receptors from the plasma membrane are endocytosed and recycled back in a Rab4 and Rab11 dependent manner (Maxfield and McGraw 2004). One possibility is that knock-down of Rab4/Rab11 or -associated proteins perturb recycling of viral receptors causing their accumulation in sorting endosomes and depletion at the plasma membrane. Another possibility of the strong RAB11FIP5 effect might be an impairment of endosomal function (Fig. 21).

The concept of RNAi profiling of several viruses with our screening platform including a “cherry-picked” siRNA library, image analysis by *InfectionCounter*, and the way we defined hits showed its usefulness in lab-scale virus infection screening. We found many expected hits and pathways and could validate new and unexpected proteins. Especially we showed by thorough validation of SV40 and SFV hits that the strong representation of the endosomal compartment is not a coincidence. It should be therefore possible to classify new viruses as dependent on endosomes.

Many hits are still unvalidated. Due to the limitations of this thesis it is not surprising. However, screening scale validations such as quantitative RT-PCR, re-screens with other siRNAs, secondary virus assays that focus on parts of the virus life cycle such as binding, endocytosis, fusion, and replication should allow quick and systematic characterization of the hits.

Can the screening distinguish between viruses that leave early the endosomal compartment such as SFV and those that are sorted into the degradative pathway such as FLU and VSV? In the hit lists we found for all these viruses primarily early endosomal hits, some of them being involved in sorting to the degradative pathway such as hrs and tsg101. However, SFV most likely fuses before this step and should not be impaired in infection when depletion of these proteins is limited to the sorting function. This implies that other early endosomal functions are also affected. Indeed depletion of tsg101 has been shown to impair acidification (Bache, Stuffers et al. 2006) and RNAi of both proteins affect morphology of late but also early endosomes (Doyotte, Russell et al. 2005; Razi and Futter 2006).

Proteins limited to other sub-compartments than early endosomes are rare and their phenotypes upon depletion not well characterized. This is true for late endosomal markers. The siRNA library contains the late endosomal proteins Rab7a and b. However, both are also found on early endosomal vesicles (Vonderheit and Helenius 2005; Bucci, Bakke et al. 2010). While Rab7a is not a hit at all indicating insufficient siRNA or depletion effects, Rab7b is a hit for SFV and VSV but not FLU. This speaks for a different role of this poorly characterized form than sorting into late endosomes. For immunofluorescence we used colocalization of SV40 with LAMP1 to show its sorting into the degradative pathway, especially lysosomes. For future screens validated siRNA against this protein as well as Rab7a might allow a better classification of the compartments.

Until then the combination of screening and thorough hit and pathway validations with diverse cell biological and virological techniques are crucial. In order to optimize the siRNA library future efforts should include searching for proteins and validated siRNA that induce pathway-specific phenotypes upon depletion and could serve as pathway markers for virus entry and infection screening.

4 MATERIALS AND METHODS

4.1 Software Development

The software *InfectionCounter* was written and tested in the technical language MATLAB (MathWorks, Natick, USA), versions 2008a – 2010a, equipped with all available toolboxes. The software consists of the GUI (Graphical User Interface) code and figure files (*InfectionCounterVblue_B2.m*, *InfectionCounterVblue_B2.fig*), the image analysis core file (*infectionwrapper_public_BLUE.m*), and the output code file (*out.m*). Primarily, the software calls MATLAB functions that are included in the core MATLAB package, as well as in the image processing toolbox. The GUI was developed in the MATLAB GUIDE (GUI Development Environment).

The user instruction manual including description of input, output, and GUI functions is provided in the Supplemental Materials as well as on the CD to this thesis.

4.2 Cell Culture

For the small compound profiling of SFV Vero cells (African green monkey kidney epithelial cells from American Tissue Culture Collection [ATCC], USA) were used. For screening, different human cervix carcinoma cell lines (HeLa ATCC - provided by ATCC; and HeLa CNX – provided by Lucas Pelkmans (Pelkmans, Fava et al. 2005)), and a lung carcinoma cell line (A549, ATCC) were used. Virus preparations were performed in Baby Hamster Kidney (BHK) cells for SFV, VACV, and VSV, and in the African green monkey kidney epithelial cell line CV-1 (ATCC) for SV40.

CV-1 cells, and A549 cells were maintained in Dulbecco's Modified Eagle's Medium (DMEM) supplemented with 10% fetal calf serum (FCS, Invitrogen). HeLa cells were maintained in DMEM with 10% FCS and 1% GlutaMAX (Invitrogen). Vero cells were cultivated in Minimal Essential Medium supplemented with Earle's salt (MEM, Invitrogen) and 1% non-essential amino acids (NEAA, Invitrogen) as well as 10% FCS. BHK-21 cells were grown in Glasgow Medium (GMEM, Invitrogen) supplemented with 10% FCS and 10% Tryptose Phosphate Broth (Invitrogen).

4.3 Drugs, Plasmids, and Antibodies

The following drugs were purchased from Sigma Aldrich: Nocodazole, o-Vanadate (w), Brefeldin A, Dynasore, Monensin, NH₄Cl (w), Wortmannin, LY294002, Deltamethrin, Chlorpromazine, and

Okadaic Acid; from Calbiochem came CGP53353, Calyculin, Tautomycetin, Calphostin C, ML-7, Blebbistatin, Endothall, Genistein (Gen). Bafilomycin A and DMSO were from Fluka. Drugs were diluted in DMSO or in water (w).

Plasmids encoding Cav-EGFP have been described before (Pelkmans, Kartenbeck et al. 2001), encoding mutant and wildtype Rab5 and Rab7 were described before (Vonderheit and Helenius 2005; Quirin, Eschli et al. 2008).

Primary antibodies for IF were purchased from Covance Inc (mouse-anti-HA), Santa Cruz (anti-LAMP1, rabbit-anti-caveolin), BD Biosciences (anti-EEA1); secondary antibodies for IF came from Molecular probes (Alexa Fluor 488/595/647 goat-anti-mouse/rabbit); for Western Blotting all antibodies came from Sigma except anti-cofilin/ezrin (cell signaling technology) and caveolin-1 (the same as for IF). The following anti-virus protein antibodies were used: 1:1000 Lady Di primary anti serum against SFV E1/E2/E3 as described in (Singh and Helenius 1992; Vonderheit and Helenius 2005); 1:1000 F-14 against VSV envelope protein as described in (Johannsdottir, Mancini et al. 2009); 1:1000 “1205” mouse antiserum against SV40 T-antigen (Pelkmans, Kartenbeck et al. 2001). The primary antibody to detect UUK infection is described in (Lozach, Mancini et al. 2010), the one for FLU is described in (Huotari).

4.4 Viruses and Virus Preparation

4.4.1 SFV

A prototype strain of Semliki Forest Virus (Smithburn, Haddow et al. 1946) was prepared essentially as described (Kaariainen, Simons et al. 1969). Briefly, 10 roller bottles (Thermo Scientific) of subconfluent BHK-21 at a low passage number were infected with SFV at a MOI of 0.01 in Earle's MEM supplemented with PenStrep for 24 hrs under slow rotation (0.2 rpm) until cells rounded up and detached. The supernatant was collected in 50ml Falcons and centrifuged for 10 min at 10'000 x g and 4°C. The supernatant was pooled and centrifuged at 25'000 rpm in a Beckman Ultracentrifuge (SW28 rotor) for 2.5 hrs at 4°C to pellet the virus. The pellet was resuspended overnight in TN buffer (50mM Tris pH7.4, 100mM NaCl). For screening unpurified SFV was used. For FACS analysis resuspended virus was purified by sedimentation centrifugation using a Pfefferkorn sucrose gradient (5%-20%, 25%-50%, and a 60% cushion – values refer to sterile sucrose in TN buffer). A faint white-bluish band was isolated by a syringe and aliquoted for storage in -80°C.

4.4.2 VSV

Vesicular Stomatitis Virus (VSV; Indiana serotype) was provided by Prof. Hans Hengartner (Institute of Experimental Immunology, University of Zurich). Stocks were prepared as previously described (White, Matlin et al. 1981; Pelkmans, Fava et al. 2005; Johannsdottir, Mancini et al. 2009). Briefly, BHK-21 cells in 4 T-175 flasks at subconfluency were infected by VSV stock at a MOI of 0.1 in 10 ml

MEM medium supplemented with 10mM HEPES pH 6.5 for 1 hr on a rocker. After addition of 30 ml of MEM alpha supplemented with 30mM HEPES pH 7.3, 10% Tryptose Phosphate Broth, and 1% FCS the cells were incubated for additional 23 hrs. Supernatant was decanted and cell debris was removed by centrifugation at 4,500 rpm for 15 min at 4°C. The stock was resuspended in TN buffer with 10 mM HEPES at pH 7.4 and stored at -80°C .

4.4.3 SV40

Simian Virus 40 was provided by Sabrina Engel and was prepared as described previously (Cole 2001; Ewers, Romer et al. 2010; Engel, Heger et al. 2011). Briefly, forty T175 flasks of sub-confluent CV-1 cells were infected with SV40 at a MOI of 0.01 in DMEM without additives for 2 hrs. Medium was exchanged by CV-1 culture medium for 14 days. To harvest virus, cells were subjected to three freeze-thaw cycles, and then centrifuged at 10'000 x g for 10 min at 4°C to remove debris. Twenty ml of virus-containing supernatant was loaded on a 10 ml cushion of CsCl (1.4 g ml⁻¹) in 10 mM HEPES, pH 7.4. Following centrifugation at 76'000 x g for 3 h at 4°C in a SW28 rotor (Beckman), the banded virus in the CsCl cushion was harvested. The density of the CsCl fraction containing SV40 was checked and the fraction was adjusted to a CsCl density of 1.34 g/ml in 10mM HEPES, pH 7.4. Following equilibrium centrifugation at 100,000 g for 16 h at 4°C in a 70.1 Ti rotor (Beckman), the lower virus band was isolated and dialyzed against 50mM HEPES, pH 8.0, 150mM NaCl, 1mM CaCl₂ (virus buffer). The purified infectious virus was stored in aliquots at -80 °C.

4.4.4 Influenza A Virus

The influenza virus strain used for screening was X31, A/Aichi/68(H3N2). Virus stocks were purified and stored in 40 % sucrose -80°C (Virapur, CA USA). Briefly, pathogen free chicken eggs inoculated with the virus were incubated for two days at 33-37°C. Harvested allantoic fluid was clarified by low speed centrifugation, and virus concentrated by high speed centrifugation and two rounds of 10-40% sucrose gradient steps. Stocks (3.0 x 10⁸ TCID50 infectious units/ml) were stored in 40 % sucrose at -80°C until usage (Huotari). Experiments with FLU were performed by Jatta Huotari.

4.4.5 Vaccinia virus

Recombinant Vaccinia viruses expressing GFP (VACV IHD-J E/L GFP) were generated based on VACV strain International Health Department J (IHD-J) as previously described (Mercer and Helenius 2008). Virus was provided and all VACV experiments were performed by Florian Schmidt.

4.4.6 Uukuniemi Virus

The prototype strain of UUKV S23 has been described previously (Pettersson and Kaariainen 1973). Experiments with Uukuniemi virus were performed by Roger Meier.

4.5 FACS Analysis of SFV Infection

SFV was bound to Vero cells at 4°C for 30 min in Earle's MEM either in the presence of the drug to be tested (or DMSO for negative controls) or without unless otherwise indicated. Pre-incubation medium was replaced by pre-warmed infection medium (Earle's MEM, 20 mM HEPES) containing the drug to be tested or DMSO for 4 h at 37°C. Cells were then trypsinized, followed by fixation with 4% formaldehyde in cell suspension for 30 min RT and washed with buffer containing 0.1% saponin (w/v), 2% FCS, 20 mM EDTA, 0.04% NaN₃ in PBS (FACS-PERM). Cells were permeabilized and stained with 1:1000 anti-E1/E2 primary antibody (Lady Di) in FACS-PERM for 2 h at 4°C, followed by secondary antibodies (goat-anti-rabbit coupled to Alexa-488/647, Invitrogen) in FACS-PERM. Cells were analyzed on a FACS calibur cytometer using CellQuest 3.1 software (Beckton). 10⁷000 cells were analyzed for each sample, each sample in at least two independent experiments.

4.6 Protocols for RNAi screening

4.6.1 Plate Layout

We used 96 well microtiter plates with flat translucent („optical“) bottom and black plastic (nunc). Since we and others (Moese, S., 3V-Biosciences; Machuy, N, Max-Planck-Institute for Infection Biology, Berlin, Germany; oral communication) found that the outermost wells of the plates often show inhomogeneous cell distribution and infection we did not use them for screening and filled them up with medium to maintain spatially homogenous thermal conditions for the inner 60 wells.

In initial tests we determined optimal parameters for cell density, type and concentration of the transfection reagent, and siRNA concentration as well as the general protocol for all screens. We decided to use a lipid-based transfection agent (Lipofectamine RNAiMAX, Invitrogen) at a final dilution of 1:1666, siRNA at a final concentration of 20nM, and 2²00 HeLa cells per well. Shortly, we pipetted 15µl of 133.3nM siRNA dissolved in pH-buffered MEM medium (MEM/HEPES), added 15µl MEM/HEPES containing 0.06µl Lipofectamine RNAiMAX (Invitrogen), let them incubate to form lipid-siRNA-complexes (30min), and filled up to 100µl final volume with 2²00 HeLa cells resuspended in full medium (DMEM/10% FCS/1% GlutaMax). The plates were incubated for 72 hours in 37°C. According to Figure 2, each siRNA was used in duplicate in adjacent wells. As transfection control („positive control“ for cell number) we used a siRNA against the kinesin-family member KIF11 (kinesin-5 / EG5) that effectively kills most of the cells by inducing apoptosis (ref). Since we aimed to perform screens also for other viruses than SFV we could not use virus-specific siRNA („positive control“ for infection). A siRNA that has been predicted as non-targeting any known human mRNA („AllStarsNegative“, ASN) served as a negative control for both screen read-outs, cell number and infection. Due to its statistically important role we used 4 wells per plate ASN. Hence, of 60 used wells per plate and 2+4 wells of control siRNA per plate as well as duplicates for each targeting siRNA, each multi well plate harbored 27 targeting siRNAs.

4.6.2 General Transfection Protocol

Depending on the virus, HeLa ATCC, HeLa CNX, and/or A549 cells were transfected in 96 well black optical bottom plates (Nunc), with three different siRNA per gene and each siRNA in duplicate, and typically in three (UUKV: four) independent experiments. Those replicates or plates within a replicate that did not pass quality controls (uneven cell seeding, no effects in positive controls, too high or too low infection, irregular infection behavior of the sample wells relative to negative control wells indicating pipetting errors, contaminated plates, low dynamic range leading to similar z-score distributions of sample versus negative control siRNA) were removed. This causes the final number of replicates for analysis in several cases to be smaller than three (see Table 1).

To monitor transfection efficiency, siRNA causing cell death (Hs_KIF11_6, Qiagen) was used in each plate (Weil, Garcon et al. 2002). AllStarsNegative (ASN) siRNA was added as a non-targeting control in quadruplets per plate. To avoid inhomogeneous cell distribution in the outermost wells, only the inner 60 wells of a 96 well plate were used, while the outermost 36 wells were filled with medium.

Transfection was performed according to a reverse transfection protocol. Briefly, 15 μ l siRNA (20nM final concentration) and 15 μ l Lipofectamine RNAiMAX (Invitrogen; 1:1000 final dilution) were both pre-diluted in OPTI-MEM (Invitrogen; Usual Suspects screens) or DMEM supplemented with 20mM HEPES pH 7.4 (PKC/PP and PIP screens), spotted into 96-well plates, and incubated for at least 10 min at RT to allow siRNA-lipid complex formation. 2200 (SV40 screen: 1200) cells per well in 70 μ l full cultivation medium (see cell culture) were added to the lipid-siRNA-complex (final volume: 100 μ l) and incubated for 72 h at 37°C. Plates that showed uneven cell distribution or insufficient cell death in AllStarsDeath positive control wells were discarded. From the other plates transfection medium was removed, and the cells were washed once with PBS prior to applying the virus-specific infection protocols (see 1.4.2).

4.6.3 Virus Infection Assays for Screening

4.6.3.1 SFV

Cells were incubated for 4 h at 37°C and 5% CO₂ with 100 μ l of a SFV stock dilution in infection medium (Earle's MEM with 20mM HEPES pH 7.4). The virus dilution factor had been determined prior to screening by titration for HeLa ATCC and CNX to lead to 20-40% infection. Cells were fixed by adding 30 μ l 16% HCHO per well (final concentration 4%) and washed three times with PBS/0.04% Azide using an ELISA washer (Thermo). Permeabilization, blocking, and primary antibody was applied in one step by incubating the cells for 2 h in an 1:1000 dilution of anti-E1/E2 polyclonal rabbit antiserum ("Lady Di") in PERM buffer (0.1% Triton X-100, 3% BSA, 0.04% Na₃N in PBS, filtered through 0.4 μ m membrane to remove fibers). Plates were 3x washed with PBS/Azide, and a dilution of secondary antibody (1:1000 of goat anti mouse coupled to Alexa Fluor 488; Invitrogen) and Hoechst 33258 (1:10,000; Invitrogen) in PERM buffer was applied for 30 min, followed by a final 3x washing step.

4.6.3.2 SV40

Cells were inoculated with SV40 suspension in R-medium (RPMI, pH 6.8) at an MOI resulting in 10-30% infected cells for 120 min at 37°C. Virus inoculum was replaced by full culture medium (see cell culture), and the cells were incubated for additional 22 h at 37°C. The cells were subjected to fixation and immunostaining with a 1:1000 dilution of primary mouse antibody 1605 (against the small T-antigen of SV40) for 120 min followed by a secondary antibody (1:1000 dilution of goat anti mouse coupled to Alexa Fluor 488; Invitrogen) together with Hoechst staining analog to the protocol for SFV.

4.6.3.3 VSV

Infection with VSV was done essentially as for SFV (1.4.2.1). Briefly, transfected cells were washed once with PBS, incubated with VSV in VSV infection medium (RPMI, 20mM HEPES pH 6.8) for 5 h and fixed in 4% HCHO. For immunostaining, the primary antibody I-14 was diluted 1:1000 in PERM and the cells incubated for 2 h. After washing secondary antibody (1:1000 goat anti mouse coupled to Alexa fluor 488) and Hoechst dye were applied as described before.

4.6.3.4 UUKV

Transfected A549N cells were washed once with infection medium (RPMI, 30 mM HEPES, pH 6.8) and infected by 100 µl of diluted UUKV stock (6250 focus-forming units / well) for 1.5 hrs at 37°C. 50 µl DMEM 30% FCS, 1% NEAA, 1% Glu, 30 mM HEPES was added per well and further incubated for additional 20 hrs until fixation. For immunostaining cells were washed three times with PBS, and incubated with primary antibody (8B11A3 at 1:500) for 1.5 hrs. After washing with PBS (3x) 200 µl of 1:1000 secondary antibody (goat-anti-mouse AF488; Invitrogen) and 1:10'000 Hoechst dye for nucleus staining was added to the cells and incubated for 45 min. After washing plates were prepared for automated microscopy and *InfectionCounter* analysis.

4.6.3.5 FLU

The transfected plates were infected and stained by Jatta Huotari. Briefly, A549 cells were infected with a virus concentration that resulted in 20-50% infection (0.005-0.02 µl/well of 96-well plate). Virus was diluted into infection medium (DMEM with 50mM Hepes and 0.2% BSA, pH 6.8). Virus infection was allowed to proceed for 10-14 hrs, after which cells were fixed. Cells were stained with an antibody against NP (HB65, ATCC, unpurified, 1:100) in order to detect newly synthesized viral protein, followed by secondary antibodies. Antibodies were diluted in permeabilization solution (PS) containing PBS with 1 % BSA and 0.1 % Saponin, and incubated 1-2 hrs (RT) before preparation for imaging. Cell nucleus staining was done by Hoechst dye as described before.

4.6.3.6 VACV

The transfected plates were infected and stained by Florian Schmid. Briefly, transfection medium was aspirated, and cells were washed and infected with 50µl minimal medium per well containing 135'000 plaque forming units (pfu) vaccinia virus IHD-J E/L GFP. After 40 min incubation at 37°C 50µl full medium (DMEM, 20% FCS, GlutaMAX, PenStrep) was added and further incubated for additional 8

hrs. Cells were fixed by adding 33 μ l of 16% HCHO in PBS and incubated for 1 hr at RT. Cell nuclei were stained by 1:10'000 Hoechst 33258 in 0.5% Triton X-100 in PBS, 0.04% Azide.

4.6.4 Imaging

Stained plates were sealed with plastic foil to avoid evaporation and to prevent spilling during imaging. Sixteen images per well for each channel (nucleus/Hoechst 33258 and infection/Alexa Fluor 488 or GFP) were acquired on a Pathway 855 automated microscope station (Becton Dickinson) using a 10x objective (Olympus) and a laser-based autofocus every second image. Cell numbers (CN) and raw infection indices (rawII) for each well were determined using *InfectionCounter*. Since cell density affects virus infection, the effect of cell density on the infection index was determined with an independent checker board for each virus and cell line. Briefly, varying amounts of cells per well, transfected with AllStarsNegative siRNA, were infected with the corresponding virus under screening conditions. From the obtained infection indices for each cell density, a polynomial regression function $\text{normII} = f(\text{CN})$ was calculated. Density-corrected, relative infection indices (corrRII) for each well of the screen were determined as $\text{corrRII} = \frac{\text{rawII}}{\text{normII}}$.

4.6.5 Normalization and Standardization

Due to virus-specific variations in the distribution of sample corrRII two normalization methods were applied for each virus and cell line. The z-score method is based on converting all replicate corrRII into z-scores, which are normalized against the MAD (median absolute deviation), a more robust i.e. outlier-tolerant method than the standard algorithms based on normalization against the mean of the sample corrRII. The ranking method is usually even more tolerant against outliers since normalization is done by ranking the plate-by-plate normalized corrRIIs of each replicate. With both methods a significance cutoff is defined based on the distribution of the negative control wells.

4.6.5.1 Z-score Method

CN and corrRII were processed using the RNAi screen analysis software package cellHTS2 (Boutros, Bras et al. 2006). Both features were independently normalized against AllStarsNegative control within each plate followed by z-score calculation (zCN and zII) and standardization over all replicate experiments essentially as described in the software manual (<http://bioconductor.org/packages/2.5/bioc/html/cellHTS2.html>). To discard all siRNA that strongly reduce cell number a virus- and cell line-specific zCN-cutoff that corresponds to 400 imaged cells per well was applied. The zCN-threshold was calculated by logarithmic regression of the replicate-averaged zCN with the replicate-averaged “raw” CN. Within the remaining siRNA, those were considered “significant”, whose zII was outside a bandwidth of ± 5 -fold the standard deviation of all AllStarsNegative control siRNA z-scores ($zII'_{\text{target siRNA}} > |5 \times STDEV(zII'_{\text{AllStarsNegative}})|$). Genes affecting virus infection (“hits”) were defined for each virus and cell line by at least 2 significant targeting siRNA decreasing virus infection. Changes of infection for hits in percent of the negative control (100%) as mentioned in the text or in hit tables were always approximated from the mean zII of all significant siRNA of a particular hit

based on logarithmic regression of the siRNA z-scores of infection to their corresponding infection index averaged over all replicate experiments (as mentioned above for calculating the zCN-threshold).

4.6.5.2 Ranking Method

All siRNA corrRII were discarded if the corresponding CN was below 400. The remaining siRNA were normalized in a plate-by-plate manner to the average corrRII of the four negative control wells and the logarithm to base 2 was calculated for each well to reach normRII. For each replicate a rank of all wells (sample and controls) were calculated and a rank bandwidth of 2.5x the standard deviation of all negative control wells were determined. A well containing a sample siRNA was considered “significant” if its normRII rank is outside this bandwidth. There was no screen that had more than one significant siRNA increasing infection. Therefore, only those siRNA that decreased infection were further analyzed and a siRNA score was determined as the rank distance to the bandwidth. A hit was defined in case of triplicates if there were at least 3 out of 6 wells of the same siRNA designated as “significant” (for duplicates: at least 1 well in each replicate, otherwise at least 3 out of 4 wells; for single screens: both wells per siRNA species). A gene was defined as “primary hit” when at least two out of three siRNA were significant. In such cases, a hit score for the ranking method was calculated by addition of the siRNA scores of all significant siRNA.

4.6.6 Hit Definition

From the method-specific hit lists the final (cell line- and method-independent) hits, termed “Final Hits” for a certain virus, were determined by overlapping all cell line- and method-specific (primary) hit lists. If a gene is listed in at least 3 out of 4 primary hit lists (2 cell lines), or in both primary hit lists (1 cell line, 2 methods), it was considered a “Final Hit”. To calculate the Final Hit score the method- and cell line-specific primary hit scores were normalized to a range from 0 to 10, and the normalized rank positions for each gene were summed up.

4.6.7 Bioinformatic tools

For classification of the 108 genes of the Usual Suspects screen into biochemical and cell physiological functions and pathways we used the tool AmiGO (<http://amigo.geneontology.org/cgi-bin/amigo/go.cgi>) (Carbon, Ireland et al. 2009). For known or predicted protein interactions based on their genomic context, high-throughput experiments such as DNA micro arrays, coexpression, and text mining from publications we used STRING 9.0, a bioinformatics tool at <http://string-db.org/> (Szklarczyk, Franceschini et al. 2011).

6 SUPPLEMENTARY INFORMATION

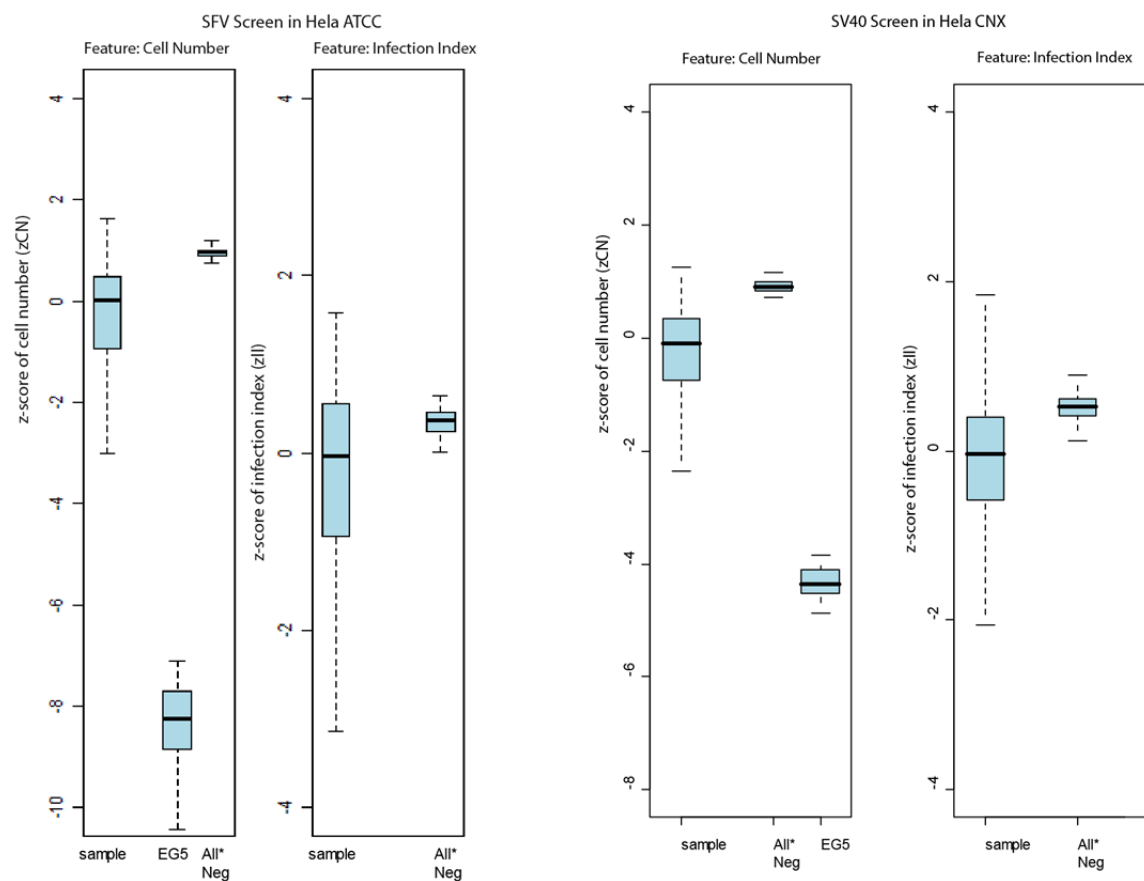


Figure S1

Example boxplots of the screens. SFV screen in HeLa ATCC (left) and SV40 in HeLa CNX (right) show z-score distributions for cell number and infection index for the populations of all replicate sample siRNA wells (“sample”), the negative controls (“All*Neg”), and the transfection (positive) control Hs_KIF11_6 (“EG5”)

7 ABBREVIATIONS

ADP/ATP	Adenosine diphosphate / triphosphate
CCP	Clathrin-coated pit
CCV	Clathrin-coated vesicle
CI-M6PR	Cation-independent mannose-6-phosphate receptor
CME	Clathrin-mediated endocytosis
CTxB	Cholera toxin B subunit
DMEM	Dulbecco's Modified Eagle's Medium
DN	Dominant-negative
(E)GFP	(Enhanced) green fluorescent protein
EE	Early endosome
EEA1	Early endosomal autoantigen-1
EGF	Epidermal growth factor
EGFR	Epidermal growth factor receptor
EM	Electron microscopy
EPS15	EGFR pathway substrate clone number 15
ER	Endoplasmic reticulum
ESCRT	Endosomal sorting complexes required for transport
FACS	Fluorescence activated cell sorter
FCS	Fetal calf serum
FLU	Influenza A virus
GDP/GTP	Guanosine diphosphate/triphosphate
GEEC	GPI-enriched early endosomal compartments
GPI-AP	Glycosylphosphatidylinositol-anchored protein
GTPase	Guanosine triphosphatase
HRS/HGS	Hepatocyte growth factor-related tyrosine kinase substrate
KD	Knock-down
LAMP	Lysosome-associated membrane protein
LBPA	Lyso-bis(phosphatidic acid)
LCMV	Lymphocytic choriomeningitis virus
LDL(R)	Low density lipoprotein (receptor)
LOG	Logarithm
(m)RFP	(monomeric) red fluorescent protein
MOI	Multiplicity of infection
PFU	Plaque forming units
PH	Pleckstrin homology
PI3,5P2	Phosphatidylinositol-3,5-bisphosphate
PI3P	Phosphatidylinositol-3-phosphate
PI4,5P2	Phosphatidylinositol-4,5-bisphosphate
PRD	Proline rich domain
Rab	Ras-like in brain
SD	Standard deviation
SEM	Standard error of the mean
SFV	Semliki forest virus
SH	Src homology
siRNA	Small interfering ribonucleic acid
SNARE	Soluble N-ethyl maleimide sensitive factor
STxB	Shiga toxin subunit B
SV40	Simian virus 40
TGN	Trans Golgi network
TIRF	Total internal reflexion fluorescence microscopy
UUK	Uukuniemi virus
VACV	Vaccinia virus
VSV	Vesicular stomatitis virus
xFP	Any fluorescent protein

8 REFERENCES

- Ablan, S., S. S. Rawat, et al. (2001). "Entry of influenza virus into a glycosphingolipid-deficient mouse skin fibroblast cell line." *Arch Virol* **146**(11): 2227-2238.
- Ahle, S. and E. Ungewickell (1990). "Auxilin, a newly identified clathrin-associated protein in coated vesicles from bovine brain." *J Cell Biol* **111**(1): 19-29.
- Ahuja, D., M. T. Saenz-Robles, et al. (2005). "SV40 large T antigen targets multiple cellular pathways to elicit cellular transformation." *Oncogene* **24**(52): 7729-7745.
- Alvi, F., J. Idkowiak-Baldys, et al. (2007). "Regulation of membrane trafficking and endocytosis by protein kinase C: emerging role of the pericentration, a novel protein kinase C-dependent subset of recycling endosomes." *Cell Mol Life Sci* **64**(3): 263-270.
- Amessou, M., A. Fradagrada, et al. (2007). "Syntaxin 16 and syntaxin 5 are required for efficient retrograde transport of several exogenous and endogenous cargo proteins." *J Cell Sci* **120**(Pt 8): 1457-1468.
- Amstutz, B., M. Gastaldelli, et al. (2008). "Subversion of CtBP1-controlled macropinocytosis by human adenovirus serotype 3." *The EMBO journal* **27**(7): 956-969.
- Amyere, M., B. Payrastre, et al. (2000). "Constitutive macropinocytosis in oncogene-transformed fibroblasts depends on sequential permanent activation of phosphoinositide 3-kinase and phospholipase C." *Molecular biology of the cell* **11**(10): 3453-3467.
- Anderson, H. A., Y. Chen, et al. (1996). "Bound simian virus 40 translocates to caveolin-enriched membrane domains, and its entry is inhibited by drugs that selectively disrupt caveolae." *Molecular biology of the cell* **7**(11): 1825-1834.
- Anderson, R. G. (1998). "The caveolae membrane system." *Annual review of biochemistry* **67**: 199-225.
- Aniento, F., N. Emans, et al. (1993). "Cytoplasmic dynein-dependent vesicular transport from early to late endosomes." *J Cell Biol* **123**(6 Pt 1): 1373-1387.
- Araki, N., T. Hatae, et al. (2003). "Phosphoinositide-3-kinase-independent contractile activities associated with Fcγ-receptor-mediated phagocytosis and macropinocytosis in macrophages." *Journal of cell science* **116**(Pt 2): 247-257.
- Araki, N., M. T. Johnson, et al. (1996). "A role for phosphoinositide 3-kinase in the completion of macropinocytosis and phagocytosis by macrophages." *The Journal of cell biology* **135**(5): 1249-1260.
- Ashok, A. and W. J. Atwood (2003). "Contrasting roles of endosomal pH and the cytoskeleton in infection of human glial cells by JC virus and simian virus 40." *Journal of virology* **77**(2): 1347-1356.
- Babuke, T. and R. Tikkanen (2007). "Dissecting the molecular function of reggie/flotillin proteins." *European journal of cell biology* **86**(9): 525-532.
- Bache, K. G., S. Stuffers, et al. (2006). "The ESCRT-III subunit hVps24 is required for degradation but not silencing of the epidermal growth factor receptor." *Mol Biol Cell* **17**(6): 2513-2523.
- Bairstow, S. F., K. Ling, et al. (2006). "Type Igγ661 phosphatidylinositol phosphate kinase directly interacts with AP2 and regulates endocytosis." *J Biol Chem* **281**(29): 20632-20642.
- Bar-Sagi, D., F. McCormick, et al. (1987). "Inhibition of cell surface ruffling and fluid-phase pinocytosis by microinjection of anti-ras antibodies into living cells." *Journal of cellular physiology. Supplement* **Suppl 5**: 69-73.
- Baravalle, G., D. Schober, et al. (2005). "Transferrin recycling and dextran transport to lysosomes is differentially affected by bafilomycin, nocodazole, and low temperature." *Cell Tissue Res* **320**(1): 99-113.
- Barriocanal, J. G., J. S. Bonifacino, et al. (1986). "Biosynthesis, glycosylation, movement through the Golgi system, and transport to lysosomes by an N-linked carbohydrate-independent mechanism of three lysosomal integral membrane proteins." *The Journal of biological chemistry* **261**(35): 16755-16763.

- Bayer, N., D. Schober, et al. (1998). "Effect of bafilomycin A1 and nocodazole on endocytic transport in HeLa cells: implications for viral uncoating and infection." *J Virol* **72**(12): 9645-9655.
- Behnia, R. and S. Munro (2005). "Organelle identity and the signposts for membrane traffic." *Nature* **438**(7068): 597-604.
- Benmerah, A., M. Bayrou, et al. (1999). "Inhibition of clathrin-coated pit assembly by an Eps15 mutant." *J Cell Sci* **112** (Pt 9): 1303-1311.
- Benmerah, A., C. Lamaze, et al. (1998). "AP-2/Eps15 interaction is required for receptor-mediated endocytosis." *J Cell Biol* **140**(5): 1055-1062.
- Bereiter-Hahn, J., M. Voth, et al. (2008). "Structural implications of mitochondrial dynamics." *Biotechnol J* **3**(6): 765-780.
- Bhattacharyya, S., K. L. Warfield, et al. (2010). "Ebola virus uses clathrin-mediated endocytosis as an entry pathway." *Virology* **401**(1): 18-28.
- Bishop, N., A. Horman, et al. (2002). "Mammalian class E vps proteins recognize ubiquitin and act in the removal of endosomal protein-ubiquitin conjugates." *J Cell Biol* **157**(1): 91-101.
- Bonazzi, M., S. Spano, et al. (2005). "CtBP3/BARS drives membrane fission in dynamin-independent transport pathways." *Nature cell biology* **7**(6): 570-580.
- Bonifacino, J. S. and R. Rojas (2006). "Retrograde transport from endosomes to the trans-Golgi network." *Nature reviews. Molecular cell biology* **7**(8): 568-579.
- Bougneres, L., S. E. Girardin, et al. (2004). "Cortactin and Crk cooperate to trigger actin polymerization during Shigella invasion of epithelial cells." *The Journal of cell biology* **166**(2): 225-235.
- Boutros, M., L. P. Bras, et al. (2006). "Analysis of cell-based RNAi screens." *Genome Biol* **7**(7): R66.
- Brown, F. D., A. L. Rozelle, et al. (2001). "Phosphatidylinositol 4,5-bisphosphate and Arf6-regulated membrane traffic." *The Journal of cell biology* **154**(5): 1007-1017.
- Bucci, C., O. Bakke, et al. (2010). "Rab7b and receptors trafficking." *Commun Integr Biol* **3**(5): 401-404.
- Bucci, C., R. G. Parton, et al. (1992). "The small GTPase rab5 functions as a regulatory factor in the early endocytic pathway." *Cell* **70**(5): 715-728.
- Canny, J. (1986). "A Computational Approach to Edge Detection." *IEEE Transactions on Pattern Analysis and Machine Intelligence PAMI-8*(6): 679-698.
- Cao, H., J. Chen, et al. (2007). "Dynamin 2 mediates fluid-phase micropinocytosis in epithelial cells." *Journal of cell science* **120**(Pt 23): 4167-4177.
- Cao, W., M. D. Henry, et al. (1998). "Identification of alpha-dystroglycan as a receptor for lymphocytic choriomeningitis virus and Lassa fever virus." *Science* **282**(5396): 2079-2081.
- Carbon, S., A. Ireland, et al. (2009). "AmiGO: online access to ontology and annotation data." *Bioinformatics* **25**(2): 288-289.
- Chalfant, C. E., S. Ohno, et al. (1996). "A carboxy-terminal deletion mutant of protein kinase C beta II inhibits insulin-stimulated 2-deoxyglucose uptake in L6 rat skeletal muscle cells." *Mol Endocrinol* **10**(10): 1273-1281.
- Chappell, T. G., W. J. Welch, et al. (1986). "Uncoating ATPase is a member of the 70 kilodalton family of stress proteins." *Cell* **45**(1): 3-13.
- Chen, P. I., C. Kong, et al. (2009). "Rab5 isoforms differentially regulate the trafficking and degradation of epidermal growth factor receptors." *J Biol Chem* **284**(44): 30328-30338.
- Chen, Y. and L. C. Norkin (1999). "Extracellular simian virus 40 transmits a signal that promotes virus enclosure within caveolae." *Experimental cell research* **246**(1): 83-90.
- Chiariello, M., C. B. Bruni, et al. (1999). "The small GTPases Rab5a, Rab5b and Rab5c are differentially phosphorylated in vitro." *FEBS Lett* **453**(1-2): 20-24.
- Christoforidis, S., M. Miaczynska, et al. (1999). "Phosphatidylinositol-3-OH kinases are Rab5 effectors." *Nat Cell Biol* **1**(4): 249-252.
- Chu, V. C. and G. R. Whittaker (2004). "Influenza virus entry and infection require host cell N-linked glycoprotein." *Proc Natl Acad Sci U S A* **101**(52): 18153-18158.
- Clague, M. J., S. Urbe, et al. (1994). "Vacuolar ATPase activity is required for endosomal carrier vesicle formation." *J Biol Chem* **269**(1): 21-24.
- Cole, C. N., Cozen, S. D. (ed. Knipe, D. M. & Howley, P. M.) (2001). "Polyomaviridae: the viruses and their replication." 2141-2229 (Lippincott-Raven Publishers, 2001).
- Collins, B. M., A. J. McCoy, et al. (2002). "Molecular architecture and functional model of the endocytic AP2 complex." *Cell* **109**(4): 523-535.

- Conner, S. D. and S. L. Schmid (2003). "Regulated portals of entry into the cell." *Nature* **422**(6927): 37-44.
- Constantinescu, S. N., C. D. Cernescu, et al. (1991). "Effects of protein kinase C inhibitors on viral entry and infectivity." *FEBS Lett* **292**(1-2): 31-33.
- Cureton, D. K., R. H. Massol, et al. (2009). "Vesicular stomatitis virus enters cells through vesicles incompletely coated with clathrin that depend upon actin for internalization." *PLoS pathogens* **5**(4): e1000394.
- Cureton, D. K., R. H. Massol, et al. (2010). "The length of vesicular stomatitis virus particles dictates a need for actin assembly during clathrin-dependent endocytosis." *PLoS pathogens* **6**(9).
- Damke, H., T. Baba, et al. (1994). "Induction of mutant dynamin specifically blocks endocytic coated vesicle formation." *The Journal of cell biology* **127**(4): 915-934.
- Damke, H., D. D. Binns, et al. (2001). "Dynamin GTPase domain mutants block endocytic vesicle formation at morphologically distinct stages." *Mol Biol Cell* **12**(9): 2578-2589.
- Damm, E. M., L. Pelkmans, et al. (2005). "Clathrin- and caveolin-1-independent endocytosis: entry of simian virus 40 into cells devoid of caveolae." *J Cell Biol* **168**(3): 477-488.
- Damm, E. M., L. Pelkmans, et al. (2005). "Clathrin- and caveolin-1-independent endocytosis: entry of simian virus 40 into cells devoid of caveolae." *The Journal of cell biology* **168**(3): 477-488.
- Danino, D., K. H. Moon, et al. (2004). "Rapid constriction of lipid bilayers by the mechanochemical enzyme dynamin." *J Struct Biol* **147**(3): 259-267.
- Dascher, C., J. Matteson, et al. (1994). "Syntaxin 5 regulates endoplasmic reticulum to Golgi transport." *J Biol Chem* **269**(47): 29363-29366.
- de Lima, M. C., J. Ramalho-Santos, et al. (1995). "Target cell membrane sialic acid modulates both binding and fusion activity of influenza virus." *Biochim Biophys Acta* **1236**(2): 323-330.
- De Vos, K. J., V. J. Allan, et al. (2005). "Mitochondrial function and actin regulate dynamin-related protein 1-dependent mitochondrial fission." *Curr Biol* **15**(7): 678-683.
- Del Conte-Zerial, P., L. Bruschi, et al. (2008). "Membrane identity and GTPase cascades regulated by toggle and cut-out switches." *Molecular systems biology* **4**: 206.
- Dermine, J. F., S. Duclos, et al. (2001). "Flotillin-1-enriched lipid raft domains accumulate on maturing phagosomes." *The Journal of biological chemistry* **276**(21): 18507-18512.
- Dharmawardhane, S., A. Schurmann, et al. (2000). "Regulation of macropinocytosis by p21-activated kinase-1." *Molecular biology of the cell* **11**(10): 3341-3352.
- Diaz-Griffero, F., A. P. Jackson, et al. (2005). "Cellular uptake of avian leukosis virus subgroup B is mediated by clathrin." *Virology* **337**(1): 45-54.
- Dikic, I. (2003). "Mechanisms controlling EGF receptor endocytosis and degradation." *Biochemical Society transactions* **31**(Pt 6): 1178-1181.
- Doherty, G. J. and H. T. McMahon (2009). "Mechanisms of endocytosis." *Annu Rev Biochem* **78**: 857-902.
- Doms, R. W., R. A. Lamb, et al. (1993). "Folding and assembly of viral membrane proteins." *Virology* **193**(2): 545-562.
- Doyotte, A., M. R. Russell, et al. (2005). "Depletion of TSG101 forms a mammalian "Class E" compartment: a multicisternal early endosome with multiple sorting defects." *J Cell Sci* **118**(Pt 14): 3003-3017.
- Driskell, O. J., A. Mironov, et al. (2007). "Dynein is required for receptor sorting and the morphogenesis of early endosomes." *Nat Cell Biol* **9**(1): 113-120.
- Dyxhoorn, D. M. and J. Lieberman (2006). "Silencing viral infection." *PLoS medicine* **3**(7): e242.
- Eddy, B. E., G. S. Borman, et al. (1962). "Identification of the oncogenic substance in rhesus monkey kidney cell culture as simian virus 40." *Virology* **17**: 65-75.
- Ehrhardt, C., H. Marjuki, et al. (2006). "Bivalent role of the phosphatidylinositol-3-kinase (PI3K) during influenza virus infection and host cell defence." *Cell Microbiol* **8**(8): 1336-1348.
- Eisenberg, E. and L. E. Greene (2007). "Multiple roles of auxilin and hsc70 in clathrin-mediated endocytosis." *Traffic* **8**(6): 640-646.
- Empig, C. J. and M. A. Goldsmith (2002). "Association of the caveola vesicular system with cellular entry by filoviruses." *Journal of virology* **76**(10): 5266-5270.
- Engel, S., T. Heger, et al. (2011). "Role of endosomes in simian virus 40 entry and infection." *J Virol* **85**(9): 4198-4211.
- Engel, S., T. Heger, et al. (2011). "The role of endosomes in SV40 entry and infection." *J Virol*.

- Ewers, H., W. Romer, et al. (2010). "GM1 structure determines SV40-induced membrane invagination and infection." *Nature cell biology* **12**(1): 11-18; sup pp 11-12.
- Ewers, H., W. Romer, et al. (2010). "GM1 structure determines SV40-induced membrane invagination and infection." *Nat Cell Biol* **12**(1): 11-18; sup pp 11-12.
- Eyster, C. A., J. D. Higginson, et al. (2009). "Discovery of new cargo proteins that enter cells through clathrin-independent endocytosis." *Traffic* **10**(5): 590-599.
- Fagerholm, S., U. Ortegren, et al. (2009). "Rapid insulin-dependent endocytosis of the insulin receptor by caveolae in primary adipocytes." *PLoS One* **4**(6): e5985.
- Falguieres, T., P. P. Luyet, et al. (2009). "Molecular assemblies and membrane domains in multivesicular endosome dynamics." *Experimental cell research* **315**(9): 1567-1573.
- Fernandez, C. J. and G. Warren (1998). "In vitro synthesis of sulfated glycosaminoglycans coupled to inter-compartmental Golgi transport." *J Biol Chem* **273**(30): 19030-19039.
- Fiers, W., R. Contreras, et al. (1978). "Complete nucleotide sequence of SV40 DNA." *Nature* **273**(5658): 113-120.
- Flinn, R. J., Y. Yan, et al. (2010). "The late endosome is essential for mTORC1 signaling." *Mol Biol Cell* **21**(5): 833-841.
- Ford, M. G., I. G. Mills, et al. (2002). "Curvature of clathrin-coated pits driven by epsin." *Nature* **419**(6905): 361-366.
- Fra, A. M., E. Williamson, et al. (1994). "Detergent-insoluble glycolipid microdomains in lymphocytes in the absence of caveolae." *The Journal of biological chemistry* **269**(49): 30745-30748.
- Fra, A. M., E. Williamson, et al. (1995). "De novo formation of caveolae in lymphocytes by expression of VIP21-caveolin." *Proceedings of the National Academy of Sciences of the United States of America* **92**(19): 8655-8659.
- Frick, M., N. A. Bright, et al. (2007). "Coassembly of flotillins induces formation of membrane microdomains, membrane curvature, and vesicle budding." *Current biology : CB* **17**(13): 1151-1156.
- Fukuda, M. (1991). "Lysosomal membrane glycoproteins. Structure, biosynthesis, and intracellular trafficking." *The Journal of biological chemistry* **266**(32): 21327-21330.
- Garcia, A., S. Cereghini, et al. (2000). "Protein phosphatase 2A and phosphatidylinositol 3-kinase regulate the activity of Sp1-responsive promoters." *J Biol Chem* **275**(13): 9385-9389.
- Garoff, H., M. Sjöberg, et al. (2004). "Budding of alphaviruses." *Virus research* **106**(2): 103-116.
- Garrett, W. S., L. M. Chen, et al. (2000). "Developmental control of endocytosis in dendritic cells by Cdc42." *Cell* **102**(3): 325-334.
- Gauthier-Rouviere, C., E. Vignal, et al. (1998). "RhoG GTPase controls a pathway that independently activates Rac1 and Cdc42Hs." *Molecular biology of the cell* **9**(6): 1379-1394.
- Geuze, H. J., J. W. Slot, et al. (1987). "Membranes of sorting organelles display lateral heterogeneity in receptor distribution." *The Journal of cell biology* **104**(6): 1715-1723.
- Gkantiragas, I., B. Brugger, et al. (2001). "Sphingomyelin-enriched microdomains at the Golgi complex." *Molecular biology of the cell* **12**(6): 1819-1833.
- Glebov, O. O., N. A. Bright, et al. (2006). "Flotillin-1 defines a clathrin-independent endocytic pathway in mammalian cells." *Nature cell biology* **8**(1): 46-54.
- Gordon, D. E., L. M. Bond, et al. (2010). "A targeted siRNA screen to identify SNAREs required for constitutive secretion in mammalian cells." *Traffic* **11**(9): 1191-1204.
- Gorvel, J. P., P. Chavrier, et al. (1991). "rab5 controls early endosome fusion in vitro." *Cell* **64**(5): 915-925.
- Gruenberg, J. (2001). "The endocytic pathway: a mosaic of domains." *Nature reviews. Molecular cell biology* **2**(10): 721-730.
- Gruenberg, J. and H. Stenmark (2004). "The biogenesis of multivesicular endosomes." *Nature reviews. Molecular cell biology* **5**(4): 317-323.
- Gruenberg, J. and F. G. van der Goot (2006). "Mechanisms of pathogen entry through the endosomal compartments." *Nat Rev Mol Cell Biol* **7**(7): 495-504.
- Gruschus, J. M., L. E. Greene, et al. (2004). "Experimentally biased model structure of the Hsc70/auxilin complex: substrate transfer and interdomain structural change." *Protein Sci* **13**(8): 2029-2044.

- Gschwendt, M., G. Furstenberger, et al. (1995). "Lack of an effect of novel inhibitors with high specificity for protein kinase C on the action of the phorbol ester 12-O-tetradecanoylphorbol-13-acetate on mouse skin in vivo." *Carcinogenesis* **16**(1): 107-111.
- Hales, C. M., J. P. Vaerman, et al. (2002). "Rab11 family interacting protein 2 associates with Myosin Vb and regulates plasma membrane recycling." *The Journal of biological chemistry* **277**(52): 50415-50421.
- Hannon, G. J. (2002). "RNA interference." *Nature* **418**(6894): 244-251.
- Hansen, C. G., N. A. Bright, et al. (2009). "SDPR induces membrane curvature and functions in the formation of caveolae." *Nature cell biology* **11**(7): 807-814.
- Hanson, P. I., R. Roth, et al. (2008). "Plasma membrane deformation by circular arrays of ESCRT-III protein filaments." *The Journal of cell biology* **180**(2): 389-402.
- Hay, J. C., D. S. Chao, et al. (1997). "Protein interactions regulating vesicle transport between the endoplasmic reticulum and Golgi apparatus in mammalian cells." *Cell* **89**(1): 149-158.
- Hayashi, S. and J. C. Hogg (2007). "Adenovirus infections and lung disease." *Current opinion in pharmacology* **7**(3): 237-243.
- Hayer, A., M. Stoeber, et al. (2010). "Biogenesis of caveolae: stepwise assembly of large caveolin and cavin complexes." *Traffic* **11**(3): 361-382.
- Hayer, A., M. Stoeber, et al. (2010). "Caveolin-1 is ubiquitinated and targeted to intraluminal vesicles in endolysosomes for degradation." *J Cell Biol* **191**(3): 615-629.
- Helenius, A., J. Kartenbeck, et al. (1980). "On the entry of Semliki forest virus into BHK-21 cells." *J Cell Biol* **84**(2): 404-420.
- Helle, F. and J. Dubuisson (2008). "Hepatitis C virus entry into host cells." *Cell Mol Life Sci* **65**(1): 100-112.
- Hill, M. M., M. Bastiani, et al. (2008). "PTRF-Cavin, a conserved cytoplasmic protein required for caveola formation and function." *Cell* **132**(1): 113-124.
- Hinshaw, J. E. (2000). "Dynamin and its role in membrane fission." *Annu Rev Cell Dev Biol* **16**: 483-519.
- Hinshaw, J. E. and S. L. Schmid (1995). "Dynamin self-assembles into rings suggesting a mechanism for coated vesicle budding." *Nature* **374**(6518): 190-192.
- Hoekstra, D., D. Tyteca, et al. (2004). "The subapical compartment: a traffic center in membrane polarity development." *Journal of cell science* **117**(Pt 11): 2183-2192.
- Hofmann, J. (1997). "The potential for isoenzyme-selective modulation of protein kinase C." *FASEB J* **11**(8): 649-669.
- Hopkins, C. R. (1983). "Intracellular routing of transferrin and transferrin receptors in epidermoid carcinoma A431 cells." *Cell* **35**(1): 321-330.
- Huang, C. Y., T. Y. Lu, et al. (2008). "A novel cellular protein, VPEF, facilitates vaccinia virus penetration into HeLa cells through fluid phase endocytosis." *Journal of virology* **82**(16): 7988-7999.
- Hummeler, K., N. Tomassini, et al. (1970). "Morphological aspects of the uptake of simian virus 40 by permissive cells." *J Virol* **6**(1): 87-93.
- Huotari, J. e. a. "Cullin-3 regulates late endosome maturation." *in submission*.
- Huotari, J. e. a. (2011). "Endosome maturation." *EMBO J*.
- Hurley, J. H. and S. D. Emr (2006). "The ESCRT complexes: structure and mechanism of a membrane-trafficking network." *Annual review of biophysics and biomolecular structure* **35**: 277-298.
- Huynh, K. K. and S. Grinstein (2007). "Regulation of vacuolar pH and its modulation by some microbial species." *Microbiology and molecular biology reviews : MMBR* **71**(3): 452-462.
- Innocenti, M., S. Gerboth, et al. (2005). "Abi1 regulates the activity of N-WASP and WAVE in distinct actin-based processes." *Nature cell biology* **7**(10): 969-976.
- Jackson, S. P., J. J. MacDonald, et al. (1990). "GC box binding induces phosphorylation of Sp1 by a DNA-dependent protein kinase." *Cell* **63**(1): 155-165.
- Jain, S. K., S. DeCandido, et al. (1991). "Processing of the p62 envelope precursor protein of Semliki Forest virus." *The Journal of biological chemistry* **266**(9): 5756-5761.
- Jentsch, T. J. (2007). "Chloride and the endosomal-lysosomal pathway: emerging roles of CLC chloride transporters." *The Journal of physiology* **578**(Pt 3): 633-640.

- Jing, S. Q., T. Spencer, et al. (1990). "Role of the human transferrin receptor cytoplasmic domain in endocytosis: localization of a specific signal sequence for internalization." The Journal of cell biology **110**(2): 283-294.
- Johansdottir, H. K., R. Mancini, et al. (2009). "Host cell factors and functions involved in vesicular stomatitis virus entry." J Virol **83**(1): 440-453.
- Jovic, M., F. Kieken, et al. (2009). "Eps15 homology domain 1-associated tubules contain phosphatidylinositol-4-phosphate and phosphatidylinositol-(4,5)-bisphosphate and are required for efficient recycling." Mol Biol Cell **20**(11): 2731-2743.
- Kaariainen, L., K. Simons, et al. (1969). "Studies in subviral components of Semliki Forest virus." Ann Med Exp Biol Fenn **47**(4): 235-248.
- Kalia, M., S. Kumari, et al. (2006). "Arf6-independent GPI-anchored protein-enriched early endosomal compartments fuse with sorting endosomes via a Rab5/phosphatidylinositol-3'-kinase-dependent machinery." Molecular biology of the cell **17**(8): 3689-3704.
- Kanaoka, Y., S. H. Kimura, et al. (1997). "GAK: a cyclin G associated kinase contains a tensin/auxilin-like domain." FEBS Lett **402**(1): 73-80.
- Kartenbeck, J., H. Stukenbrok, et al. (1989). "Endocytosis of simian virus 40 into the endoplasmic reticulum." J Cell Biol **109**(6 Pt 1): 2721-2729.
- Kasahara, K., Y. Nakayama, et al. (2007). "Role of Src-family kinases in formation and trafficking of macropinosomes." Journal of cellular physiology **211**(1): 220-232.
- Kerr, M. C. and R. D. Teasdale (2009). "Defining macropinocytosis." Traffic **10**(4): 364-371.
- Khor, R., L. J. McElroy, et al. (2003). "The ubiquitin-vacuolar protein sorting system is selectively required during entry of influenza virus into host cells." Traffic **4**(12): 857-868.
- Kielian, M., C. Chanel-Vos, et al. (2010). "Alphavirus Entry and Membrane Fusion." Viruses **2**(4): 796-825.
- Kielian, M. C., M. Marsh, et al. (1986). "Kinetics of endosome acidification detected by mutant and wild-type Semliki Forest virus." EMBO J **5**(12): 3103-3109.
- King, C. C., E. M. Gardiner, et al. (2000). "p21-activated kinase (PAK1) is phosphorylated and activated by 3-phosphoinositide-dependent kinase-1 (PDK1)." The Journal of biological chemistry **275**(52): 41201-41209.
- Kirchhausen, T., E. Macia, et al. (2008). "Use of dynasore, the small molecule inhibitor of dynamin, in the regulation of endocytosis." Methods Enzymol **438**: 77-93.
- Kirkham, M., A. Fujita, et al. (2005). "Ultrastructural identification of uncoated caveolin-independent early endocytic vehicles." The Journal of cell biology **168**(3): 465-476.
- Kirkham, M., S. J. Nixon, et al. (2008). "Evolutionary analysis and molecular dissection of caveola biogenesis." Journal of cell science **121**(Pt 12): 2075-2086.
- Klimstra, W. B., E. M. Nangle, et al. (2003). "DC-SIGN and L-SIGN can act as attachment receptors for alphaviruses and distinguish between mosquito cell- and mammalian cell-derived viruses." Journal of virology **77**(22): 12022-12032.
- Kojic, L. D., B. Joshi, et al. (2007). "Raft-dependent endocytosis of autocrine motility factor is phosphatidylinositol 3-kinase-dependent in breast carcinoma cells." The Journal of biological chemistry **282**(40): 29305-29313.
- Kolokoltsov, A. A., D. Deniger, et al. (2007). "Small interfering RNA profiling reveals key role of clathrin-mediated endocytosis and early endosome formation for infection by respiratory syncytial virus." J Virol **81**(14): 7786-7800.
- Kolter, T. and K. Sandhoff (2010). "Lysosomal degradation of membrane lipids." FEBS letters **584**(9): 1700-1712.
- Kononchik, J. P., Jr., R. Hernandez, et al. (2011). "An alternative pathway for alphavirus entry." Virology journal **8**: 304.
- Kornfeld, S. and I. Mellman (1989). "The biogenesis of lysosomes." Annual review of cell biology **5**: 483-525.
- Krauss, M., M. Kinuta, et al. (2003). "ARF6 stimulates clathrin/AP-2 recruitment to synaptic membranes by activating phosphatidylinositol phosphate kinase type Igamma." The Journal of cell biology **162**(1): 113-124.
- Kumari, S. and S. Mayor (2008). "ARF1 is directly involved in dynamin-independent endocytosis." Nature cell biology **10**(1): 30-41.
- Lajoie, P. and I. R. Nabi (2010). "Lipid rafts, caveolae, and their endocytosis." International review of cell and molecular biology **282**: 135-163.

- Lamaze, C., A. Dujeancourt, et al. (2001). "Interleukin 2 receptors and detergent-resistant membrane domains define a clathrin-independent endocytic pathway." *Molecular cell* **7**(3): 661-671.
- Langhorst, M. F., A. Reuter, et al. (2008). "Trafficking of the microdomain scaffolding protein reggie-1/flotillin-2." *European journal of cell biology* **87**(4): 211-226.
- Langhorst, M. F., A. Reuter, et al. (2005). "Scaffolding microdomains and beyond: the function of reggie/flotillin proteins." *Cellular and molecular life sciences : CMLS* **62**(19-20): 2228-2240.
- Lanzetti, L., A. Palamidessi, et al. (2004). "Rab5 is a signalling GTPase involved in actin remodelling by receptor tyrosine kinases." *Nature* **429**(6989): 309-314.
- Laporte, S. A., R. H. Oakley, et al. (2000). "The interaction of beta-arrestin with the AP-2 adaptor is required for the clustering of beta 2-adrenergic receptor into clathrin-coated pits." *J Biol Chem* **275**(30): 23120-23126.
- Le Blanc, I., P. P. Luyet, et al. (2005). "Endosome-to-cytosol transport of viral nucleocapsids." *Nat Cell Biol* **7**(7): 653-664.
- Le, P. U., G. Guay, et al. (2002). "Caveolin-1 is a negative regulator of caveolae-mediated endocytosis to the endoplasmic reticulum." *The Journal of biological chemistry* **277**(5): 3371-3379.
- Liberali, P., E. Kakkonen, et al. (2008). "The closure of Pak1-dependent macropinosomes requires the phosphorylation of CtBP1/BARS." *The EMBO journal* **27**(7): 970-981.
- Liddington, R. C., Y. Yan, et al. (1991). "Structure of simian virus 40 at 3.8-A resolution." *Nature* **354**(6351): 278-284.
- Liebl, D., F. Difato, et al. (2006). "Mouse polyomavirus enters early endosomes, requires their acidic pH for productive infection, and meets transferrin cargo in Rab11-positive endosomes." *Journal of virology* **80**(9): 4610-4622.
- Lin, S. X., B. Grant, et al. (2001). "Rme-1 regulates the distribution and function of the endocytic recycling compartment in mammalian cells." *Nat Cell Biol* **3**(6): 567-572.
- Lin, S. X., G. G. Gundersen, et al. (2002). "Export from pericentriolar endocytic recycling compartment to cell surface depends on stable, detyrosinated (glu) microtubules and kinesin." *Molecular biology of the cell* **13**(1): 96-109.
- Lindeberg, T. (1998). "Edge Detection and Ridge Detection with Automatic Scale Selection." *International Journal of Computer Vision* **30**(2): 117-154.
- Lindmo, K. and H. Stenmark (2006). "Regulation of membrane traffic by phosphoinositide 3-kinases." *Journal of cell science* **119**(Pt 4): 605-614.
- Lombardi, D., T. Soldati, et al. (1993). "Rab9 functions in transport between late endosomes and the trans Golgi network." *The EMBO journal* **12**(2): 677-682.
- Longva, K. E., F. D. Blystad, et al. (2002). "Ubiquitination and proteasomal activity is required for transport of the EGF receptor to inner membranes of multivesicular bodies." *J Cell Biol* **156**(5): 843-854.
- Lozach, P. Y., A. Kuhbacher, et al. (2011). "DC-SIGN as a Receptor for Phleboviruses." *Cell host & microbe* **10**(1): 75-88.
- Lozach, P. Y., R. Mancini, et al. (2010). "Entry of bunyaviruses into mammalian cells." *Cell Host Microbe* **7**(6): 488-499.
- Lozach, P. Y., R. Mancini, et al. (2010). "Entry of bunyaviruses into mammalian cells." *Cell host & microbe* **7**(6): 488-499.
- Lundmark, R. and S. R. Carlsson (2003). "Sorting nexin 9 participates in clathrin-mediated endocytosis through interactions with the core components." *J Biol Chem* **278**(47): 46772-46781.
- Lundmark, R. and S. R. Carlsson (2004). "Regulated membrane recruitment of dynamin-2 mediated by sorting nexin 9." *J Biol Chem* **279**(41): 42694-42702.
- Luzio, J. P., P. R. Pryor, et al. (2007). "Lysosomes: fusion and function." *Nature reviews. Molecular cell biology* **8**(8): 622-632.
- Macia, E., M. Ehrlich, et al. (2006). "Dynasore, a cell-permeable inhibitor of dynamin." *Dev Cell* **10**(6): 839-850.
- Maddali, K. K., D. H. Korzick, et al. (2005). "PKCdelta mediates testosterone-induced increases in coronary smooth muscle Cav1.2." *J Biol Chem* **280**(52): 43024-43029.
- Marechal, V., M. C. Prevost, et al. (2001). "Human immunodeficiency virus type 1 entry into macrophages mediated by macropinocytosis." *Journal of virology* **75**(22): 11166-11177.
- Marsh, M., E. Bolzau, et al. (1983). "Penetration of Semliki Forest virus from acidic prelysosomal vacuoles." *Cell* **32**(3): 931-940.

- MathWorks (2010). MATLAB Software Help Index.
- Matlin, K. S., H. Reggio, et al. (1981). "Infectious entry pathway of influenza virus in a canine kidney cell line." *J Cell Biol* **91**(3 Pt 1): 601-613.
- Matlin, K. S., H. Reggio, et al. (1982). "Pathway of vesicular stomatitis virus entry leading to infection." *J Mol Biol* **156**(3): 609-631.
- Matlin, K. S., H. Reggio, et al. (1982). "Pathway of vesicular stomatitis virus entry leading to infection." *Journal of molecular biology* **156**(3): 609-631.
- Matrosovich, M. N., T. Y. Matrosovich, et al. (2004). "Neuraminidase is important for the initiation of influenza virus infection in human airway epithelium." *J Virol* **78**(22): 12665-12667.
- Matsuo, K., H. Hotokezaka, et al. (2006). "Analysis of amphotericin B-induced cell signaling with chemical inhibitors of signaling molecules." *Microbiol Immunol* **50**(4): 337-347.
- Maurer, M. E. and J. A. Cooper (2006). "The adaptor protein Dab2 sorts LDL receptors into coated pits independently of AP-2 and ARH." *J Cell Sci* **119**(Pt 20): 4235-4246.
- Maxfield, F. R. and T. E. McGraw (2004). "Endocytic recycling." *Nat Rev Mol Cell Biol* **5**(2): 121-132.
- Maxfield, F. R. and D. J. Yamashiro (1987). "Endosome acidification and the pathways of receptor-mediated endocytosis." *Advances in experimental medicine and biology* **225**: 189-198.
- Mayor, S., J. F. Presley, et al. (1993). "Sorting of membrane components from endosomes and subsequent recycling to the cell surface occurs by a bulk flow process." *The Journal of cell biology* **121**(6): 1257-1269.
- McMahon, K. A., H. Zajicek, et al. (2009). "SRBC/cavin-3 is a caveolin adapter protein that regulates caveolae function." *The EMBO journal* **28**(8): 1001-1015.
- Medina-Kauwe, L. K. (2003). "Endocytosis of adenovirus and adenovirus capsid proteins." *Adv Drug Deliv Rev* **55**(11): 1485-1496.
- Meister, G. and T. Tuschl (2004). "Mechanisms of gene silencing by double-stranded RNA." *Nature* **431**(7006): 343-349.
- Mellman, I. (1996). "Endocytosis and molecular sorting." *Annu Rev Cell Dev Biol* **12**: 575-625.
- Mellman, I. (1996). "Endocytosis and molecular sorting." *Annual review of cell and developmental biology* **12**: 575-625.
- Mercer, J. and A. Helenius (2008). "Vaccinia virus uses macropinocytosis and apoptotic mimicry to enter host cells." *Science* **320**(5875): 531-535.
- Mercer, J. and A. Helenius (2009). "Virus entry by macropinocytosis." *Nat Cell Biol* **11**(5): 510-520.
- Mercer, J. and A. Helenius (2010). "Apoptotic mimicry: phosphatidylserine-mediated macropinocytosis of vaccinia virus." *Ann N Y Acad Sci* **1209**: 49-55.
- Mercer, J., S. Knebel, et al. (2010). "Vaccinia virus strains use distinct forms of macropinocytosis for host-cell entry." *Proc Natl Acad Sci U S A* **107**(20): 9346-9351.
- Mercer, J., M. Schelhaas, et al. (2010). "Virus entry by endocytosis." *Annu Rev Biochem* **79**: 803-833.
- Merrifield, C. J., M. E. Feldman, et al. (2002). "Imaging actin and dynamin recruitment during invagination of single clathrin-coated pits." *Nat Cell Biol* **4**(9): 691-698.
- Mesaki, K., K. Tanabe, et al. (2011). "Fission of tubular endosomes triggers endosomal acidification and movement." *PLoS One* **6**(5): e19764.
- Mettlen, M., T. Pucadyil, et al. (2009). "Dissecting dynamin's role in clathrin-mediated endocytosis." *Biochem Soc Trans* **37**(Pt 5): 1022-1026.
- Mire, C. E., J. M. White, et al. (2010). "A spatio-temporal analysis of matrix protein and nucleocapsid trafficking during vesicular stomatitis virus uncoating." *PLoS pathogens* **6**(7): e1000994.
- Motley, A., N. A. Bright, et al. (2003). "Clathrin-mediated endocytosis in AP-2-depleted cells." *J Cell Biol* **162**(5): 909-918.
- Muhlberg, A. B., D. E. Warnock, et al. (1997). "Domain structure and intramolecular regulation of dynamin GTPase." *EMBO J* **16**(22): 6676-6683.
- Murray, J. T., C. Panaretou, et al. (2002). "Role of Rab5 in the recruitment of hVps34/p150 to the early endosome." *Traffic* **3**(6): 416-427.
- Nakano, M. Y., K. Boucke, et al. (2000). "The first step of adenovirus type 2 disassembly occurs at the cell surface, independently of endocytosis and escape to the cytosol." *J Virol* **74**(15): 7085-7095.
- Nanbo, A., M. Imai, et al. (2010). "Ebola virus is internalized into host cells via macropinocytosis in a viral glycoprotein-dependent manner." *PLoS pathogens* **6**(9).

- Nesterov, A., R. E. Carter, et al. (1999). "Inhibition of the receptor-binding function of clathrin adaptor protein AP-2 by dominant-negative mutant mu2 subunit and its effects on endocytosis." *EMBO J* **18**(9): 2489-2499.
- Newcomb, W. W., G. J. Tobin, et al. (1982). "In vitro reassembly of vesicular stomatitis virus skeletons." *Journal of virology* **41**(3): 1055-1062.
- Newmyer, S. L., A. Christensen, et al. (2003). "Auxilin-dynamin interactions link the uncoating ATPase chaperone machinery with vesicle formation." *Dev Cell* **4**(6): 929-940.
- Nichols, B. J. and H. R. Pelham (1998). "SNAREs and membrane fusion in the Golgi apparatus." *Biochim Biophys Acta* **1404**(1-2): 9-31.
- Niebuhr, K., S. Giuriato, et al. (2002). "Conversion of PtdIns(4,5)P(2) into PtdIns(5)P by the *S. flexneri* effector IpgD reorganizes host cell morphology." *The EMBO journal* **21**(19): 5069-5078.
- Nishi, K. and K. Saigo (2007). "Cellular internalization of green fluorescent protein fused with herpes simplex virus protein VP22 via a lipid raft-mediated endocytic pathway independent of caveolae and Rho family GTPases but dependent on dynamin and Arf6." *The Journal of biological chemistry* **282**(37): 27503-27517.
- Norkin, L. C. (2001). "Caveolae in the uptake and targeting of infectious agents and secreted toxins." *Advanced drug delivery reviews* **49**(3): 301-315.
- Nossal, R. (2001). "Energetics of clathrin basket assembly." *Traffic* **2**(2): 138-147.
- Nunes-Correia, I., J. Ramalho-Santos, et al. (1999). "Interactions of influenza virus with cultured cells: detailed kinetic modeling of binding and endocytosis." *Biochemistry* **38**(3): 1095-1101.
- Oehlke, O., H. W. Martin, et al. (2011). "Rab11b and its effector Rip11 regulate the acidosis-induced traffic of V-ATPase in salivary ducts." *J Cell Physiol* **226**(3): 638-651.
- Oh, P., D. P. McIntosh, et al. (1998). "Dynamin at the neck of caveolae mediates their budding to form transport vesicles by GTP-driven fission from the plasma membrane of endothelium." *The Journal of cell biology* **141**(1): 101-114.
- Ohuchi, M., N. Asaoka, et al. (2006). "Roles of neuraminidase in the initial stage of influenza virus infection." *Microbes Infect* **8**(5): 1287-1293.
- Overby, A. K., R. F. Pettersson, et al. (2008). "Insights into bunyavirus architecture from electron cryotomography of Uukuniemi virus." *Proceedings of the National Academy of Sciences of the United States of America* **105**(7): 2375-2379.
- Paleotti, O., E. Macia, et al. (2005). "The small G-protein Arf6GTP recruits the AP-2 adaptor complex to membranes." *The Journal of biological chemistry* **280**(22): 21661-21666.
- Palese, P. and M. L. Shaw (2006). Orthomyxoviridae: The viruses and their replication. *Fields Virology*. D. M. Knipe and P. M. Howley. Philadelphia, Lippincott Williams & Wilkins: 1647-1690.
- Parton, R. G., B. Joggerst, et al. (1994). "Regulated internalization of caveolae." *The Journal of cell biology* **127**(5): 1199-1215.
- Parton, R. G. and K. Simons (2007). "The multiple faces of caveolae." *Nature reviews. Molecular cell biology* **8**(3): 185-194.
- Payne, C. K., S. A. Jones, et al. (2007). "Internalization and trafficking of cell surface proteoglycans and proteoglycan-binding ligands." *Traffic* **8**(4): 389-401.
- Pelham, H. R. (1998). "Getting through the Golgi complex." *Trends Cell Biol* **8**(1): 45-49.
- Pelkmans, L., T. Burli, et al. (2004). "Caveolin-stabilized membrane domains as multifunctional transport and sorting devices in endocytic membrane traffic." *Cell* **118**(6): 767-780.
- Pelkmans, L., E. Fava, et al. (2005). "Genome-wide analysis of human kinases in clathrin- and caveolae/raft-mediated endocytosis." *Nature* **436**(7047): 78-86.
- Pelkmans, L. and A. Helenius (2002). "Endocytosis via caveolae." *Traffic* **3**(5): 311-320.
- Pelkmans, L. and A. Helenius (2003). "Insider information: what viruses tell us about endocytosis." *Current opinion in cell biology* **15**(4): 414-422.
- Pelkmans, L., J. Kartenbeck, et al. (2001). "Caveolar endocytosis of simian virus 40 reveals a new two-step vesicular-transport pathway to the ER." *Nat Cell Biol* **3**(5): 473-483.
- Pelkmans, L., D. Puntener, et al. (2002). "Local actin polymerization and dynamin recruitment in SV40-induced internalization of caveolae." *Science* **296**(5567): 535-539.
- Peter, B. J., H. M. Kent, et al. (2004). "BAR domains as sensors of membrane curvature: the amphiphysin BAR structure." *Science* **303**(5657): 495-499.

- Pettersson, R. and L. Kaariainen (1973). "The ribonucleic acids of Uukuniemi virus, a noncubical tick-borne arbovirus." *Virology* **56**(2): 608-619.
- Pike, L. J. (2006). "Rafts defined: a report on the Keystone Symposium on Lipid Rafts and Cell Function." *Journal of lipid research* **47**(7): 1597-1598.
- Pingale, K. K. (1969). *Visual perception by computer*, Academic Press, New York.
- Poupart, M. E., D. Fessart, et al. (2007). "ARF6 regulates angiotensin II type 1 receptor endocytosis by controlling the recruitment of AP-2 and clathrin." *Cellular signalling* **19**(11): 2370-2378.
- Prewitt, J. M. S. (1965). *Object enhancement and extraction*, Academic Press, New York.
- Progida, C., L. Cogli, et al. (2010). "Rab7b controls trafficking from endosomes to the TGN." *J Cell Sci* **123**(Pt 9): 1480-1491.
- Puto, L. A., K. Pestonjamas, et al. (2003). "p21-activated kinase 1 (PAK1) interacts with the Grb2 adapter protein to couple to growth factor signaling." *The Journal of biological chemistry* **278**(11): 9388-9393.
- Quirin, K., B. Eschli, et al. (2008). "Lymphocytic choriomeningitis virus uses a novel endocytic pathway for infectious entry via late endosomes." *Virology* **378**(1): 21-33.
- Radhakrishna, H., R. D. Klausner, et al. (1996). "Aluminum fluoride stimulates surface protrusions in cells overexpressing the ARF6 GTPase." *The Journal of cell biology* **134**(4): 935-947.
- Raiborg, C., K. G. Bache, et al. (2002). "Hrs sorts ubiquitinated proteins into clathrin-coated microdomains of early endosomes." *Nat Cell Biol* **4**(5): 394-398.
- Raiborg, C., J. Wesche, et al. (2006). "Flat clathrin coats on endosomes mediate degradative protein sorting by scaffolding Hrs in dynamic microdomains." *Journal of cell science* **119**(Pt 12): 2414-2424.
- Razi, M. and C. E. Futter (2006). "Distinct roles for Tsg101 and Hrs in multivesicular body formation and inward vesiculation." *Mol Biol Cell* **17**(8): 3469-3483.
- Razi, M. and C. E. Futter (2006). "Distinct roles for Tsg101 and Hrs in multivesicular body formation and inward vesiculation." *Molecular biology of the cell* **17**(8): 3469-3483.
- Ridley, A. J., H. F. Paterson, et al. (1992). "The small GTP-binding protein rac regulates growth factor-induced membrane ruffling." *Cell* **70**(3): 401-410.
- Rink, J., E. Ghigo, et al. (2005). "Rab conversion as a mechanism of progression from early to late endosomes." *Cell* **122**(5): 735-749.
- Robinson, M. S. (2004). "Adaptable adaptors for coated vesicles." *Trends Cell Biol* **14**(4): 167-174.
- Rojek, J. M., M. Perez, et al. (2008). "Cellular entry of lymphocytic choriomeningitis virus." *Journal of virology* **82**(3): 1505-1517.
- Roth, M. G. (2006). "Clathrin-mediated endocytosis before fluorescent proteins." *Nature reviews. Molecular cell biology* **7**(1): 63-68.
- Rothberg, K. G., J. E. Heuser, et al. (1992). "Caveolin, a protein component of caveolae membrane coats." *Cell* **68**(4): 673-682.
- Roux, A., K. Uyhazi, et al. (2006). "GTP-dependent twisting of dynamin implicates constriction and tension in membrane fission." *Nature* **441**(7092): 528-531.
- Ruegg, U. T. and G. M. Burgess (1989). "Staurosporine, K-252 and UCN-01: potent but nonspecific inhibitors of protein kinases." *Trends Pharmacol Sci* **10**(6): 218-220.
- Rust, M. J., M. Lakadamyali, et al. (2004). "Assembly of endocytic machinery around individual influenza viruses during viral entry." *Nat Struct Mol Biol* **11**(6): 567-573.
- Rust, M. J., M. Lakadamyali, et al. (2004). "Assembly of endocytic machinery around individual influenza viruses during viral entry." *Nature structural & molecular biology* **11**(6): 567-573.
- Sabharanjak, S., P. Sharma, et al. (2002). "GPI-anchored proteins are delivered to recycling endosomes via a distinct cdc42-regulated, clathrin-independent pinocytotic pathway." *Developmental cell* **2**(4): 411-423.
- Saeed, M. F., A. A. Kolokoltsov, et al. (2010). "Cellular entry of ebola virus involves uptake by a macropinocytosis-like mechanism and subsequent trafficking through early and late endosomes." *PLoS pathogens* **6**(9).
- Saeed, M. F., A. A. Kolokoltsov, et al. (2008). "Phosphoinositide-3 kinase-Akt pathway controls cellular entry of Ebola virus." *PLoS pathogens* **4**(8): e1000141.
- Sandvig, K., M. L. Torgersen, et al. (2008). "Clathrin-independent endocytosis: from nonexisting to an extreme degree of complexity." *Histochemistry and cell biology* **129**(3): 267-276.
- Santolini, E., C. Puri, et al. (2000). "Numb is an endocytic protein." *J Cell Biol* **151**(6): 1345-1352.

- Santy, L. C. and J. E. Casanova (2001). "Activation of ARF6 by ARNO stimulates epithelial cell migration through downstream activation of both Rac1 and phospholipase D." The Journal of cell biology **154**(3): 599-610.
- Saraste, J. and B. Goud (2007). "Functional symmetry of endomembranes." Molecular biology of the cell **18**(4): 1430-1436.
- Sarli, V. and A. Giannis (2006). "Inhibitors of mitotic kinesins: next-generation antimetabolites." ChemMedChem **1**(3): 293-298.
- Scheiffele, P., P. Verkade, et al. (1998). "Caveolin-1 and -2 in the exocytic pathway of MDCK cells." The Journal of cell biology **140**(4): 795-806.
- Schelhaas, M., J. Malmstrom, et al. (2007). "Simian Virus 40 depends on ER protein folding and quality control factors for entry into host cells." Cell **131**(3): 516-529.
- Schlunck, G., H. Damke, et al. (2004). "Modulation of Rac localization and function by dynamin." Molecular biology of the cell **15**(1): 256-267.
- Schmid, E. M., M. G. Ford, et al. (2006). "Role of the AP2 beta-appendage hub in recruiting partners for clathrin-coated vesicle assembly." PLoS Biol **4**(9): e262.
- Schmid, E. M. and H. T. McMahon (2007). "Integrating molecular and network biology to decode endocytosis." Nature **448**(7156): 883-888.
- Schmid, S., R. Fuchs, et al. (1989). "Acidification of endosome subpopulations in wild-type Chinese hamster ovary cells and temperature-sensitive acidification-defective mutants." J Cell Biol **108**(4): 1291-1300.
- Schmid, S. L. and V. A. Frolov (2011). "Dynamin: Functional Design of a Membrane Fission Catalyst." Annu Rev Cell Dev Biol.
- Schmid, S. L., R. Fuchs, et al. (1988). "Two distinct subpopulations of endosomes involved in membrane recycling and transport to lysosomes." Cell **52**(1): 73-83.
- Schnatwinkel, C., S. Christoforidis, et al. (2004). "The Rab5 effector Rabankyrin-5 regulates and coordinates different endocytic mechanisms." PLoS biology **2**(9): E261.
- Schonteich, E., G. M. Wilson, et al. (2008). "The Rip11/Rab11-FIP5 and kinesin II complex regulates endocytic protein recycling." J Cell Sci **121**(Pt 22): 3824-3833.
- Sever, S. (2002). "Dynamin and endocytosis." Curr Opin Cell Biol **14**(4): 463-467.
- Shajahan, A. N., B. K. Timblin, et al. (2004). "Role of Src-induced dynamin-2 phosphorylation in caveolae-mediated endocytosis in endothelial cells." The Journal of biological chemistry **279**(19): 20392-20400.
- Sharma, D. K., A. Choudhury, et al. (2003). "Glycosphingolipids internalized via caveolar-related endocytosis rapidly merge with the clathrin pathway in early endosomes and form microdomains for recycling." The Journal of biological chemistry **278**(9): 7564-7572.
- Shimura, H., Y. Umeno, et al. (1987). "Effects of inhibitors of the cytoplasmic structures and functions on the early phase of infection of cultured cells with simian virus 40." Virology **158**(1): 34-43.
- Sieczkarski, S. B., H. A. Brown, et al. (2003). "Role of protein kinase C betaII in influenza virus entry via late endosomes." J Virol **77**(1): 460-469.
- Sieczkarski, S. B. and G. R. Whittaker (2002). "Influenza virus can enter and infect cells in the absence of clathrin-mediated endocytosis." J Virol **76**(20): 10455-10464.
- Sieczkarski, S. B. and G. R. Whittaker (2003). "Differential requirements of Rab5 and Rab7 for endocytosis of influenza and other enveloped viruses." Traffic **4**(5): 333-343.
- Sigismund, S., T. Woelk, et al. (2005). "Clathrin-independent endocytosis of ubiquitinated cargos." Proc Natl Acad Sci U S A **102**(8): 2760-2765.
- Simons, K. and E. Ikonen (1997). "Functional rafts in cell membranes." Nature **387**(6633): 569-572.
- Singh, I. and A. Helenius (1992). "Role of ribosomes in Semliki Forest virus nucleocapsid uncoating." Journal of virology **66**(12): 7049-7058.
- Skehel, J. J. and D. C. Wiley (2000). "Receptor binding and membrane fusion in virus entry: the influenza hemagglutinin." Annu Rev Biochem **69**: 531-569.
- Smit, J. M., B. L. Waarts, et al. (2002). "Adaptation of alphaviruses to heparan sulfate: interaction of Sindbis and Semliki forest viruses with liposomes containing lipid-conjugated heparin." Journal of virology **76**(20): 10128-10137.
- Smith, A. E., H. Lilie, et al. (2003). "Ganglioside-dependent cell attachment and endocytosis of murine polyomavirus-like particles." FEBS Lett **555**(2): 199-203.
- Smithburn, K. C., A. J. Haddow, et al. (1946). "A neurotropic virus isolated from Aedes mosquitoes caught in the Semliki forest." Am J Trop Med Hyg **26**: 189-208.

- Snijder, B. and L. Pelkmans (2011). "Origins of regulated cell-to-cell variability." Nat Rev Mol Cell Biol **12**(2): 119-125.
- Snijder, B., R. Sacher, et al. (2009). "Population context determines cell-to-cell variability in endocytosis and virus infection." Nature **461**(7263): 520-523.
- Sobo, K., I. Le Blanc, et al. (2007). "Late endosomal cholesterol accumulation leads to impaired intra-endosomal trafficking." PLoS One **2**(9): e851.
- Sonnichsen, B., S. De Renzis, et al. (2000). "Distinct membrane domains on endosomes in the recycling pathway visualized by multicolor imaging of Rab4, Rab5, and Rab11." J Cell Biol **149**(4): 901-914.
- Sontag, E., J. M. Sontag, et al. (1997). "Protein phosphatase 2A is a critical regulator of protein kinase C zeta signaling targeted by SV40 small t to promote cell growth and NF-kappaB activation." EMBO J **16**(18): 5662-5671.
- Spuul, P., G. Balistreri, et al. (2010). "Phosphatidylinositol 3-kinase-, actin-, and microtubule-dependent transport of Semliki Forest Virus replication complexes from the plasma membrane to modified lysosomes." J Virol **84**(15): 7543-7557.
- Stang, E., J. Kartenbeck, et al. (1997). "Major histocompatibility complex class I molecules mediate association of SV40 with caveolae." Molecular biology of the cell **8**(1): 47-57.
- Steinman, R. M., I. S. Mellman, et al. (1983). "Endocytosis and the recycling of plasma membrane." The Journal of cell biology **96**(1): 1-27.
- Stephens, L., C. Ellson, et al. (2002). "Roles of PI3Ks in leukocyte chemotaxis and phagocytosis." Current opinion in cell biology **14**(2): 203-213.
- Strauss, J. H. and E. G. Strauss (1994). "The alphaviruses: gene expression, replication, and evolution." Microbiological reviews **58**(3): 491-562.
- Stray, S. J., R. D. Cummings, et al. (2000). "Influenza virus infection of desialylated cells." Glycobiology **10**(7): 649-658.
- Stuermer, C. A., D. M. Lang, et al. (2001). "Glycosylphosphatidyl inositol-anchored proteins and fyn kinase assemble in noncaveolar plasma membrane microdomains defined by reggie-1 and -2." Molecular biology of the cell **12**(10): 3031-3045.
- Sun, W., Q. Yan, et al. (2003). "Hrs regulates early endosome fusion by inhibiting formation of an endosomal SNARE complex." The Journal of cell biology **162**(1): 125-137.
- Sun, X., V. K. Yau, et al. (2005). "Role of clathrin-mediated endocytosis during vesicular stomatitis virus entry into host cells." Virology **338**(1): 53-60.
- Swanson, J. A. (1989). "Phorbol esters stimulate macropinocytosis and solute flow through macrophages." Journal of cell science **94** (Pt 1): 135-142.
- Szklarczyk, D., A. Franceschini, et al. (2011). "The STRING database in 2011: functional interaction networks of proteins, globally integrated and scored." Nucleic Acids Res **39**(Database issue): D561-568.
- Tagawa, A., A. Mezzacasa, et al. (2005). "Assembly and trafficking of caveolar domains in the cell: caveolae as stable, cargo-triggered, vesicular transporters." The Journal of cell biology **170**(5): 769-779.
- Tai, G., L. Lu, et al. (2004). "Participation of the syntaxin 5/Ykt6/GS28/GS15 SNARE complex in transport from the early/recycling endosome to the trans-Golgi network." Mol Biol Cell **15**(9): 4011-4022.
- Takai, Y., A. Kishimoto, et al. (1977). "Studies on a cyclic nucleotide-independent protein kinase and its proenzyme in mammalian tissues. I. Purification and characterization of an active enzyme from bovine cerebellum." J Biol Chem **252**(21): 7603-7609.
- Takei, K., P. S. McPherson, et al. (1995). "Tubular membrane invaginations coated by dynamin rings are induced by GTP-gamma S in nerve terminals." Nature **374**(6518): 186-190.
- Tamaoki, T., H. Nomoto, et al. (1986). "Staurosporine, a potent inhibitor of phospholipid/Ca⁺⁺-dependent protein kinase." Biochem Biophys Res Commun **135**(2): 397-402.
- Thomsen, P., K. Roepstorff, et al. (2002). "Caveolae are highly immobile plasma membrane microdomains, which are not involved in constitutive endocytic trafficking." Molecular biology of the cell **13**(1): 238-250.
- Tsai, B., J. M. Gilbert, et al. (2003). "Gangliosides are receptors for murine polyoma virus and SV40." EMBO J **22**(17): 4346-4355.

- Tsai, B., J. M. Gilbert, et al. (2003). "Gangliosides are receptors for murine polyoma virus and SV40." The EMBO journal **22**(17): 4346-4355.
- Tuschl, T. (2001). "RNA interference and small interfering RNAs." ChemBiochem : a European journal of chemical biology **2**(4): 239-245.
- Ungewickell, E., H. Ungewickell, et al. (1995). "Role of auxilin in uncoating clathrin-coated vesicles." Nature **378**(6557): 632-635.
- van der Blik, A. M. (1999). "Is dynamin a regular motor or a master regulator?" Trends Cell Biol **9**(7): 253-254.
- van der Schaar, H. M., M. J. Rust, et al. (2008). "Dissecting the cell entry pathway of dengue virus by single-particle tracking in living cells." PLoS Pathog **4**(12): e1000244.
- van der Sluijs, P., M. Hull, et al. (1992). "The small GTP-binding protein rab4 controls an early sorting event on the endocytic pathway." Cell **70**(5): 729-740.
- van Ijzendoorn, S. C. (2006). "Recycling endosomes." Journal of cell science **119**(Pt 9): 1679-1681.
- van, I. S. C. and D. Hoekstra (1999). "The subapical compartment: a novel sorting centre?" Trends in cell biology **9**(4): 144-149.
- van Kerkhof, P., C. M. Alves dos Santos, et al. (2001). "Proteasome inhibitors block a late step in lysosomal transport of selected membrane but not soluble proteins." Mol Biol Cell **12**(8): 2556-2566.
- Van Kolen, K. and H. Slegers (2006). "Atypical PKCzeta is involved in RhoA-dependent mitogenic signaling by the P2Y(12) receptor in C6 cells." FEBS J **273**(8): 1843-1854.
- Varshavsky, A. J., S. A. Nedospasov, et al. (1977). "Compact form of SV40 viral minichromosome is resistant to nuclease: possible implications for chromatin structure." Nucleic acids research **4**(10): 3303-3325.
- Vonderheit, A. and A. Helenius (2005). "Rab7 associates with early endosomes to mediate sorting and transport of Semliki forest virus to late endosomes." PLoS Biol **3**(7): e233.
- Wang, L. H., K. G. Rothberg, et al. (1993). "Mis-assembly of clathrin lattices on endosomes reveals a regulatory switch for coated pit formation." J Cell Biol **123**(5): 1107-1117.
- Wang, X., S. M. Huong, et al. (2003). "Epidermal growth factor receptor is a cellular receptor for human cytomegalovirus." Nature **424**(6947): 456-461.
- Webb, B. L., S. J. Hirst, et al. (2000). "Protein kinase C isoenzymes: a review of their structure, regulation and role in regulating airways smooth muscle tone and mitogenesis." Br J Pharmacol **130**(7): 1433-1452.
- Wegner, C. S., L. Malerod, et al. (2010). "Ultrastructural characterization of giant endosomes induced by GTPase-deficient Rab5." Histochem Cell Biol **133**(1): 41-55.
- Weil, D., L. Garcon, et al. (2002). "Targeting the kinesin Eg5 to monitor siRNA transfection in mammalian cells." Biotechniques **33**(6): 1244-1248.
- Wenk, M. R. and P. De Camilli (2004). "Protein-lipid interactions and phosphoinositide metabolism in membrane traffic: insights from vesicle recycling in nerve terminals." Proc Natl Acad Sci U S A **101**(22): 8262-8269.
- West, M. A., A. R. Prescott, et al. (2000). "Rac is required for constitutive macropinocytosis by dendritic cells but does not control its downregulation." Current biology : CB **10**(14): 839-848.
- White, J., K. Matlin, et al. (1981). "Cell fusion by Semliki Forest, influenza, and vesicular stomatitis viruses." J Cell Biol **89**(3): 674-679.
- Wolfe, B. L. and J. Trejo (2007). "Clathrin-dependent mechanisms of G protein-coupled receptor endocytosis." Traffic **8**(5): 462-470.
- Woodman, P. G. and C. E. Futter (2008). "Multivesicular bodies: co-ordinated progression to maturity." Current opinion in cell biology **20**(4): 408-414.
- Yamashiro, D. J. and F. R. Maxfield (1987). "Acidification of morphologically distinct endosomes in mutant and wild-type Chinese hamster ovary cells." The Journal of cell biology **105**(6 Pt 1): 2723-2733.
- Yamashiro, D. J., B. Tycko, et al. (1984). "Segregation of transferrin to a mildly acidic (pH 6.5) para-Golgi compartment in the recycling pathway." Cell **37**(3): 789-800.
- Young, V. B., S. Falkow, et al. (1992). "The invasin protein of *Yersinia enterocolitica*: internalization of invasin-bearing bacteria by eukaryotic cells is associated with reorganization of the cytoskeleton." The Journal of cell biology **116**(1): 197-207.

- Zerial, M. and H. McBride (2001). "Rab proteins as membrane organizers." Nat Rev Mol Cell Biol **2**(2): 107-117.
- Zhou, B. B., H. Li, et al. (1998). "Caspase-dependent activation of cyclin-dependent kinases during Fas-induced apoptosis in Jurkat cells." Proc Natl Acad Sci U S A **95**(12): 6785-6790.
- Zhu, C., J. Zhao, et al. (2005). "Functional analysis of human microtubule-based motor proteins, the kinesins and dyneins, in mitosis/cytokinesis using RNA interference." Mol Biol Cell **16**(7): 3187-3199.
- Zhu, W., L. Wang, et al. (2010). "Interaction of E2 glycoprotein with heparan sulfate is crucial for cellular infection of Sindbis virus." PLoS One **5**(3): e9656.
- Zoncu, R., R. M. Perera, et al. (2009). "A phosphoinositide switch controls the maturation and signaling properties of APPL endosomes." Cell **136**(6): 1110-1121.

9 ACKNOWLEDGEMENTS

First of all I would like to thank Ari that I could do my PhD in his lab, and for his help throughout my thesis. Especially I want to thank him that he and his family visited me during my rehabilitation and that he encouraged me many times to finish this project although I confronted him quite often with my concerns.

I also want to thank my thesis committee member Daniel Gerlich, who always had time for discussions and supported me a lot. Also I would like to thank the members of his lab, especially Julien, Michael Held, Claudia, Andrea, and Michael Schmitz for friendship and many tea breaks.

A great “thank you” to all former and current members of the Helenius lab for all the nice time during research and outside the lab. Thanks for all your support, discussions, and wishes during my hard time in the hospital. It was great to have so many friends during all the years. I want to thank especially Roger M, Sabrina, Jatta, Miriam, Flo, Hrefna, and Olivia for the deep friendship that hopefully will last forever. We together went through all the ups and downs during the years. I thank the other lab members for the fruitful discussions and the great atmosphere in the lab, which improved continuously throughout the years. I want to thank Vondi to introduce me to virus work and his support during screening and application for the RISC. I want to thank my two students that they made such a good job and worked so independently. My special thanks are for you, Roberta, that you are not only a really good technician but are so kind despite of all our former problems. I would like to thank all of you who visited me in the hospital and during rehabilitation – I enjoyed it so much during this hard time.

I would like to emphasize how great Toni supported me and the whole lab in any kind of technical questions and problems. Without you, Toni, everything would break apart! Also I thank the staff of the IBC, especially Sonia, for all your help. My special thanks go to the LMC and RISC facility, especially Mike, Vondi und Justine for trouble shooting at the microscopes. Roland and Nico, I thank you for your instant help whenever something IT-related did not work properly. Thanks Roland for your TV and the good and deep chats about life!

Last but not least I thank my mom that she always believed in me, supported me throughout my life. It is so hard that you are gone. I thank my dad, my sister, Mirko, and Lilli that they are always here to help and support me. I thank also my deep old friends Jörg, Didac, Bernd, and Maike. It is good to have you.

10 CURRICULUM VITAE

Personal Information

Name: Thomas Heger
Date of birth: 28th March 1978
Citizenship: Germany
Place of birth: Ruit

Higher Education

12/2004 – 08/2011 PhD Student
Prof. Dr. Ari Helenius lab
Institute of Biochemistry, ETH Zurich

11/2003 – 07/2004 Diploma Thesis
Prof. Dr. med. Hanns Lochmüller
Laboratory for Gene Therapy, GeneCenter, Ludwig-Maximilians-Universität
München, Germany

09/2001 – 07/2002 Exchange Year at University of Washington, Seattle
Prof. John A. Glomset, Institute of Biochemistry

10/1998 – 07/2004 Study of Biochemistry
Eberhard-Karls-University Tübingen, Germany
Degree: Diplom-Biochemist

07/1997 Abitur
Friedrich-Ebert-Gymnasium, Esslingen, Germany

Fellowships and Awards

2006 TH-Grant from the ETH Vice President for PhD project

2001 “Baden-Württemberg-Stipendium” of the “Landesstiftung Baden-Württemberg”
Grant for exchange students of the National Foundation of the German Federal State Baden-Wurttemberg

1997 High school award for the best *Abitur*
Award from the Foundation of the German Chemical Industry for the best performance in high school chemistry
Scheffel Price for the best German *Abitur* essay

Publications

Engel S, Heger T, Mancini R, Herzog F, Kartenbeck J, Hayer A, Helenius A
The role of endosomes in SV40 entry and infection.
J Virol 2011 May;85(9):4198-211.

Geiger R, Andritschke D, Friebe S, Herzog F, Luisoni S, Heger T, Helenius A.
BAP31 and BiP are essential for dislocation of SV40 from the endoplasmic reticulum to the cytosol.
Nat Cell Biol. 2011 Sep 25.

Snijder B, Sacher R, Rämö P, Mench K, Burleigh L, Wolfrum N, Verheije H, Mercer J, Moese S, Heger T, Theusner K, Jurgéit A, Schelhaas M, De Haan X, Marjomäki V, Hyypiä T, Rottier P, Sodeik B, Marsh M, Amara A, Greber U, Helenius A, and Pelkmans L
Cell-to-cell variability modeling reveals complex RNAi phenotypes in virus infection.
In preparation.

Heger T.
Winzig, wandelbar und bedrohlich.
Focus article, VSAO Journal, Nr. 5, p16-17, Sept 2010

